NONLINEAR ASSIMILATION VIA SCORE-BASED SEQUENTIAL LANGEVIN SAMPLING

ZHAO DING[1], CHENGUANG DUAN[1], YULING JIAO[1], JERRY ZHIJIAN YANG[1], CHENG YUAN[2], AND PINGWEN ZHANG[1,3]

ABSTRACT. This paper presents score-based sequential Langevin sampling (SSLS), a novel approach to nonlinear data assimilation within a recursive Bayesian framework. The proposed method decomposes the assimilation process into alternating prediction and update steps, leveraging dynamic models for state prediction while incorporating observational data through score-based Langevin Monte Carlo during updates. To address challenges in posterior sampling, we introduce an annealing strategy within the update mechanism. We provide theoretical guarantees for SSLS convergence in total variation (TV) distance under certain conditions, providing insights into error behavior with respect to key hyper-parameters. Our numerical experiments across challenging scenarios – including high-dimensional systems, strong nonlinearity, and sparse observations – demonstrate the robust performance of the proposed method. Furthermore, SSLS effectively quantifies the uncertainty associated with the estimated states, making it particularly valuable for the error calibration.

1. INTRODUCTION

Data assimilation aims to estimate the time-varying latent states given noisy observation data and the state transition dynamics (Law et al., 2015, Reich and Cotter, 2015, Reich, 2019). This task is essential in various application scenarios such as weather forecasting (Katsafados et al., 2020, Evensen et al., 2022), digital twin technology (Thelen et al., 2022, 2023), and mathematical finance (Bhar, 2010, Frey and Schmidt, 2012, Elliott and Siu, 2013). Despite its importance and widespread application, data assimilation remains a challenging task. The major difficulties in data assimilation lie in the nonlinear nature of both the state transition dynamics and the measurement model, as well as the high dimensionality of the state. Moreover, in many cases, only noisy and sparse observation data are available, introducing further difficulties to the data assimilation. Apart from estimating the latent states, researchers also need to quantify the uncertainties of the estimated states, which is crucial for assessing and calibrating the estimation error (Sullivan, 2015). These constraints and requirements pose significant challenges for data assimilation.

Although various widely-used methods have been proposed for data assimilation, none fully addresses the aforementioned challenges. These approaches generally fall into two categories: variational methods (Evensen et al., 2022) and Bayesian filtering (Särkkä and Svensson, 2023). Variational methods, such as 3D-Var and 4D-Var (Le Dimet and Talagrand, 1986), estimate latent states through maximum-a-posteriori inference. In contrast, Bayesian filtering approaches, including the ensemble Kalman filter (EnKF) (Houtekamer and Mitchell,

---

1998) and particle filter (PF) (Gordon et al., 1993, Kitagawa, 1996, Doucet et al., 2001), aim to sample from the posterior distribution. Despite their widespread adoption, both categories encounter significant limitations in complex assimilation scenarios. The fundamental rationale behind variational methods and EnKF relies on Gaussian approximations of the posterior distribution (Särkkä and Svensson, 2023). These methods assume both Gaussian prior and measurement noise, while linearizing the dynamics and measurement models. However, in highly nonlinear assimilation scenarios with non-Gaussian prior and likelihood, the true posterior may deviate substantially from a Gaussian distribution (Mandel et al., 2012), severely compromising the effectiveness of Gaussian approximations. The PF, while free from linear and Gaussian assumptions, encounters particle degeneracy or impoverishment in high-dimensional settings (Snyder et al., 2008, Bengtsson et al., 2008, Bickel et al., 2008). This phenomenon occurs when the number of ensemble particles is limited: with high probability, multiple particles in the ensemble converge to identical values (Snyder et al., 2008).

Recently, score-based generative models (Ho et al., 2020, Song and Ermon, 2019, Song et al., 2021) have emerged as a promising approach in data assimilation (Rozet and Louppe, 2023a, Li et al., 2024, Bao et al., 2024, Si and Chen, 2024), driven by their exceptional ability to learn and sample from complex distributions. While these approaches demonstrate encouraging empirical performance in certain nonlinear and high-dimensional problems, they face two key limitations: they either depend on restrictive assumptions about Gaussian priors and likelihoods (Li et al., 2024), or they lack rigorous theoretical foundations (Rozet and Louppe, 2023a, Bao et al., 2024, Si and Chen, 2024). A detailed discussion of these limitations is provided in Appendix A.

In this work, we introduce a provable method for nonlinear and high-dimensional data assimilation that is both empirically validated and theoretically rigorous. Our main contributions are summarized as follows:

(i) We present a novel method for nonlinear assimilation, named **s**core-based **s**equential **L**angevin **s**ampling (SSLS), within a recursive Bayesian framework. SSLS decomposes the assimilation process into a sequence of iterations invoking prediction and update steps. During the prediction step, we utilize the dynamics model to predict states, from which the score of the prior distribution can be learned. Subsequently, in the update step, we incorporate the observation data as the likelihood and sample from the posterior distribution using the score-based Langevin Monte Carlo. To improve convergence and facilitate multi-modal sampling, an annealing strategy is integrated into the Langevin algorithm.

(ii) We analyze the convergence of SSLS in TV-distance under certain mild conditions. Our theoretical findings characterize precisely how the assimilation error is affected by the various hyper-parameters including the step size, the number of iterations, the score matching error, and the initial distribution shift (Theorem 3.4). In addition, our theoretical results provide valuable insights into the convergence of score-based Langevin-type algorithms for posterior sampling (Theorem 3.2), which is of independent interest.

(iii) We utilize SSLS in various numerical examples to assess its performance and compare it with baseline approaches from multiple perspectives. According to our experimental results, SSLS yields significant advantages in high-dimensional and nonlinear data assimilation, even with only sparse observations. Furthermore, the standard deviation

of SSLS accurately indicates estimation errors, highlighting the proficiency of our method in quantifying uncertainty.

1.1. **Notations.** We now introduce some basic notations. The set of positive integers is denoted by $\mathbb{N} = \{1, 2, \ldots\}$. Denote $\mathbb{N}_0 = \{0\} \cup \mathbb{N}$ for convenience. For a positive integer $k \in \mathbb{N}$, let $[k]$ denote the set $\{1, \ldots, k\}$. We employ the notations $A \lesssim B$ and $B \gtrsim A$ to signify that there exists an absolute constant $c > 0$ such that $A \leq cB$. In addition, $A = \Theta(B)$ means both $A \lesssim B$ and $A \gtrsim B$. Appendix B summarizes the notations used in Sections 2 and 3 for easy reference and cross-checking.

1.2. **Organization.** The rest of this paper is organized as follows. Section 2 presents the score-based sequential Langevin sampling for data assimilation, while Section 3 provides a thorough theoretical guarantee. The efficiency of our methods is demonstrated through a series of numerical experiments in Section 4. Finally, Section 5 summarizes the conclusions and outlines future work. The supplementary material provides a review of existing approaches, a notation summary, complete theoretical proofs, additional numerical experiments, and detailed experimental settings.

2. Score-based Sequential Langevin Sampling

This section begins with an introduction to data assimilation in Section 2.1, followed by a presentation of the recursive Bayesian framework in Section 2.2. Then Sections 2.3 and 2.4 propose the prediction and update procedures, respectively. The complete assimilation algorithm is summarized in Section 2.5.

2.1. **Problem formulation.** The data assimilation refers to a class of problems that aim to estimate the state of a time-varying system that is indirectly observed through noisy measurements. Let $(\mathbf{X}_k)_{k\in\mathbb{N}}$ be a sequence of unobservable latent states taking values in $\mathbb{R}^d$, which satisfies the dynamics model

$$(2.1) \qquad\qquad \mathbf{X}_{k+1} = \mathcal{F}_k(\mathbf{X}_k, \mathbf{V}_k).$$

Here $k \in \mathbb{N}$ is the time index, $\mathcal{F}_k$ is a time-dependent forward propagation operator, and $(\mathbf{V}_k)_{k\in\mathbb{N}}$ is a sequence of independent random variables with known distribution. The dynamics model (2.1) implies that $(\mathbf{X}_k)_{k\in\mathbb{N}}$ is a non-homogeneous Markov chain, defined in terms of the transition probability density $\rho_k(\mathbf{x}|\mathbf{x}_k) := p_{\mathbf{X}_{k+1}|\mathbf{X}_k}(\mathbf{x}|\mathbf{x}_k)$. The stochastic process $(\mathbf{Y}_k)_{k\in\mathbb{N}}$ represents the indirect and noisy observations, linked with the latent states $(\mathbf{X}_k)_{k\in\mathbb{N}}$ by the measurement model

$$(2.2) \qquad\qquad \mathbf{Y}_k = \mathcal{G}_k(\mathbf{X}_k, \mathbf{W}_k),$$

where $\mathcal{G}_k$ is a time-dependent measurement operator, and $(\mathbf{W}_k)_{k\in\mathbb{N}}$ is a sequence of independent noise with known distribution. Denote the conditional density associated with the measurement model (2.2) by $g_k(\mathbf{y}|\mathbf{x}) := p_{\mathbf{Y}_k|\mathbf{X}_k}(\mathbf{y}|\mathbf{x})$, which is known as the measurement likelihood. The dynamics model (2.1) together the measurement model (2.2) characterize a state-space model illustrated in Figure 1.

The goal of the data assimilation is to estimate the posterior distribution of the latent state $\mathbf{X}_{k+1}$ conditioned on all available observations $\mathbf{Y}_{[k+1]}$, that is,

$$(2.3) \qquad\quad \pi_{k+1}(\mathbf{x}|\mathbf{y}_{[k+1]}) := p_{\mathbf{X}_{k+1}|\mathbf{Y}_{[k+1]}}(\mathbf{x}|\mathbf{y}_{[k+1]}), \quad k \in \mathbb{N}.$$

In practical scenarios, researchers predominantly focus on posterior sampling rather than posterior density estimation. This preference arises because posterior sampling provides
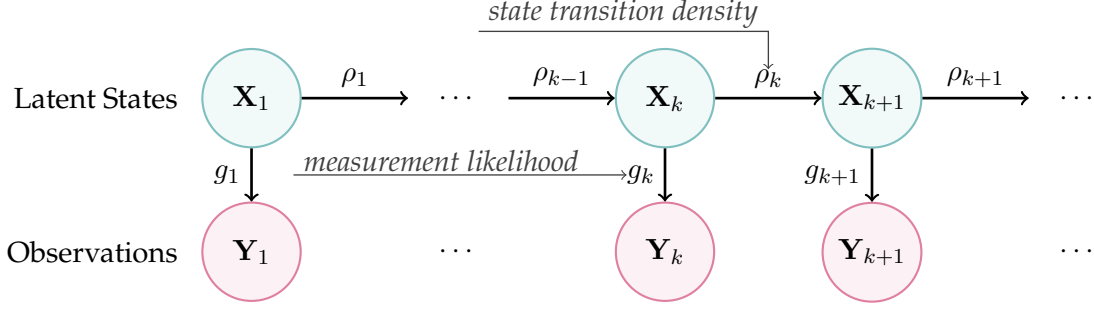
FIGURE 1. An illustrative schematic of the state-space model. The latent states $(\mathbf{X}_k)_{k \in \mathbb{N}}$ are unobservable and evolves according to known transition densities $(\rho_k)_{k \in \mathbb{N}}$, which are specified by a dynamics model (2.1). The observations $(\mathbf{Y}_k)_{k \in \mathbb{N}}$ are linked with states by a known likelihood g_k characterized by the measurement model (2.2).

direct access to statistical inference through the computation of essential measures such as means, standard deviations, and confidence intervals, which are crucial for decision-making and uncertainty quantification. Consequently, data assimilation can be reformulated as a sequence of posterior sampling problems.

2.2. **Recursive Bayesian framework.** In this subsection, we present the recursive Bayesian framework Särkkä and Svensson (2023) for data assimilation. Given the previous posterior distribution $\pi_k(\cdot|\mathbf{y}_{[k+1]})$, the current state $\mathbf{X}_{k+1}$ can be predicted using the dynamics model (2.1). The distribution of the predicted state given all historical measurements is given by

$$(2.4) \qquad q_{k+1}(\mathbf{x}|\mathbf{y}_{[k]}) := p_{\mathbf{X}_{k+1}|\mathbf{Y}_{[k]}}(\cdot|\mathbf{y}_{[k]}) = \int \rho_k(\mathbf{x}|\mathbf{x}_k)\pi_k(\mathbf{x}_k|\mathbf{y}_{[k]})\,\mathrm{d}\mathbf{x}_k,$$

where the Chapman-Kolmogorov identity is applied. The posterior distribution in (2.3) can be expressed as the product of the measurement likelihood $g_{k+1}(\mathbf{y}_{k+1}|\cdot)$ (2.2) and the prediction distribution $q_{k+1}(\cdot|\mathbf{y}_{[k]})$ via the Bayes' rule:

$$(2.5) \qquad \pi_{k+1}(\mathbf{x}|\mathbf{y}_{[k+1]}) \propto g_{k+1}(\mathbf{y}_{k+1}|\mathbf{x})q_{k+1}(\mathbf{x}|\mathbf{y}_{[k]}),$$

where we omit a constant independent of $\mathbf{x}$. The prediction (2.4) and update (2.5) stages can be combined to characterize a recursion from the previous posterior $\pi_k(\cdot|\mathbf{y}_{[k]})$ to the current posterior $\pi_{k+1}(\cdot|\mathbf{y}_{[k+1]})$ as

$$(2.6) \qquad \pi_{k+1}(\mathbf{x}|\mathbf{y}_{[k+1]}) \propto g_{k+1}(\mathbf{y}_{k+1}|\mathbf{x}) \int \rho_k(\mathbf{x}|\mathbf{x}_k)\pi_k(\mathbf{x}_k|\mathbf{y}_{[k]})\,\mathrm{d}\mathbf{x}_k.$$

This recursion serves as the central object throughout our method, which enables us to decompose the data assimilation into a sequence of posterior sampling problems. Each of these sub-problems can be solved by alternating between prediction (2.4) and update (2.5) steps. The complete procedure of the prediction-update recursion is illustrated in Figure 2. We will present these two steps in detail as Sections 2.3 and 2.4, respectively.

2.3. **Prediction and score matching.** This section focuses on estimating the score, i.e., the gradient of log-density, of the prediction distribution $q_{k+1}(\cdot|\mathbf{y}_{[k]})$ (2.4). The prediction score estimator will be utilized in the update step for sampling through Langevin-type algorithms, as demonstrated in the subsequent subsection.
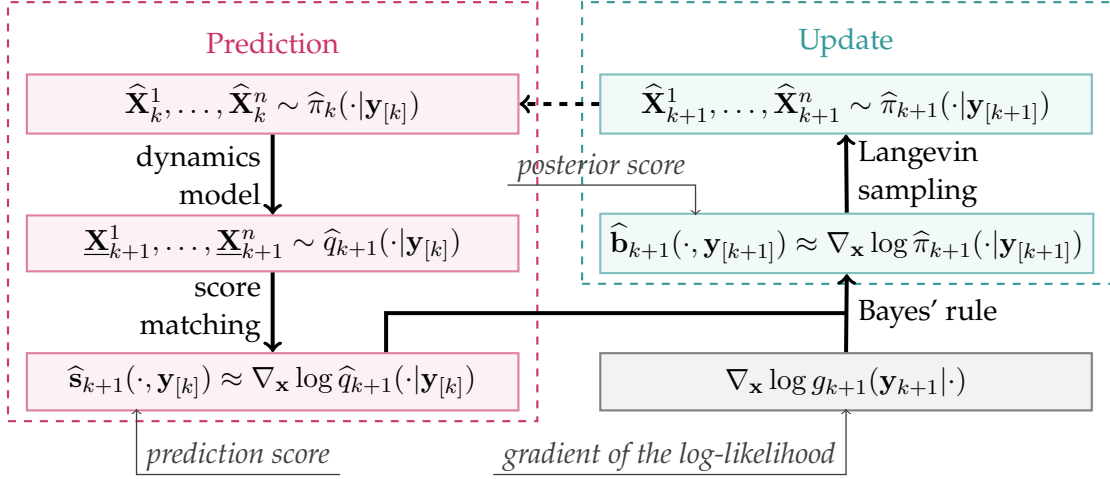
FIGURE 2. Schematic representation of score-based sequential Langevin sampling. (Left) The prediction step involves sampling from the approximated prediction distribution and estimating the prediction score. (Right) The posterior score is then obtained by combining the prediction score with the gradient of the log-likelihood. The update step samples from the posterior distribution using ALMC. Combining these two phases characterizes a recursion from the previous posterior to the current posterior.

Given that the exact previous posterior distribution $\pi_k(\cdot|\mathbf{y}_{[k]})$ in (2.4) is intractable, and only an estimator $\widehat{\pi}_k(\cdot|\mathbf{y}_{[k]})$ is available within the recursive Bayesian framework, we substitute the exact posterior distribution in (2.4) with its estimator to derive the approximated prediction distribution:

$$(2.7) \qquad \widehat{q}_{k+1}(\mathbf{x}|\mathbf{y}_{[k]}) := \int \rho_k(\mathbf{x}|\mathbf{x}_k)\widehat{\pi}_k(\mathbf{x}_k|\mathbf{y}_{[k]})\,\mathrm{d}\mathbf{x}_k \approx q_{k+1}(\mathbf{x}|\mathbf{y}_{[k]}).$$

This approximation closely resembles the prediction distribution (2.4) when $\widehat{\pi}_k(\cdot|\mathbf{y}_{[k]})$ provides an accurate approximation of the previous posterior distribution $\pi_k(\cdot|\mathbf{y}_{[k]})$. Our task thus becomes estimating the score for the approximated prediction distribution (2.7).

According to the dynamics model (2.1), a particle approximation to the approximated prediction distribution (2.7) can be constructed as

$$(2.8) \qquad \underline{\mathbf{X}}_{k+1}^i = \mathcal{F}_k(\widehat{\mathbf{X}}_k^i, \mathbf{V}_k^i), \quad 1 \le i \le n,$$

where $\widehat{\mathbf{X}}_k^1, \ldots, \widehat{\mathbf{X}}_k^n$ are independent random variables drawn from the previous estimated posterior $\widehat{\pi}_k(\cdot|\mathbf{y}_{[k]})$, and $\mathbf{V}_k^1, \ldots, \mathbf{V}_k^n$ are independent random copies of $\mathbf{V}_k$. However, in regions where the approximated prediction density is low, score matching using the particle approximation (2.8) fails to accurately estimate the score due to insufficient prediction samples (Song and Ermon, 2019).

Gaussian smoothing. To address this limitation, we incorporate Gaussian smoothing into the score matching procedure, building upon the approach developed by Song and Ermon (2019). For a fixed smoothing level $\sigma > 0$, define the Gaussian smoothed counterpart of (2.7) as

$$(2.9) \qquad q_{k+1}^\sigma(\mathbf{x}|\mathbf{y}_{[k]}) = \int N(\mathbf{x}; \mathbf{x}_0, \sigma^2\mathbf{I}_d)\widehat{q}_{k+1}(\mathbf{x}_0|\mathbf{y}_{[k]})\,\mathrm{d}\mathbf{x}_0 \approx \widehat{q}_{k+1}(\mathbf{x}|\mathbf{y}_{[k]}),$$

where $N(\cdot; \mathbf{x}_0, \sigma^2 \mathbf{I}_d)$ represents the density of Gaussian distribution with mean $\mathbf{x}_0$ and covariance matrix $\sigma^2 \mathbf{I}_d$. The Gaussian smoothing serves two important purposes. First, it fills in low density regions in the original approximated prediction distribution (2.7), making the estimation of the smoothed density (2.9) more tractable than estimating the original distribution (Song and Ermon, 2019). Second, for sufficiently small $\sigma > 0$, the score function of the smoothed distribution approximates that of the original prediction density $\widehat{q}_{k+1}(\cdot|\mathbf{y}_{[k]})$ (Tang and Yang, 2024). Consequently, the score function of (2.9) serves as an effective surrogate that closely approximates the original score while being easier to estimate.

Remark 2.1 (Inflation). The Gaussian smoothing (2.9) is commonly known as inflation in the field of data assimilation, and has demonstrated empirical success in practical applications (Anderson and Anderson, 1999, Anderson, 2009, Sacher and Bartello, 2008, Evensen et al., 2022). Inflation serves a main purpose to mitigate the excessive reduction of variance resulting from spurious correlations in the update step.

Denoising score matching. Three mainstream approaches exist for score matching: implicit score matching (Hyvärinen, 2005), sliced score matching (Song et al., 2020), and denoising score matching (Vincent, 2011). Among these, we adopt denoising score matching because it eliminates the need to compute the gradient of the score network, unlike the other two methods which require this computation.

Following denoising score matching (Vincent, 2011), the score function of the smoothed density (2.9) minimizes the objective functional:

$$L_{k+1}(\mathbf{s}) = \mathbb{E}_{\underline{\mathbf{X}}_{k+1} \sim \widehat{q}_{k+1}(\cdot|\mathbf{y}_{[k]})} \mathbb{E}_{\boldsymbol{\varepsilon} \sim N(0,\mathbf{I}_d)} \left[\|\sigma \mathbf{s}(\underline{\mathbf{X}}_{k+1} + \sigma\boldsymbol{\varepsilon}, \mathbf{y}_{[k]}) + \boldsymbol{\varepsilon}\|_2^2 \right].$$

Since this population risk is analytically intractable in practical applications, we estimate the score function through empirical risk minimization:

$$(2.10) \qquad \widehat{\mathbf{s}}_{k+1}(\cdot, \mathbf{y}_{[k]}) \in \arg\min_{\mathbf{s} \in \mathcal{S}} \widehat{L}_{k+1}(\mathbf{s}) = \frac{1}{n} \sum_{i=1}^{n} \|\sigma \mathbf{s}(\underline{\mathbf{X}}_{k+1}^i + \sigma\boldsymbol{\varepsilon}_i, \mathbf{y}_{[k]}) + \boldsymbol{\varepsilon}_i\|_2^2,$$

where $\mathcal{S}$ is a deep neural network class, $\{\underline{\mathbf{X}}_{k+1}^i\}_{i=1}^{n}$ is a set of independent predicted states defined as (2.8), and $\{\boldsymbol{\varepsilon}_i\}_{i=1}^{n}$ is a set of independent standard Gaussian variables.

2.4. **Update via Langevin Sampling.** This subsection introduces a Langevin algorithm to sample from the posterior distribution $\pi_{k+1}(\cdot|\mathbf{y}_{[k+1]})$ in (2.5). We begin by introducing the Langevin diffusion associated with the target posterior distribution, defined as the solution to the following stochastic differential equation:

$$(2.11) \qquad d\mathbf{Z}_t = \nabla_{\mathbf{x}} \log \pi_{k+1}(\mathbf{Z}_t|\mathbf{y}_{[k+1]}) \, dt + \sqrt{2} \, d\mathbf{B}_t, \quad \mathbf{Z}_0 \sim q_{k+1}(\cdot|\mathbf{y}_{[k]}),$$

where $(\mathbf{B}_t)_{t \geq 0}$ is a Brownian motion. Classical theory establishes that when $\pi_{k+1}(\cdot|\mathbf{y}_{[k+1]})$ satisfies a functional inequality such as the log-Sobolev inequality, the law of Langevin diffusion (2.11) converges exponentially fast to the target distribution $\pi_{k+1}(\cdot|\mathbf{y}_{[k+1]})$ (Bakr et al., 2014). By applying the Bayes' rule (2.5), we can approximate the drift term of the Langevin diffusion (2.11) as:

$$\nabla_{\mathbf{x}} \log \pi_{k+1}(\mathbf{x}|\mathbf{y}_{[k+1]}) \approx \nabla_{\mathbf{x}} \log g_{k+1}(\mathbf{y}_{k+1}|\mathbf{x}) + \widehat{\mathbf{s}}_{k+1}(\mathbf{x}, \mathbf{y}_{[k]}),$$

where the second term represents the score estimated in the prediction step (2.10). Sampling from the posterior distribution requires simulating the Langevin diffusion with this estimated score. However, in most cases, the Langevin diffusion cannot be simulated analytically. We

employ the Euler-Maruyama discretization to approximate the Langevin diffusion (2.11) with the estimated score, leading to the Langevin Monte Carlo (LMC).

Limitations of vanilla Langevin Monte Carlo. Notice that the initial distribution of Langevin diffusion (2.11) is chosen as the prediction distribution $q_{k+1}(\cdot|\mathbf{y}_{[k]})$, which can be practically implemented using the approximated prediction distribution (2.7). This choice is necessitated by the fact that the prediction distribution represents our only available knowledge about the state variables $\mathbf{X}_k$. However, this initialization strategy may become inefficient when there is a substantial discrepancy between the target posterior distribution $\pi_{k+1}(\cdot|\mathbf{y}_{[k+1]})$ and the prediction distribution $q_{k+1}(\cdot|\mathbf{y}_{[k]})$.

Specifically, regions of high prediction density may not coincide with regions of high posterior density, particularly when the likelihood is highly informative or concentrated in regions where the prediction density is low. This misalignment creates two significant limitations for the vanilla LMC: it wastes computational resources exploring regions with high prediction density but low likelihood, and it may fail to locate important regions of the posterior distribution where the prediction density is low but the likelihood is high.

Annealing strategy. To overcome these limitations, we incorporate an annealing strategy into the Langevin algorithm. The rationale behind annealing involves gradually transitioning from the prediction distribution to the target posterior distribution (Del Moral et al., 2006, Kantas et al., 2014, Beskos et al., 2015, Brosse et al., 2018, Song and Ermon, 2019, Ge et al., 2020, Jalal et al., 2021, Wu and Xie, 2024). Specifically, we construct a sequence of interpolations between these two distributions

$$(2.12) \qquad \pi_{k+1}^m(\mathbf{x}|\mathbf{y}_{[k+1]}) \propto \pi_{k+1}(\mathbf{x}|\mathbf{y}_{[k+1]})^{\beta_m} q_{k+1}(\mathbf{x}|\mathbf{y}_{[k]})^{1-\beta_m}, \quad 0 \leq m \leq M,$$

where $0 \equiv \beta_0 < \beta_1 < \cdots < \beta_M \equiv 1$ represents a sequence of inverse temperatures. Here $\beta_0 = 0$ corresponds to the prediction distribution, while $\beta_M = 1$ corresponds to the target posterior. When β_m is small, the intermediate distribution $\pi_{k+1}^m(\cdot|\mathbf{y}_{[k+1]})$ is predominantly influenced by the prediction distribution, enabling efficient sampling via LMC initialized from the prediction distribution. As β_m approaches 1, the intermediate distribution $\pi_{k+1}^m(\cdot|\mathbf{y}_{[k+1]})$ converges to the target posterior distribution. Through this gradual increase in inverse temperatures from $\beta_0 = 0$ to $\beta_M = 1$, the easily sampleable prediction distribution $q_{k+1}(\cdot|\mathbf{y}_{[k]})$ smoothly transitions toward the target posterior distribution $\pi_{k+1}(\cdot|\mathbf{y}_{[k+1]})$.

At each inverse temperature β_m, we sample from the intermediate distribution $\pi_{k+1}^m(\cdot|\mathbf{y}_{[k+1]})$ using the Langevin diffusion

$$(2.13) \qquad \mathrm{d}\mathbf{Z}_t^m = \nabla_{\mathbf{x}} \log \pi_{k+1}^m(\mathbf{Z}_t^m|\mathbf{y}_{[k+1]})\,\mathrm{d}t + \sqrt{2}\,\mathrm{d}\mathbf{B}_t, \quad \mathbf{Z}_0^m \sim \pi_{k+1}^{m-1}(\cdot|\mathbf{y}_{[k+1]}),$$

where the score of the intermediate distribution is given by:

$$\nabla_{\mathbf{x}} \log \pi_{k+1}^m(\mathbf{x}|\mathbf{y}_{[k+1]}) = \beta_m \nabla_{\mathbf{x}} \log \pi_{k+1}(\mathbf{x}|\mathbf{y}_{[k+1]}) + (1-\beta_m)\nabla_{\mathbf{x}} \log q_{k+1}(\mathbf{x}|\mathbf{y}_{[k]})$$
$$= \beta_m \nabla_{\mathbf{x}} \log g_{k+1}(\mathbf{y}_{k+1}|\mathbf{x}) + \nabla_{\mathbf{x}} \log q_{k+1}(\mathbf{x}|\mathbf{y}_{[k]}).$$

Based on the construction of the intermediate distributions (2.12), when consecutive temperatures are sufficiently close, the target distribution $\pi_{k+1}^m(\cdot|\mathbf{y}_{[k+1]})$ and the initial distribution $\pi_{k+1}^{m-1}(\cdot|\mathbf{y}_{[k+1]})$ exhibit minimal discrepancy, facilitating rapid convergence of the Langevin diffusion (2.13). Through this annealing strategy, we effectively decompose the challenging posterior sampling problem (2.11) into a sequence of more tractable posterior sampling steps (2.13). Figure 3 presents a comparison between the original Langevin algorithm and

its annealed variant. Besides, this annealing procedure has been shown to enable effective sampling from multi-modal distributions (Wu and Xie, 2024).
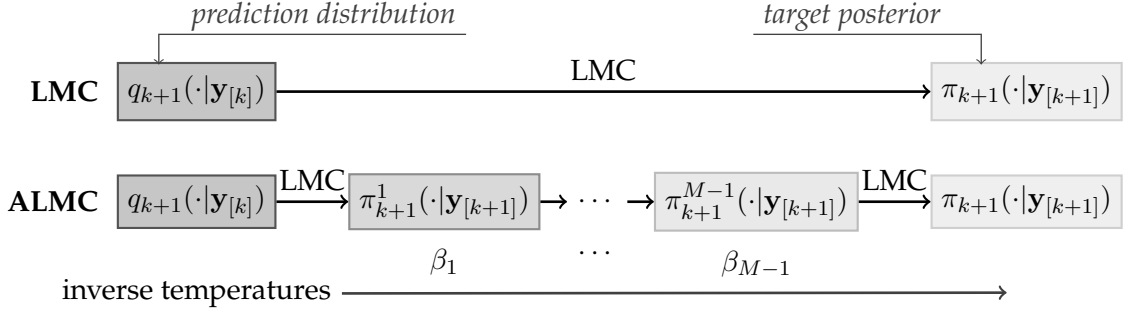

FIGURE 3. Schematic comparison of vanilla and annealed Langevin algorithms. (Top) The vanilla Langevin algorithm samples from the target posterior distribution, using the prediction distribution as initialization. (Bottom) The annealed Langevin algorithm employs a sequence of interpolations that smoothly transition from the prediction distribution to the target posterior distribution.

Since the Langevin diffusion (2.13) cannot be simulated analytically, we employ the Euler-Maruyama discretization to approximate it, yielding the following sampling scheme:

$$\widehat{\mathbf{Z}}_{(\ell+1)h}^m = \widehat{\mathbf{Z}}_{\ell h}^m + h\widehat{\mathbf{b}}_{k+1}^m(\widehat{\mathbf{Z}}_{\ell h}, \mathbf{y}_{[k+1]}) + \sqrt{2h}\boldsymbol{\xi}_\ell^m, \quad 0 \le \ell \le K-1,$$
(2.14)
$$\widehat{\mathbf{Z}}_0^1 \sim \widehat{q}_{k+1}(\cdot|\mathbf{y}_{[k]}), \quad \widehat{\mathbf{Z}}_0^m = \widehat{\mathbf{Z}}_{Kh}^{m-1}, \quad 2 \le m \le M,$$

where $h > 0$ is the step size, $(\boldsymbol{\xi}_\ell^m)_{m,\ell}$ is a sequence of independent standard Gaussian variables, and the drift term is a weighted sum of the gradient of log-likelihood and the estimated prediction score function (2.10)

(2.15) $\quad \widehat{\mathbf{b}}_{k+1}^m(\mathbf{x}, \mathbf{y}_{[k+1]}) = \beta_m \nabla_{\mathbf{x}} \log g_{k+1}(\mathbf{y}_{k+1}|\mathbf{x}) + \widehat{\mathbf{s}}_{k+1}(\mathbf{x}, \mathbf{y}_{[k]}) \approx \nabla_{\mathbf{x}} \log \pi_{k+1}^m(\mathbf{x}|\mathbf{y}_{[k+1]}).$

The complete procedure for the $(k+1)$-th update step is presented in Algorithm 1.

2.5. **Summary of the procedure.** Building upon the methods described in Sections 2.3 and 2.4, we can sample from the current posterior distribution $\pi_{k+1}(\cdot|\mathbf{y}_{[k+1]})$ given a particle approximation to the previous posterior distribution $\pi_k(\cdot|\mathbf{y}_{[k]})$.

To obtain a particle approximation to the initial posterior distribution $\pi_1(\cdot|\mathbf{y}_1)$, we apply Bayes' rule, yielding:

(2.16) $\qquad \nabla_{\mathbf{x}} \log \pi_1(\mathbf{x}|\mathbf{y}_1) = \nabla_{\mathbf{x}} \log g_1(\mathbf{y}_1|\mathbf{x}) + \nabla_{\mathbf{x}} \log p_{\mathbf{X}_1}(\mathbf{x}),$

where $q_1 := p_{\mathbf{X}_1}$ denotes the initial prior distribution. Thus, sampling from the initial posterior distribution $\pi_1(\cdot|\mathbf{y}_1)$ requires only an estimate of the score of the initial prior distribution $\nabla_{\mathbf{x}} \log q_1$. In practice, one typically has access to a set of samples drawn independently from $\widehat{q}_1$, an approximation of the initial prior q_1. Using these samples, we can estimate the initial prior score $\nabla_{\mathbf{x}} \log q_1$ through Gaussian smoothing and denoising score matching as shown in (2.10), which we denote as $\widehat{\mathbf{s}}_1$. The complete procedure for score-based sequential Langevin sampling is presented in Algorithm 2.

Remark 2.2 (Computational cost reduction). The implementation of Algorithm 2 requires learning a score network from predicted states at each time step, which introduces substantial computational overhead. However, we demonstrate that in practical applications, one can

---

Algorithm 1: Update by Annealed Langevin Monte Carlo (ALMC).

1 **Input:** Predicted samples $\underline{\mathbf{X}}_{k+1}^1, \ldots, \underline{\mathbf{X}}_{k+1}^n$, a prediction score estimator $\widehat{\mathbf{s}}_{k+1}(\cdot, \mathbf{y}_{[k]})$, the measurement likelihood $g_{k+1}(\mathbf{y}_{k+1}|\cdot)$.

2 **Output:** A particle approximation $\widehat{\mathbf{X}}_{k+1}^1, \ldots, \widehat{\mathbf{X}}_{k+1}^n$ to the posterior $\pi_{k+1}(\cdot|\mathbf{y}_{[k+1]})$.

3 Set inverse temperatures $0 \equiv \beta_0 < \beta_1 < \cdots < \beta_M \equiv 1$, and a step size $h > 0$.

4 Initialize the particles $\widehat{\mathbf{Z}}_0^{1,i} \leftarrow \underline{\mathbf{X}}_{k+1}^i$ for each $1 \le i \le n$.

5 **for** $m = 1, \ldots, M$ **do**

6   **for** $\ell = 0, \ldots, K-1$ **do**

7   Sample independent Gaussian noises $\boldsymbol{\xi}_\ell^{m,1}, \ldots, \boldsymbol{\xi}_\ell^{m,n} \sim^{\text{i.i.d.}} N(0, \mathbf{I}_d)$.

8   Compute the estimated posterior score
$$\widehat{\mathbf{b}}_{k+1}^m(\cdot, \mathbf{y}_{[k+1]}) \leftarrow \beta_m \nabla_{\mathbf{x}} \log g_{k+1}(\mathbf{y}_{k+1}|\cdot) + \widehat{\mathbf{s}}_{k+1}(\cdot, \mathbf{y}_{[k]}).$$

9   Update by the LMC, for $1 \le i \le n$,
$$\widehat{\mathbf{Z}}_{(\ell+1)h}^{m,i} \leftarrow \widehat{\mathbf{Z}}_{\ell h}^{m,i} + h\widehat{\mathbf{b}}_{k+1}^m(\widehat{\mathbf{Z}}_{\ell h}^{m,i}, \mathbf{y}_{[k+1]}) + \sqrt{2h}\boldsymbol{\xi}_\ell^{m,i}.$$

10   **end**

11   Initialize the particles for the next temperature $\widehat{\mathbf{Z}}_0^{m+1,i} \leftarrow \widehat{\mathbf{Z}}_{Kh}^{m,i}$ for $1 \le i \le n$.

12 **end**

13 $\widehat{\mathbf{X}}_{k+1}^i \leftarrow \widehat{\mathbf{Z}}_{Kh}^{M,i}$ for $1 \le i \le n$.

Algorithm 2: Score-based sequential Langevin sampling for data assimilation.

1 **Input:** The observations $(\mathbf{y}_k)_{k\in\mathbb{N}}$, the dynamics model $(\mathcal{F}_k)_{k\in\mathbb{N}}$, the measurement likelihood $\{g_k(\mathbf{y}_k|\cdot)\}_{k\in\mathbb{N}}$.

2 **Output:** A particle approximation $\widehat{\mathbf{X}}_{k+1}^1, \ldots, \widehat{\mathbf{X}}_{k+1}^n$ to the distribution $\pi_{k+1}(\cdot|\mathbf{y}_{[k+1]})$.

3 # Initial posterior sampling.

4 Choose a gauss for prior distribution $\widehat{q}_1$.

5 Sample from the gauss of prior distribution $\underline{\mathbf{X}}_1^1, \ldots, \underline{\mathbf{X}}_1^n \sim^{\text{i.i.d.}} \widehat{q}_1$.

6 Estimate the score from $\{\underline{\mathbf{X}}_1^i\}_{i=1}^n$ by score matching $\widehat{\mathbf{s}}_1$.

7 Sample from the posterior distribution $\widehat{\pi}_1(\cdot|\mathbf{y}_1)$ by the ALMC (Algorithm 1):
$$\widehat{\mathbf{X}}_1^1, \ldots, \widehat{\mathbf{X}}_1^n \leftarrow \text{ALMC}(\underline{\mathbf{X}}_1^1, \ldots, \underline{\mathbf{X}}_1^n, \widehat{\mathbf{s}}_1, g_1(\mathbf{y}_1|\cdot)).$$

8 # Recursive posterior sampling.

9 **for** $k = 1, 2, \ldots$ **do**

10   # Prediction step.

11   Run the dynamics model: $\underline{\mathbf{X}}_{k+1}^i \leftarrow \mathcal{F}_k(\widehat{\mathbf{X}}_k^i, \mathbf{V}_k^i)$ with $\mathbf{V}_k^i \sim p_{\mathbf{V}}$ for $1 \le i \le n$.

12   Estimate the prediction score from $\{\underline{\mathbf{X}}_{k+1}^i\}_{i=1}^n$ by score matching $\widehat{\mathbf{s}}_{k+1}(\cdot, \mathbf{y}_{[k]})$.

13   # Update step.

14   Sample from the posterior distribution $\pi_{k+1}(\cdot|\mathbf{y}_{[k+1]})$ by the ALMC (Algorithm 1):
$$\widehat{\mathbf{X}}_{k+1}^1, \ldots, \widehat{\mathbf{X}}_{k+1}^n \leftarrow \text{ALMC}(\underline{\mathbf{X}}_{k+1}^1, \ldots, \underline{\mathbf{X}}_{k+1}^n, \widehat{\mathbf{s}}_{k+1}(\cdot, \mathbf{y}_{[k]}), g_{k+1}(\mathbf{y}_{k+1}|\cdot)).$$

15 **end**

---

effectively fine-tune the score network using the current predicted states while initializing it with parameters obtained from the previous time step. This approach eliminates the need for complete network retraining with random initialization, thereby achieving significant computational efficiency.

3. Non-asymptotic Convergence Guarantees

In this section, we present a convergence analysis for the score-based sequential Langevin sampling (SSLS). Our theoretical analysis focuses on the core algorithm of the SSLS:

$$
\begin{aligned}
\widehat{\mathbf{Z}}_{(\ell+1)h} &= \widehat{\mathbf{Z}}_{\ell h} + h\widehat{\mathbf{b}}_{k+1}(\widehat{\mathbf{Z}}_{\ell h}, \mathbf{y}_{[k+1]}) + \sqrt{2h}\boldsymbol{\xi}_\ell, \quad 1 \le \ell \le K-1, \\
\widehat{\mathbf{Z}}_0 &\sim \pi_{k+1}^0(\cdot|\mathbf{y}_{[k+1]}),
\end{aligned}
$$

(3.1)

where $h > 0$ represents the time step, $(\boldsymbol{\xi}_\ell)_\ell$ is a sequence of independent standard Gaussian variables, and $\pi_{k+1}^0(\cdot|\mathbf{y}_{[k+1]})$ denotes the initial distribution at the $(k+1)$-th update step. While this initial distribution is typically selected as $\widehat{q}_{k+1}(\cdot|\mathbf{y}_{[k]})$, our analysis can generalize to any choice of initial distribution. The estimated posterior score takes the form:

$$
\widehat{\mathbf{b}}_{k+1}(\mathbf{x}, \mathbf{y}_{[k+1]}) = \nabla_{\mathbf{x}} \log g_{k+1}(\mathbf{y}_{k+1}|\mathbf{x}) + \widehat{\mathbf{s}}_{k+1}(\mathbf{x}, \mathbf{y}_{[k]}),
$$

(3.2)

where the prediction score $\widehat{\mathbf{s}}_{k+1}$ is estimated using score matching (2.10).

Through this analysis, we establish rigorous theoretical guarantees for data assimilation using SSLS and provide theoretical understandings for the benefits of the annealing strategy employed in Section 2.4.

3.1. Notations and assumptions.

Before proceeding with our analysis, we introduce some notations and assumptions. Let $\widehat{\pi}_{k+1}$ denote the law of $\widehat{\mathbf{Z}}_T$ with $T = Kh$, representing the SSLS estimate of the target posterior distribution. We denote $\varepsilon_{\mathrm{TV}}^k$ as the total variation distance between the target posterior distribution and its SSLS estimate:

$$
\varepsilon_{\mathrm{TV}}^k := \mathrm{TV}\left(\pi_k(\cdot|\mathbf{y}_{[k]}), \widehat{\pi}_k(\cdot|\mathbf{y}_{[k]})\right), \quad k \in \mathbb{N}.
$$

(3.3)

For a comprehensive list of notations used throughout this section, we refer readers to Appendix B.

Assumption 1 (Lipschitz score). For each $k \in \mathbb{N}$, the posterior score is λ-Lipschitz on $\mathbb{R}^d$, that is, for each $\mathbf{x}_1, \mathbf{x}_2 \in \mathbb{R}^d$,

$$
\|\nabla_{\mathbf{x}} \log \pi_{k+1}(\mathbf{x}_1|\mathbf{y}_{[k+1]}) - \nabla_{\mathbf{x}} \log \pi_{k+1}(\mathbf{x}_2|\mathbf{y}_{[k+1]})\|_2 \le \lambda\|\mathbf{x}_1 - \mathbf{x}_2\|_2.
$$

Assumption 1 is a fundamental requirement in the convergence analysis of Langevin-type sampling methods (Chewi et al., 2024, Chewi, 2024, Lee et al., 2022). This assumption ensures the existence and uniqueness of strong solution to the Langevin diffusion (2.11). Moreover, it plays a crucial role in analyzing the discretization errors that arise in Langevin sampling (Chewi et al., 2024).

Our analysis relies heavily on certain isoperimetric properties of the target posterior distribution, which we formalize in the following assumption.

Assumption 2 (Log-Sobolev inequality). For each $k \in \mathbb{N}$, the posterior distribution satisfies a log-Sobolev inequality with constant C_{LSI}, that is, for each function $f \in C_0^\infty(\mathbb{R}^d)$,

$$
\mathrm{Ent}(f^2) \le 2C_{\mathrm{LSI}}\mathbb{E}\left[\|\nabla f\|_2^2\right],
$$

where the entropy is defined as $\mathrm{Ent}(g) = \mathbb{E}[g \log g] - \mathbb{E}[g] \log \mathbb{E}[g]$, and the expectation is taken with respect to the posterior distribution $\pi_{k+1}(\cdot|\mathbf{y}_{[k+1]})$.

Assumption 2 is crucial for establishing the convergence analysis for both the Langevin diffusion and its discretized counterpart, Langevin sampling (Chewi et al., 2024, Lee et al., 2022, Tang and Yang, 2024). The Gaussian distribution serves as a canonical example satisfying Assumption 2. Consequently, this assumption holds in linear data assimilation

problems with Gaussian prior and likelihood – precisely the setting where Kalman filtering is optimal. This connection implies that SSLS maintains effectiveness in scenarios where Kalman filtering succeeds. More generally, the class of strongly log-concave distributions satisfies Assumption 2 (Chewi, 2024), extending the applicability of our results beyond the Gaussian case.

Assumption 3 (Boundedness and condition number). For each $k \in \mathbb{N}$,

   (i) there exists $B \geq 1$ such that $\rho_k(\mathbf{x}|\mathbf{x}_k), \|\nabla_{\mathbf{x}}\rho_k(\mathbf{x}|\mathbf{x}_k)\|_{\infty} \leq B$ for $\mathbf{x} \in \mathbb{R}^d$,
  (ii) there exists $D \geq 1$ such that $q_{k+1}(\mathbf{x}|\mathbf{y}_{[k]}) \geq D^{-1}$ for $\mathbf{x} \in \Omega_{k+1} := \operatorname{supp}(q_{k+1}(\cdot|\mathbf{y}_{[k]}))$,
 (iii) $q_1(\mathbf{x}), \|\nabla_{\mathbf{x}}q_1(\mathbf{x})\|_{\infty} \leq B$ and $q_1(\mathbf{x}) \geq D^{-1}$ for $\mathbf{x} \in \Omega_1 := \operatorname{supp}(q_1)$, and
 (iv) there exists $\kappa > 0$ such that

$$(3.4) \qquad \frac{\sup_{\mathbf{x}} g_1(\mathbf{y}_1|\mathbf{x})}{\int g_1(\mathbf{y}_1|\mathbf{x})q_1(\mathbf{x})\,\mathrm{d}\mathbf{x}}, \frac{\sup_{\mathbf{x}} g_{k+1}(\mathbf{y}_{k+1}|\mathbf{x})}{\int g_{k+1}(\mathbf{y}_{k+1}|\mathbf{x})q_{k+1}(\mathbf{x}|\mathbf{y}_{[k]})\,\mathrm{d}\mathbf{x}} \leq \kappa.$$

Assumption 3 (i) to (iii) establish essential regularity conditions for the state transition density, prediction density, measurement likelihood, and initial prior score. The upper and lower boundedness of these densities is crucial for controlling both the score estimation error and the error propagated from the prior distribution. This importance of density boundedness is well-documented in the statistical literature, as highlighted by Tsybakov (2009), where distributions lacking such boundedness properties can exhibit arbitrarily poor statistical properties.

Remark 3.1 (Condition number). Assumption 3 (iv) introduces a condition number κ, which, as noted by Purohit et al. (2024), quantifies the inherent challenges in the posterior sampling. To illustrate this concept, consider the $(k+1)$-th step. When the likelihood function $g_{k+1}(\mathbf{y}_{k+1}|\cdot)$ primarily concentrates on the support Ω_{k+1} of the prediction distribution $q_{k+1}(\cdot|\mathbf{y}_{[k]})$, the denominator in (3.4) remains sufficiently bounded away from zero, resulting in a moderate value of κ. Conversely, if the likelihood $g_{k+1}(\mathbf{y}_{k+1}|\cdot)$ concentrates on a region with low prediction probability and vanishes elsewhere, the denominator in (3.4) approaches zero, yielding a large condition number and indicating significant ill-posedness. As demonstrated in Theorem 3.2, the error of the posterior sampling grows with this condition number.

We next introduce a "black-box" assumption on score matching (2.10).

Assumption 4 (Error of score matching). There exists a score matching tolerance $\Delta \in (0, 1)$ such that

$$\mathbb{E}_{\underline{\mathbf{X}}_1}\big[\|\nabla_{\mathbf{x}}\log\widehat{q}_1(\underline{\mathbf{X}}_1) - \widehat{\mathbf{s}}_1(\underline{\mathbf{X}}_1)\|_2^2\big] \leq \Delta^2,$$

$$\mathbb{E}_{\underline{\mathbf{X}}_{k+1}}\big[\|\nabla_{\mathbf{x}}\log\widehat{q}_{k+1}(\underline{\mathbf{X}}_{k+1}|\mathbf{y}_{[k]}) - \widehat{\mathbf{s}}_{k+1}(\underline{\mathbf{X}}_{k+1}, \mathbf{y}_{[k]})\|_2^2\big] \leq \Delta^2,$$

for each $k \in \mathbb{N}$. Here the expectation $\mathbb{E}_{\underline{\mathbf{X}}_1}[\cdot]$ is taken with respect to $\underline{\mathbf{X}}_1 \sim \widehat{q}_1$, and the expectation $\mathbb{E}_{\underline{\mathbf{X}}_{k+1}}[\cdot]$ is taken with respect to $\underline{\mathbf{X}}_{k+1} \sim \widehat{q}_{k+1}(\cdot|\mathbf{y}_{[k]})$.

Assumption 4 requires the L^2-error of prediction score estimator $\widehat{\mathbf{s}}_{k+1}$ (2.10) to be sufficiently small, where the error is measured with respect to the approximated prediction distribution $\widehat{q}_{k+1}(\cdot|\mathbf{y}_{[k]})$. While this assumption could be substituted with explicit score matching bounds, we maintain this formulation for clarity of presentation. Specifically, some standard techniques of non-parametric regression using deep neural networks (Schmidt-Hieber, 2020, Kohler and Langer, 2021, Jiao et al., 2023) demonstrates that

$$\mathbb{E}_{\underline{\mathbf{X}}_{k+1}}\big[\|\nabla_{\mathbf{x}}\log\widehat{q}_{k+1}(\underline{\mathbf{X}}_{k+1}|\mathbf{y}_{[k]}) - \widehat{\mathbf{s}}_{k+1}(\underline{\mathbf{X}}_{k+1}, \mathbf{y}_{[k]})\|_2^2\big] \to 0$$

with high probability, as the number of samples n approaches infinity and the smoothing level $\sigma > 0$ in (2.9) converges to zero. A complete proof of this convergence result can be found in Tang and Yang (2024, Theorem 1).

3.2. **Convergence analysis for posterior sampling.** Our main theoretical result for posterior sampling is stated as the following theorem.

Theorem 3.2 (Posterior sampling). *Suppose Assumptions 1, 2, 3, and 4 hold. Then for each $k \in \mathbb{N}$ and each terminal time $T = Kh$,*

$$
(\varepsilon_{\mathrm{TV}}^{k+1})^2 \lesssim \underbrace{\exp\Big(-\frac{T}{5C_{\mathrm{LSI}}}\Big)\eta_\chi^2}_{\text{convergence of LD}} + \underbrace{dC_{\mathrm{LSI}}\lambda^2 h}_{\text{discretization error}} + \underbrace{\sqrt{\kappa B^3 D^3}(T + C_{\mathrm{LSI}}\eta_\chi)\Delta}_{\text{score estimation error}} + \underbrace{B^4 D^4 T(\varepsilon_{\mathrm{TV}}^k)^2}_{\text{prior error}},
$$

where the step size h and the initial distribution $\pi_k^0(\cdot|\mathbf{y}_{[k]})$ satisfies

$$
h \lesssim \frac{1}{dC_{\mathrm{LSI}}\lambda^2}, \quad \chi^2\big(\pi_{k+1}^0(\cdot|\mathbf{y}_{[k+1]})\|\pi_{k+1}(\cdot|\mathbf{y}_{[k+1]})\big) \le \eta_\chi^2.
$$

Error decomposition. Theorem 3.2 decomposes the total variation error into four fundamental components: the convergence of Langevin diffusion, the discretization error, the score estimation error, and the prior error.

(i) The error of the Langevin diffusion (2.11) exhibits exponential convergence to zero as the terminal time T increases (Vempala and Wibisono, 2019, Chewi et al., 2024).
(ii) The discretization error, arising from the Euler-Maruyama approximation (3.1), converges linearly with respect to the step size h.
(iii) The score estimation error decreases as the score matching tolerance Δ in Assumption 4 tends to zero.
(iv) The prior error stems from inaccuracies in the prior distribution and is governed by the error $\varepsilon_{\mathrm{TV}}^k$ from the previous posterior distribution estimation.

Early-stopping. The first term in Theorem 3.2 diminishes with increasing terminal time T. However, both the score estimation error and the prior error grow with T, establishing a fundamental trade-off in the sampling error decomposition. This trade-off necessitates early-stopping in score-based Langevin sampling, as noted by Lee et al. (2022). Corollary 3.3 derives the optimal number of iterations based on this trade-off.

The following corollary provides a theoretical guidance for selecting hyper-parameters in the score-based Langevin sampling, as well as outlines its computational complexity.

Corollary 3.3. *Suppose Assumptions 1, 2, 3, and 4 hold. Then for each $k \in \mathbb{N}$ and error tolerance $\varepsilon \in (0,1)$,*

$$
(\varepsilon_{\mathrm{TV}}^{k+1})^2 \lesssim C_{\mathrm{LSI}}B^4 D^4 \log\Big(\frac{\eta_\chi^2}{\varepsilon^2}\Big)(\varepsilon_{\mathrm{TV}}^k)^2 + \varepsilon^2,
$$

where the step size h, the number of the Langevin iterations K, and the score matching error Δ satisfy:

$$
h = \Theta\Big(\frac{\varepsilon^2}{dC_{\mathrm{LSI}}\lambda^2}\Big), \quad K = \Theta\Big(\frac{d\lambda^2 C_{\mathrm{LSI}}^2}{\varepsilon^2}\log\Big(\frac{\eta_\chi^2}{\varepsilon^2}\Big)\Big),
$$

$$
\Delta = \Theta\Big(\frac{\varepsilon^2}{\sqrt{\kappa B^3 D^3}C_{\mathrm{LSI}}}\frac{1}{\log(\varepsilon^{-2}\eta_\chi^2) + \eta_\chi}\Big).
$$

Warm-start. In Theorem 3.2 and Corollary 3.3, a warm-start condition in terms of χ^2-divergence is essential, requiring that the initial distribution remains sufficiently close to the target posterior distribution:

$$(3.5) \qquad \chi^2\big(\pi_{k+1}^0(\cdot|\mathbf{y}_{[k+1]}) \| \pi_{k+1}(\cdot|\mathbf{y}_{[k+1]})\big) \le \eta_\chi^2.$$

This warm-start condition (3.5) influences both the convergence of Langevin diffusion and the score estimation error in Theorem 3.2. Regarding the score estimation, a critical observation is that the score estimator $\widehat{s}_{k+1}(\cdot, \mathbf{y}_{[k+1]})$ (2.10) approximates the prediction score in the L^2-norm (Assumption 4), where the L^2-error is measured with respect to the approximated prediction distribution $\widehat{q}_{k+1}(\cdot|\mathbf{y}_{[k]})$ (2.7). However, the Girsanov theorem (Chen et al., 2023) indicates that the score estimation error is bounded by the L^2-error of the score with respect to the law of Langevin sampling using the exact score. This discrepancy necessitates the warm-start condition in χ^2-divergence, as it ensures the out-of-distribution generalization of the score estimator from the approximated prediction distribution to the law of Langevin sampling using the exact score (Lee et al., 2022, Tang and Yang, 2024).

3.3. **Discussions on annealing.** In this subsection, we demonstrate theoretical advantages of annealing strategy introduced in Section 2.4.

Theorem 3.2 and Corollary 3.3 reveal two critical factors affecting the posterior sampling error: the condition number and the warm-start condition. Specifically, the score matching tolerance Δ decreases polynomially with both the condition number and the initial χ^2-divergence. Consequently, addressing the challenge posed by large condition numbers and substantial initial χ^2-divergence necessitates the use of larger deep neural networks and increased ensemble size, substantially raising computational costs.

We next demonstrate how the annealing strategy introduced in Section 2.4 effectively reduces the condition number and ensures the warm-start condition is satisfied.

Reduction of condition number. According to Theorem 3.2, the error of score-based Langevin sampling depends critically on the quantity (3.4)

$$\frac{\sup_\mathbf{x} g_{k+1}(\mathbf{y}_{k+1}|\mathbf{x})}{\int g_{k+1}(\mathbf{y}_{k+1}|\mathbf{x}) q_{k+1}(\mathbf{x}|\mathbf{y}_{[k]}) \, \mathrm{d}\mathbf{x}}.$$

This factor can become arbitrarily large in highly ill-posed problems, as discussed below Assumption 3. In contrast, for the annealed Langevin sampling (2.13) at temperature β_m, the corresponding factor satisfies:

$$\frac{\sup_\mathbf{x} g_{k+1}^{\beta_m - \beta_{m-1}}(\mathbf{y}_{k+1}|\mathbf{x})}{\int g_{k+1}^{\beta_m - \beta_{m-1}}(\mathbf{y}_{k+1}|\mathbf{x}) \pi_{k+1}^{m-1}(\mathbf{x}|\mathbf{y}_{[k+1]}) \, \mathrm{d}\mathbf{x}}$$
$$= \sup_\mathbf{x} g_{k+1}^{\beta_m - \beta_{m-1}}(\mathbf{y}_{k+1}|\mathbf{x}) \frac{\int g_{k+1}^{\beta_{m-1}}(\mathbf{y}_{k+1}|\mathbf{x}) q_{k+1}^{1-\beta_{m-1}}(\mathbf{x}|\mathbf{y}_{[k]}) \, \mathrm{d}\mathbf{x}}{\int g_{k+1}^{\beta_m}(\mathbf{y}_{k+1}|\mathbf{x}) q_{k+1}^{1-\beta_{m-1}}(\mathbf{x}|\mathbf{y}_{[k]}) \, \mathrm{d}\mathbf{x}} \approx 1,$$

when $\beta_m - \beta_{m-1}$ approaches zero. Thus, annealing can substantially reduce the condition number through a sufficiently dense annealing temperature schedule.

Warm-start condition. In Section 2.4, the score-based Langevin sampling initializes from the prediction distribution $q_{k+1}(\cdot|\mathbf{y}_{[k]})$. The χ^2-divergence between this initial distribution and the target posterior distribution $\pi_{k+1}(\cdot|\mathbf{y}_{[k+1]})$ can be arbitrarily large. In contrast, for the annealed Langevin sampling (2.13) at temperature β_m, the sampling process initializes from $\pi_{k+1}^{m-1}(\cdot|\mathbf{y}_{[k+1]})$, which remains close to the target distribution $\pi_{k+1}^m(\cdot|\mathbf{y}_{[k+1]})$ given that β_{m-1}

approaches β_m. Consequently, annealing strategy reduces the initial χ^2-divergence, thereby decreasing the posterior sampling error as demonstrated in Theorem 3.2

3.4. **Convergence analysis for assimilation.** Building upon the convergence results for score-based Langevin sampling in posterior estimation established in the previous subsection, we now analyze the convergence properties of score-based sequential Langevin sampling (SSLS). Let q_1 be the ground-truth prior distribution of the initial state in the assimilation process, and $\widehat{q}_1$ be the prior distribution employed in SSLS. The discrepancy between these initial distributions can be quantified by the following metric:

$$\varepsilon_{\text{init}} := \|\nabla_{\mathbf{x}} \log q_1 - \nabla_{\mathbf{x}} \log \widehat{q}_1\|_{L^\infty(\mathbb{R}^d)}.$$

The convergence behavior of the assimilation process under SSLS can be characterized by the following theorem.

Theorem 3.4 (Assimilation). *Suppose Assumptions 1, 2, 3, and 4 hold. Then for each time step $k \in \mathbb{N}$ and error tolerance $\varepsilon \in (0,1)$,*

$$\varepsilon_{\text{TV}}^{k+1} \leq \widetilde{\mathcal{O}}(\varepsilon_{\text{init}} + \varepsilon),$$

where the $\widetilde{\mathcal{O}}$ notation omits logarithmic factors of $\varepsilon_{\text{init}}$ and ε, and the constant behind the $\widetilde{\mathcal{O}}$ notation is independent of $\varepsilon_{\text{init}}$ and ε. Moreover, the step size h, the number of the Langevin iterations K and the score matching error Δ satisfy:

$$h = \Theta\Big(\frac{\varepsilon^2}{dC_{\text{LSI}}\lambda^2}\Big), \quad K = \Theta\Big(\frac{d\lambda^2 C_{\text{LSI}}^2}{\varepsilon^2} \log\Big(\frac{\eta_\chi^2}{\varepsilon^2}\Big)\Big),$$

$$\Delta = \Theta\Big(\frac{\varepsilon^2}{\sqrt{\kappa B^3 D^3}C_{\text{LSI}}} \frac{1}{\log(\varepsilon^{-2}\eta_\chi^2) + \eta_\chi}\Big).$$

Consistency. Theorem 3.4 establishes that SSLS serves as a consistent estimator of the posterior distribution when there is no initial distribution shift. As discussed by Remark 3.1, the score matching error Δ converges to zero as the ensemble size grows to infinity. Therefore, Theorem 3.4 reveals that the SSLS error asymptotically vanishes when both the ensemble size and the number of iterations approach infinity simultaneously. This stands in contrast to Kalman filter and diffusion-based methods examined in Section A.1, which exhibit inconsistency in assimilation scenarios where linear and Gaussian assumptions do not hold.

4. Numerical Experiments

In this section, we demonstrate the effectiveness of score-based sequential Langevin sampling (SSLS) through numerical experiments.

(1) In Section 4.1, we examine the assimilation of Langevin diffusion with a double-well potential. This investigation compares SSLS against the auxiliary particle filter (APF) and ensemble Kalman filter (EnKF) in scenarios featuring state mutations and model nonlinearity.

(2) In Section 4.2, we apply SSLS to the assimilation of Kolmogorov flow under sparse and partial observations. We highlight the crucial role of the prior score through comparisons with standard maximum likelihood estimation (MLE) and demonstrate methods for quantifying the uncertainty of states estimated by SSLS.

4.1. **The double-well potential.** A classic problem in molecular dynamics involves a one-dimensional Langevin diffusion with a double-well potential, governed by the nonlinear SDE:

$$\mathrm{d}X_t = -\nabla U(X_t)\,\mathrm{d}t + \beta\,\mathrm{d}B_t, \tag{4.1}$$

where $U(x) := x^4 - 2x^2$ is a double-well potential, $\beta > 0$ is the temperature parameter, and $(B_t)_{t\geq 0}$ denotes the standard Brownian motion. In this experiment, we focus on the dynamics model defined as the Euler-Maruyama discretization of (4.1)

$$X_{k+1} = X_k - \delta t \nabla U(X_k) + \beta\sqrt{\delta t}V_k, \tag{4.2}$$

where $\delta t > 0$ and $V_k \sim N(0,1)$. As we will demonstrate, this dynamic model exhibits state mutations that introduce ill-posedness to the assimilation process. This experiment is designed to showcase SSLS's effectiveness in handling such mutations.

State mutations in dynamics model. Since the dynamics model (4.2) has similar behaviors as its time-continuous counterpart (4.1) when δt is sufficiently small, we illustrate state mutations in (4.1) for the sake of simplicity. The dynamics model (4.1) exhibits two local stable states at $x = -1$ and $x = 1$. A particle initialized at any position is drawn toward one of these stable states by the drift term in (4.1), while the diffusion term models thermal collisions with the environment, introducing stochasticity into the particle's trajectory. At low temperatures (small β), the particle typically remains confined near one stable state, making only rare transitions to the other potential well. At higher temperatures (large β), the particle transitions more frequently between the two potential wells, leading to state mutations.

When state mutations occur, the true state can deviate significantly from the support of the prediction distribution. Such deviation results in an extremely large condition number (3.4), indicating severe ill-posedness in the posterior sampling, as discussed by Remark 3.1.

Reference states generation. To evaluate the assimilation methods, we simulate the dynamics model (4.2) with temperature $\beta = 0.3$ and time step $\delta t = 0.1$ to generate true states. To effectively demonstrate how different assimilation methods respond to state mutations, we manually induce mutations by switching states from X_k to $-X_k$ every 20 time steps.

Baseline. For comparison, we evaluate SSLS alongside two widely-used assimilation techniques: the auxiliary particle filter (APF) (Pitt and Shephard, 1999) and the ensemble Kalman filter (Houtekamer and Mitchell, 1998). In SSLS, prediction scores at each assimilation step are learned from 1000 particles. For fair comparison, we maintain the same ensemble size of 1000 for both APF and EnKF.

4.1.1. *Linear measurement model.* We first consider a linear measurement model with Gaussian additive noise

$$Y_k = X_k + \sigma_{\mathrm{obs}}W_k, \tag{4.3}$$

where $k \in \mathbb{N}$ and $W_k \sim N(0,1)$. Figure 4 plots the results of assimilation for the state-space model (4.2) and (4.3). The observation noise level is set as $\sigma_{\mathrm{obs}} = 0.1$.

As shown in Figure 4, all assimilation methods provide estimates that closely track the reference states before state mutations occur. However, APF exhibits a notable delay following state mutations. This delay arises because APF approximates the prediction distribution using a weighted particle set. Due to state mutations, particles sampled from the prediction distribution may be far from the observation, resulting in small assigned weights. These particles thus contribute minimally to the posterior distribution approximation (Särkkä and
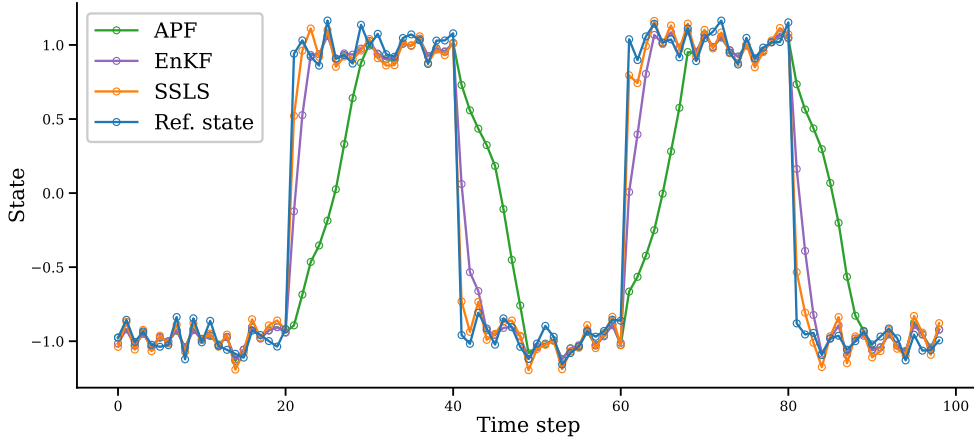
FIGURE 4. Results of assimilation for Langevin diffusion with a double-well potential (4.2) with a linear measurement model (4.3). The ensemble mean of SSLS, APF, and EnKF at each time steps are shown in the figure.

Svensson, 2023, Chapter 11.6). This phenomenon, known as particle degeneracy, persists even though APF offers some improvement over the standard PF.

In contrast, SSLS and EnKF avoid reliance on particle approximations. SSLS employs a score network, while EnKF uses a Gaussian distribution to approximate the prediction distribution. Both methods can generalize to regions near the observation where predicted particles may be absent, enabling them to respond more rapidly to state mutations.

4.1.2. *Nonlinear measurement model.* As illustrated in Figure 4, SSLS outperforms EnKF due to the nonlinearity of dynamics model (4.2). This advantage arises because EnKF only captures linear components while disregarding higher-order structures of the dynamics model. To further demonstrate the advantages of SSLS over EnKF in nonlinear settings, we consider a nonlinear measurement model:

$$(4.4) \qquad Y_k = \exp(X_k - \gamma_k) + \sigma_{\text{obs}} W_k,$$

where $\gamma_k = 0.6$, $\sigma_{\text{obs}} = 0.2$, and $W_k \sim N(0,1)$.

Figure 5 presents the numerical results, revealing that EnKF fails to effectively assimilate observation data in the fully nonlinear state-space model (4.2) and (4.4). In contrast, SSLS and APF maintain their performance despite the nonlinear measurement model. These results establish SSLS as a robust method for handling nonlinear scenarios, even under full nonlinearity.

4.2. **Kolmogorov flow.** In this example, we consider the assimilation of a Kolmogorov flow, which arises in atmospherical sciences and fluid dynamics (Cotter et al., 2009, Rozet and Louppe, 2023a). Kolmogorov flow is a viscous and incompressible fluid flow governed by the Navier-Stokes (NS) equation on the two-dimensional torus $[0, 2\pi]^2$,

$$(4.5) \qquad \begin{cases} \partial_t \mathbf{u} = -(\mathbf{u} \cdot \nabla)\mathbf{u} + \dfrac{1}{\text{Re}} \nabla^2 \mathbf{u} - \dfrac{1}{\rho} \nabla p + \mathbf{F}, \\[2mm] 0 = \nabla \cdot \mathbf{u}, \end{cases}$$
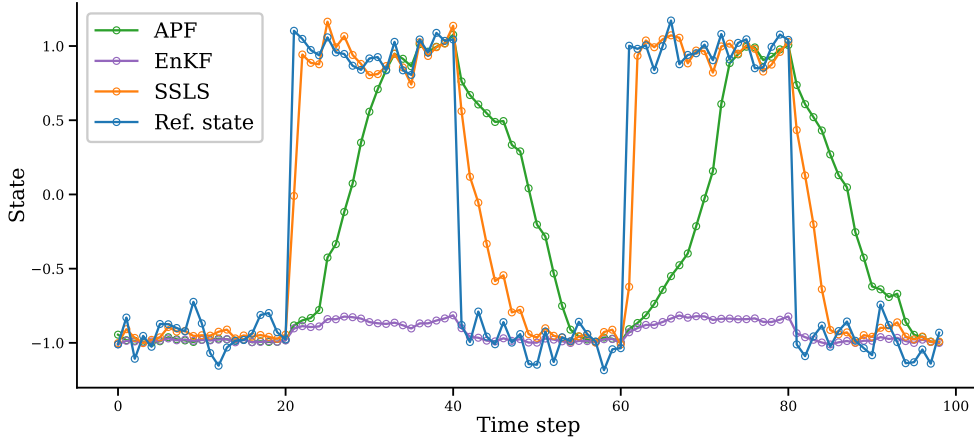
FIGURE 5. Results of assimilation for Langevin diffusion with a double-well potential (4.2) with a nonlinear measurement model (4.4). The ensemble mean of SSLS, APF, and EnKF at each time steps are shown in the figure.

where $\mathbf{u}$ represents the velocity field, Re is the Reynolds number, ρ denotes the fluid density, p is the pressure field, and $\mathbf{F}$ is the external forcing. This example uses the periodic boundary conditions, a large Reynolds number $\mathrm{Re} = 10^3$, a constant density $\rho \equiv 1$ and an external forcing $\mathbf{F}$ corresponding to Kolmogorov forcing with linear damping. Our objective is to track a velocity field describing the solutions to the NS equation (4.5) with unknown initial condition.

Reference states generation. Let $\mathbf{u}_0$ be a initial random state sampled from a Gaussian random field. The NS equation (4.5) is evolved from this initial state $\mathbf{u}_0$. Following a warm-up period of $T_0 = 10$, reference states are downsampled from the trajectory between $T_0 = 10$ and $T = 20$ with a spatial resolution of 128×128 and a temporal resolution of $\Delta t = 0.2$. Here the NS equation (4.5) is solved using the `jax-cfd` package (Kochkov et al., 2021).

Initial prior distribution shift. The SSLS assimilation process begins with a set of independent random realizations of $\mathbf{u}_0$. A crucial consideration is that the initial reference state $\mathbf{u}_{T_0}$ follows a distribution that differs from the initial distribution employed in SSLS. Such initial distributional shifts are prevalent in practical applications, where the true distribution of the initial state often remains unknown. Therefore, successful assimilation under these distributional shifts represents both a critical requirement and a significant challenge in the field.

4.2.1. *Assimilation with sparse or partial observation data.* This subsection demonstrates the effectiveness of SSLS under various sparse and partial observation scenarios through three distinct tasks: (i) super-resolution, (ii) sparse reconstruction, and (iii) box reconstruction. For the super-resolution task, observations are generated by applying average pooling to the reference states, followed by the addition of pointwise Gaussian noise. The sparse reconstruction task employs a measurement model combining uniform-stride downsampling with Gaussian perturbation. In the box reconstruction task, measurements within a specified

domain are unavailable, while measurements outside this domain are perturbed by Gaussian noise.
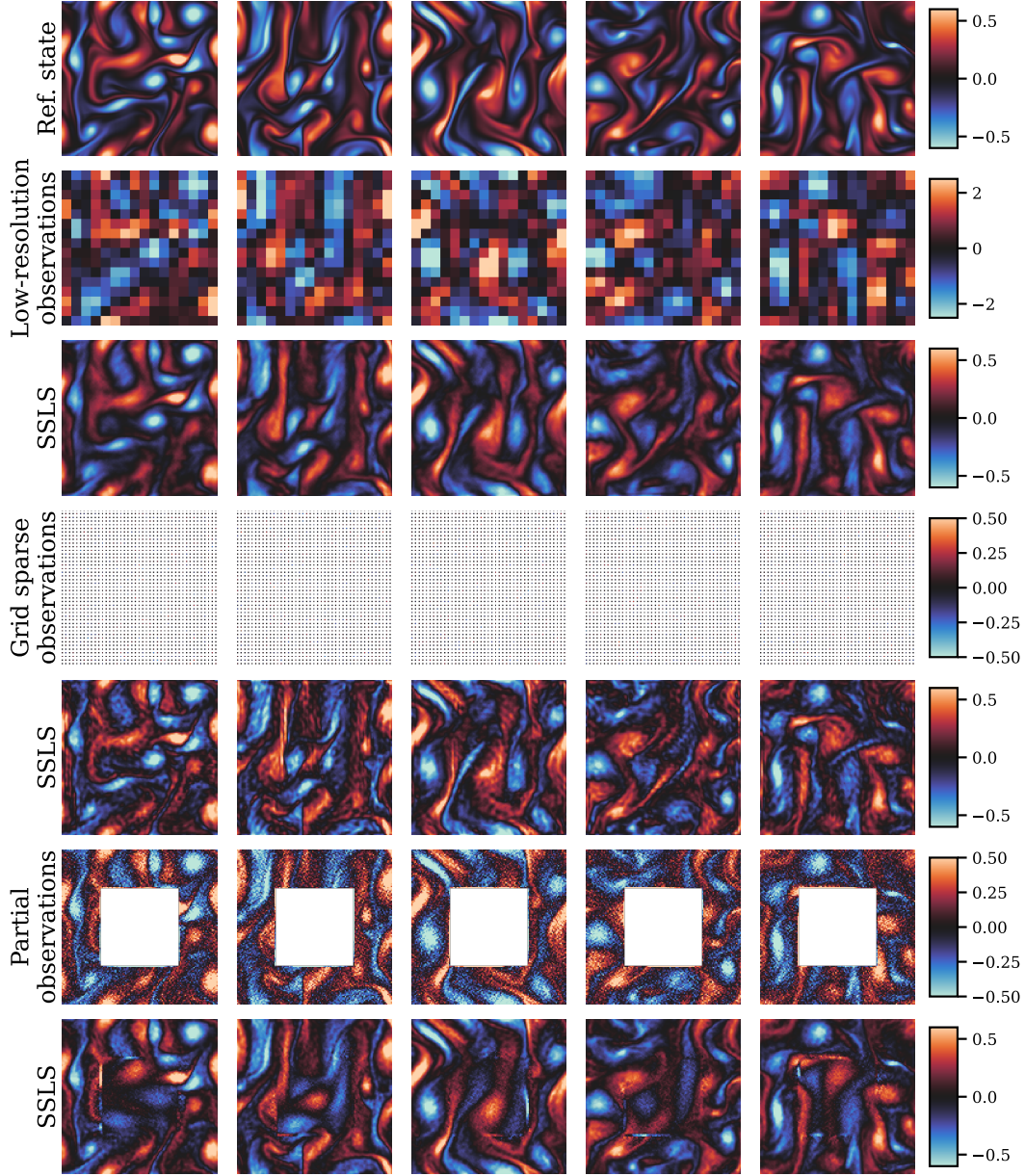

FIGURE 6. Results of assimilation for Kolmogorov flow (4.5) with different measurement models. Each column corresponds to distinct time steps (states are plotted for every 10 time steps). The first row displays the reference state. (i) Super-resolution: The 2nd and 3rd rows display the noisy observations with 8x average pooling and the corresponding SSLS estimations, respectively. (ii) Sparse reconstruction: The 4th and 5th rows show the noisy observations with a uniform mask and the corresponding SSLS estimations, respectively. (iii) Box reconstruction: The 6th and 7th rows demonstrate the noisy observations with a centering square mask and the corresponding SSLS estimations, respectively.

Figure 6 presents the experimental results of SSLS under these measurement models, visualized through the vorticity field $\omega = \nabla \times \mathbf{u}$. The results demonstrate the exceptional performance of SSLS across all three tasks:

(i) In the super-resolution task, while the observation data lacks most micro-structures present in the reference vorticity field, SSLS successfully reconstructs the majority of these intricate details.

(ii) The sparse reconstruction results showcase SSLS's remarkable capability to reconstruct the field even when 88.72% of observation points are masked. This robustness to sparse observations is particularly valuable in applications where measurement acquisition is costly or limited.

(iii) In the box reconstruction task, SSLS demonstrates impressive performance by accurately reconstructing the field even within the completely masked region where no observations are available.

Notably, across aforementioned tasks, the estimated states exhibit significant deviations from the observation data, indicating the substantial influence of prediction information on the assimilation process. The effectiveness of this prediction information will be further examined through ablation studies in subsequent experiments. Furthermore, a mathematical analysis of this efficiency under sparse or partial measurements is presented in Section 4.2.2.

4.2.2. *Ablation study: influence of the prediction score.* Previous experiments demonstrate that the estimated states closely align with reference states, even under significant observational noise and occlusion. This remarkable performance underscores the fundamental importance of prior information encoded in the prediction score. We now investigate the specific contribution of the prediction score in SSLS through comprehensive comparisons with score-free methods.

Baseline. To evaluate the impact of the prediction score in SSLS, we employ two comparative methods:

(i) Langevin sampling without prediction score, and

(ii) ensemble maximum likelihood estimation (MLE).

Method (i) employs Langevin sampling where the drift term consists solely of the log-likelihood gradient, with the prediction score component removed. This formulation can be interpreted as a noise-augmented gradient method for maximum likelihood estimation. Method (ii) represents a pure gradient-based MLE approach, obtained by additionally removing the Gaussian noise term from the Langevin sampling formulation.

To ensure fair comparison, both methods are initialized using the approximated prediction distribution (2.7), consistent with the SSLS framework. Consequently, although these methods do not explicitly incorporate the prediction score, their state estimates inherently reflect the influence of historical observations through their initialization.

Influence of the prediction score. As illustrated in Figure 7, both Langevin sampling without the prediction score (method (i)) and ensemble MLE (method (ii)) produce notably non-smooth state estimations. This phenomenon has a clear mathematical explanation: the log-likelihood gradient exists only at locations with available measurements and vanishes elsewhere. This gradient absence presents a fundamental challenge in assimilation with sparse or partial measurements. In such scenarios, methods (i) and (ii) can only update in measured locations, while unmeasured locations either experience random perturbations
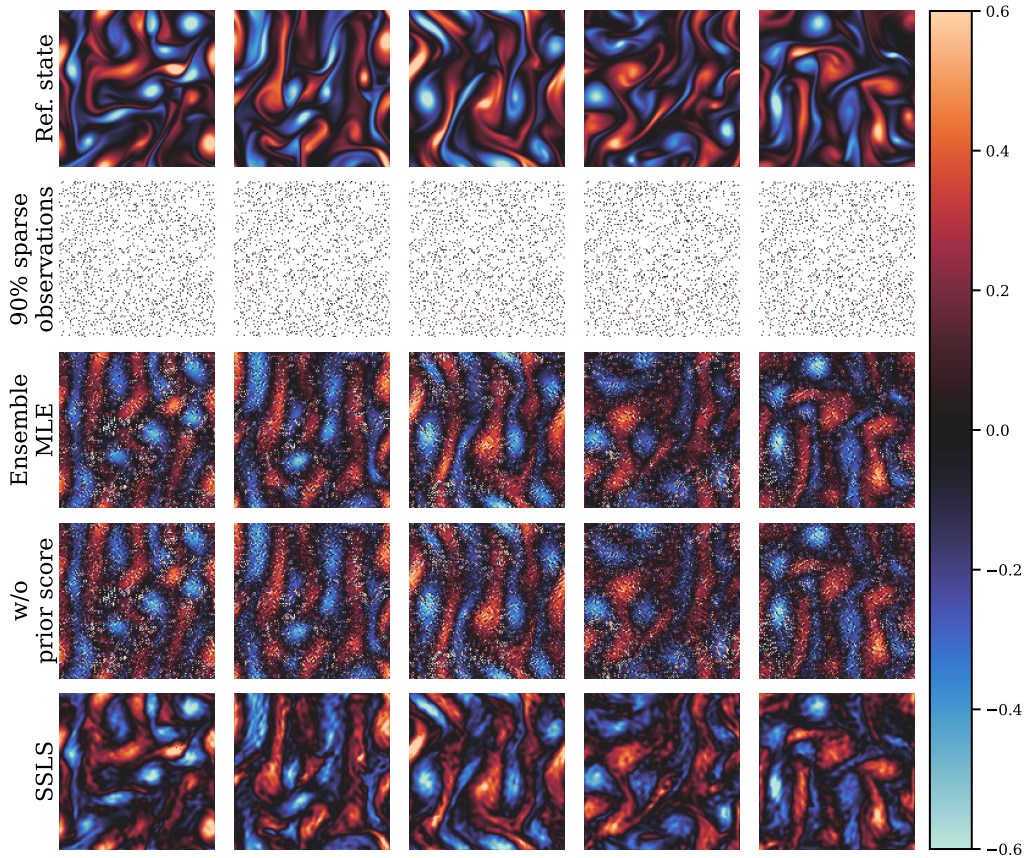
FIGURE 7. Comparison of results of SSLS and methods without prediction score. From top to bottom: the reference state, observations, estimations of the ensemble MLE, estimations of Langevin sampling without the prediction score, and estimations of SSLS. Here the noise level is set as $\sigma_{\mathrm{obs}} = 0.3$ and let 90% points be randomly masked.

(method (i)) or remain unchanged (method (ii)). This spatially inconsistent updating mechanism leads to discontinuous and non-smooth state estimations in both methods.

In contrast, SSLS produces estimations that exhibit strong alignment with the reference states, attributed to the prediction score's incorporation of dynamics-based spatiotemporal correlations. This score term enables meaningful updates even at unmeasured locations by leveraging the physical constraints and dynamics embedded within it. The score effectively bridges information gaps between measured and unmeasured regions, ensuring appropriate smoothness and physical consistency throughout the domain. This capacity to maintain physical coherence while assimilating sparse measurements allows SSLS to achieve superior reconstruction quality, particularly in regions where observational data is limited or absent.

4.2.3. *Uncertainty quantification in assimilation.* The preceding experiments demonstrate that the states estimated by the SSLS closely align with reference states, even when significant occlusion and noise are present. However, point estimation alone proves insufficient, particularly in contexts where estimation reliability is paramount. In such high-stakes scenarios, the quantification of estimation uncertainties becomes critical for informed decision-making (Sullivan, 2015, Adler and Öktem, 2025).

In this experiment, we will demonstrate how to quantify the uncertainties associated with the states estimated by SSLS. To this end, we consider the random reconstruction task as an example, where the observation data are obtained by masking 95% of grid points randomly and perturbating with Gaussian noise. The experimental results are shown in Figure 8.
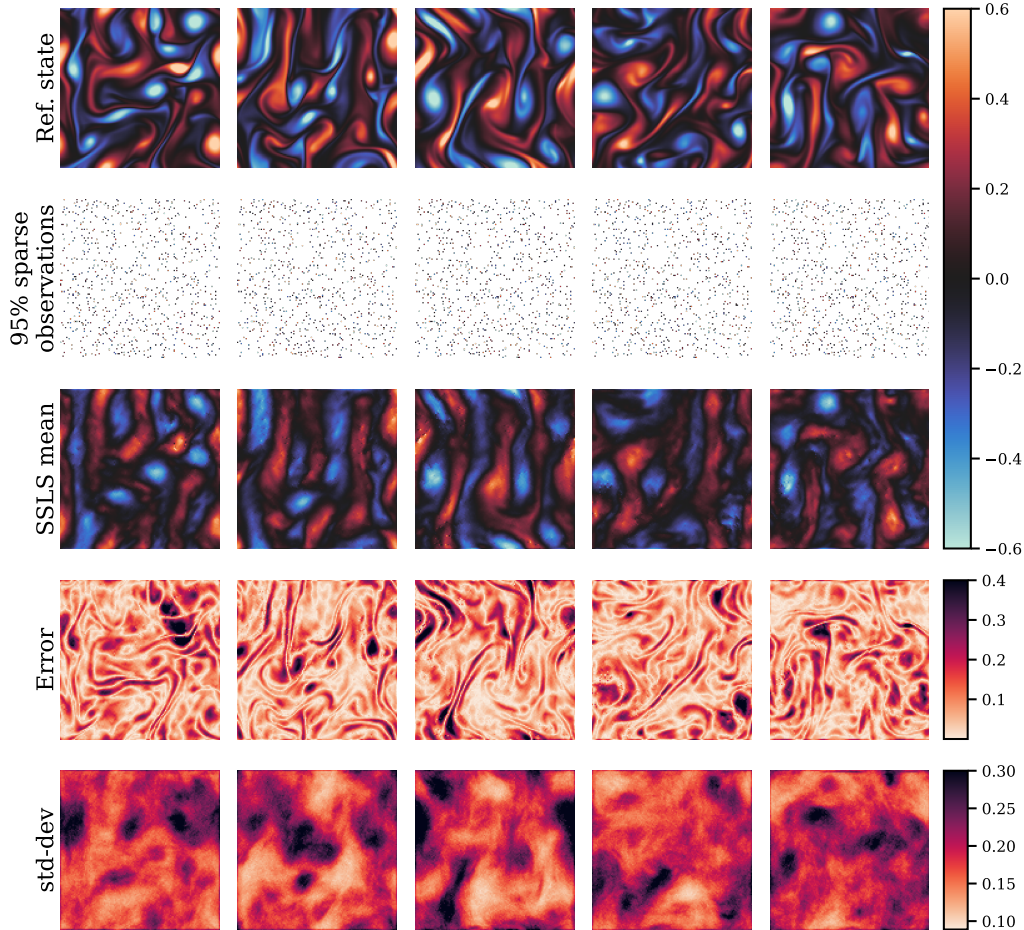

FIGURE 8. Quantify the uncertainty associated with states estimated by SSLS. From top to bottom: the reference states, observations (95% random mask), the SSLS assimilated states, point-wise error (in absolute value) and standard deviation. The noise level is set as $\sigma_{\text{obs}} = 0.4$.

Standard deviation and uncertainty. A notable advantage of SSLS is its ability to generate multiple ensemble samples from the posterior distribution, enabling the computation of standard deviations that illuminate the quality of the estimated states (Patel and Oberai, 2021, Adler and Öktem, 2025). The estimated pointwise standard deviations are presented in the last row of Figure 8.

The first and last rows of Figure 8 reveal that the standard deviation concentrates in regions of high reference vorticity magnitude. This empirical observation aligns with physical intuition. Vorticity, defined as the curl of the velocity field, quantifies the local fluid rotation. Regions of high vorticity indicate intense rotational and swirling motion in the fluid. The uniformly distributed measurement positions prove insufficient to capture high-frequency

information in these high-vorticity regions, resulting in greater uncertainty in the estimated states for these areas.

Well-calibrated uncertainty estimation. One critical measure of uncertainty estimation quality is calibration. A well-calibrated uncertainty estimation ensures that the estimated standard deviation aligns with the pointwise error (Raad et al., 2022, Antoran et al., 2023, Raad et al., 2024).
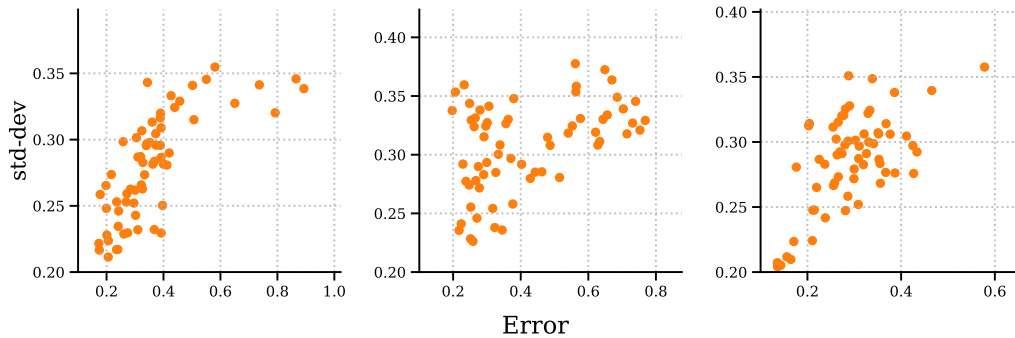

FIGURE 9. The correlation between the standard deviation and estimation error of the SSLS. The standard deviation and error are down-sampled by max pooling for clearer visualization. From left to right: the results at three equally separated time points of the assimilation process.

The last two rows of Figure 8 demonstrate that the standard deviation estimated by SSLS correlates with the pointwise error. To analyze this correlation quantitatively, Figure 9 plots the standard deviation against the error for pixels down-sampled via max-pooling with a kernel size of 16. The correlation is examined at three equally spaced time points, revealing a consistent positive correlation between standard deviation and error across all temporal snapshots.

Both Figures 8 and 9 establish that SSLS provides well-calibrated uncertainty estimations, with the computed standard deviation serving as a reliable indicator of state estimation error. This robust uncertainty quantification proves crucial for assessing the reliability of estimated states and offers valuable insights for optimizing observational positions and refining the model.

5. CONCLUSIONS

This paper presents score-based sequential Langevin sampling, a novel approach for nonlinear assimilation within a recursive Bayesian framework. The theoretical analysis establishes SSLS convergence in TV-distance under mild conditions, providing insights into error behavior with respect to hyper-parameters. Extensive numerical experiments demonstrate SSLS's exceptional performance in high-dimensional and nonlinear scenarios, particularly with sparse or partial measurements. Furthermore, SSLS effectively quantifies state estimation uncertainty, enabling error calibration.

Several promising directions exist for future research and methodological enhancement. While the current framework assumes a known state-space model, practical applications often involve uncertain parameters in both dynamics and measurement models. Future work will extend SSLS to enable simultaneous estimation of latent states and model parameters.

Additionally, we aim to address the computational burden of score network training at each time step through techniques such as in-context learning.

References

Jonas Adler and Ozan Öktem. Deep Bayesian inversion. In Tatiana A. Bubba, editor, *Data-driven Models in Inverse Problems*, volume 31 of *Radon Series on Computational and Applied Mathematics*, pages 359–412. Berlin, Boston: De Gruyter, 2025.

Jeffrey L. Anderson. Spatially and temporally varying adaptive covariance inflation for ensemble filters. *Tellus A*, 61(1):72–83, 2009.

Jeffrey L. Anderson and Stephen L. Anderson. A Monte Carlo implementation of the nonlinear filtering problem to produce ensemble assimilations and forecasts. *Monthly Weather Review*, 121:2741–2758, 1999.

Javier Antoran, Riccardo Barbano, Johannes Leuschner, José Miguel Hernández-Lobato, and Bangti Jin. Uncertainty estimation for computed tomography with a linearised deep image prior. *Transactions on Machine Learning Research*, 2023. ISSN 2835–8856.

Dominique Bakr, Ivan Gentil, and Michel Ledoux. *Analysis and Geometry of Markov Diffusion Operators*, volume 348 of *Grundlehren der mathematischen Wissenschaften (GL)*. Springer Cham, first edition, 2014.

Feng Bao, Zezhong Zhang, and Guannan Zhang. A score-based filter for nonlinear data assimilation. *Journal of Computational Physics*, 514:113207, 2024. ISSN 0021-9991.

Thomas Bengtsson, Peter Bickel, and Bo Li. Curse-of-dimensionality revisited: Collapse of the particle filter in very large scale systems. In Deborah Nolan and Terry Speed, editors, *Institute of Mathematical Statistics Collections*, Probability and Statistics: Essays in Honor of David A. Freedman, pages 316–334. Institute of Mathematical Statistics, 2008.

Alexandros Beskos, Ajay Jasra, Ege A. Muzaffer, and Andrew M. Stuart. Sequential Monte Carlo methods for Bayesian elliptic inverse problems. *Statistics and Computing*, 25:727–737, 2015.

Ramaprasad Bhar. *Stochastic Filtering with Applications in Finance*. World Scientific, 2010.

Peter Bickel, Bo Li, and Thomas Bengtsson. Sharp failure rates for the bootstrap particle filter in high dimensions. In Bertrand Clarke and Subhashis Ghosal, editors, *Institute of Mathematical Statistics Collections*, Pushing the Limits of Contemporary Statistics: Contributions in Honor of Jayanta K. Ghosh, pages 318–329. Institute of Mathematical Statistics, 2008.

Jochen Bröcker. Evaluating raw ensembles with the continuous ranked probability score. *Quarterly Journal of the Royal Meteorological Society*, 138(667):1611–1617, 2012.

Nicolas Brosse, Alain Durmus, and Éric Moulines. Normalizing constants of log-concave densities. *Electronic Journal of Statistics*, 12(1):851 – 889, 2018.

Sitan Chen, Sinho Chewi, Jerry Li, Yuanzhi Li, Adil Salim, and Anru Zhang. Sampling is as easy as learning the score: theory for diffusion models with minimal data assumptions. In *The Eleventh International Conference on Learning Representations*, 2023.

Sinho Chewi. Log-concave sampling, 2024. URL https://chewisinho.github.io/main.pdf. unfinished draft.

Sinho Chewi, Murat A. Erdogdu, Mufan Li, Ruoqi Shen, and Matthew S. Zhang. Analysis of Langevin Monte Carlo from Poincaré to log-Sobolev. *Foundations of Computational Mathematics*, 2024.

Hyungjin Chung, Jeongsol Kim, Michael Thompson Mccann, Marc Louis Klasky, and Jong Chul Ye. Diffusion posterior sampling for general noisy inverse problems. In *The Eleventh International Conference on Learning Representations*, 2023.

S L Cotter, M Dashti, J C Robinson, and A M Stuart. Bayesian inverse problems for functions and applications to fluid mechanics. *Inverse Problems*, 25(11):115008, 2009.

Pierre Del Moral, Arnaud Doucet, and Ajay Jasra. Sequential Monte Carlo samplers. *Journal of the Royal Statistical Society Series B: Statistical Methodology*, 68(3):411–436, 05 2006.

Arnaud Doucet, Nando Freitas, and Neil Gordon, editors. *Sequential Monte Carlo Methods in Practice*. Information Science and Statistics (ISS). Springer New York, NY, first edition, 2001.

John C. Duchi. Information theory and statistics, 2024. URL http://web.stanford.edu/class/stats311/lecture-notes.pdf. unfinished draft.

Robert J. Elliott and Tak Kuen Siu. Option pricing and filtering with hidden Markov-modulated pure-jump processes. *Applied Mathematical Finance*, 20(1):1–25, 2013.

Geir Evensen, Femke C. Vossepoel, and Peter Jan van Leeuwen. *Data Assimilation Fundamentals: A Unified Formulation of the State and Parameter Estimation Problem*. Springer Textbooks in Earth Sciences, Geography and Environment (STEGE). Springer Cham, first edition, 2022.

Rüdiger Frey and Thorsten Schmidt. Pricing and hedging of credit derivatives via the innovations approach to nonlinear filtering. *Finance and Stochastics*, 16:105–133, 2012.

Rong Ge, Holden Lee, and Jianfeng Lu. Estimating normalizing constants for log-concave distributions: algorithms and lower bounds. In *Proceedings of the 52nd Annual ACM SIGACT Symposium on Theory of Computing*, STOC 2020, pages 579–586. Association for Computing Machinery, 2020.

Tilmann Gneiting, Fadoua Balabdaoui, and Adrian E. Raftery. Probabilistic forecasts, calibration and sharpness. *Journal of the Royal Statistical Society: Series B (Statistical Methodology)*, 69(2):243–268, 2007.

N.J. Gordon, D.J. Salmond, and A.F.M. Smith. Novel approach to nonlinear/non-Gaussian Bayesian state estimation. *IEE Proceedings on Radar and Signal Processing*, 140:107–113, 1993.

Yingqing Guo, Hui Yuan, Yukang Yang, Minshuo Chen, and Mengdi Wang. Gradient guidance for diffusion models: An optimization perspective, 2024. arXiv:2404.14743.

Jonathan Ho, Ajay Jain, and Pieter Abbeel. Denoising diffusion probabilistic models. In H. Larochelle, M. Ranzato, R. Hadsell, M.F. Balcan, and H. Lin, editors, *Advances in Neural Information Processing Systems*, volume 33, pages 6840–6851. Curran Associates, Inc., 2020.

Peter L Houtekamer and Herschel L Mitchell. Data assimilation using an ensemble kalman filter technique. *Monthly weather review*, 126(3):796–811, 1998.

Aapo Hyvärinen. Estimation of non-normalized statistical models by score matching. *Journal of Machine Learning Research*, 6(24):695–709, 2005.

Ajil Jalal, Marius Arvinte, Giannis Daras, Eric Price, Alexandros G Dimakis, and Jon Tamir. Robust compressed sensing MRI with deep generative priors. In M. Ranzato, A. Beygelzimer, Y. Dauphin, P.S. Liang, and J. Wortman Vaughan, editors, *Advances in Neural Information Processing Systems*, volume 34, pages 14938–14954. Curran Associates, Inc., 2021.

Yuling Jiao, Guohao Shen, Yuanyuan Lin, and Jian Huang. Deep nonparametric regression on approximate manifolds: Nonasymptotic error bounds with polynomial prefactors. *The Annals of Statistics*, 51(2):691 – 716, 2023.

Nikolas Kantas, Alexandros Beskos, and Ajay Jasra. Sequential Monte Carlo methods for high-dimensional inverse problems: A case study for the Navier-Stokes equations.

SIAM/ASA Journal on Uncertainty Quantification, 2(1):464–489, 2014.

Petros Katsafados, Elias Mavromatidis, and Christos Spyrou. *Numerical Weather Prediction and Data Assimilation.* John Wiley & Sons, Ltd, 2020.

Genshiro Kitagawa. Monte Carlo filter and smoother for non-Gaussian nonlinear state space models. *Journal of Computational and Graphical Statistics*, 5(1):1–25, 1996.

Dmitrii Kochkov, Jamie A. Smith, Ayya Alieva, Qing Wang, Michael P. Brenner, and Stephan Hoyer. Machine learning-accelerated computational fluid dynamics. *Proceedings of the National Academy of Sciences*, 118(21):e2101784118, 2021.

Michael Kohler and Sophie Langer. On the rate of convergence of fully connected deep neural network regression estimates. *The Annals of Statistics*, 49(4):2231–2249, 2021.

Kody Law, Andrew Stuart, and Konstantinos Zygalakis. *Data Assimilation: A Mathematical Introduction*, volume 62 of *Texts in Applied Mathematics (TAM)*. Springer Cham, first edition, 2015.

François-Xavier Le Dimet and Olivier Talagrand. Variational algorithms for analysis and assimilation of meteorological observations: theoretical aspects. *Tellus A*, 38A(2):97–110, 1986.

Holden Lee, Jianfeng Lu, and Yixin Tan. Convergence for score-based generative modeling with polynomial complexity. In S. Koyejo, S. Mohamed, A. Agarwal, D. Belgrave, K. Cho, and A. Oh, editors, *Advances in Neural Information Processing Systems*, volume 35, pages 22870–22882. Curran Associates, Inc., 2022.

Zhuoyuan Li, Bin Dong, and Pingwen Zhang. State-observation augmented diffusion model for nonlinear assimilation, 2024. arXiv:2407.21314.

Andrew J. Majda and John Harlim. *Filtering Complex Turbulent Systems*. Cambridge University Press, 2012.

Jan Mandel, Loren Cobb, and Jonathan D. Beezley. On the convergence of the ensemble kalman filter. *Applications of Mathematics*, 56:533–541, 2012.

Dhruv V. Patel and Assad A. Oberai. GAN-based priors for quantifying uncertainty in supervised learning. *SIAM/ASA Journal on Uncertainty Quantification*, 9(3):1314–1343, 2021.

Grigorios A. Pavliotis. *Stochastic Processes and Applications: Diffusion Processes, the Fokker-Planck and Langevin Equations*, volume 60 of *Texts in Applied Mathematics (TAM)*. Springer New York, NY, 2014.

Michael K Pitt and Neil Shephard. Filtering via simulation: Auxiliary particle filters. *Journal of the American statistical association*, 94(446):590–599, 1999.

Vishal Purohit, Matthew Repasky, Jianfeng Lu, Qiang Qiu, Yao Xie, and Xiuyuan Cheng. Posterior sampling via Langevin dynamics based on generative priors, 2024. arXiv:2410.02078.

Ragheb Raad, Dhruv Patel, Chiao-Chih Hsu, Vijay Kothapalli, Deep Ray, Bino Varghese, Darryl Hwang, Inderbir Gill, Vinay Duddalwar, and Assad A. Oberai. Probabilistic medical image imputation via deep adversarial learning. *Engineering with Computers*, 38:3975–3986, 2022.

Ragheb Raad, Deep Ray, Bino Varghese, Darryl Hwang, Inderbir Gill, Vinay Duddalwar, and Assad A. Oberai. Conditional generative learning for medical image imputation. *Scientific Reports*, 14(171), 2024.

Firas Rassoul-Agha and Timo Seppäläinen. *A Course on Large Deviations with an Introduction to Gibbs Measures*, volume 162 of *Graduate Studies in Mathematics*. American Mathematical Society (AMS), 2015.

Sebastian Reich. Data assimilation: The Schrödinger perspective. *Acta Numerica*, 28:635–711, 2019.

Sebastian Reich and Colin Cotter. *Probabilistic Forecasting and Bayesian Data Assimilation*. Cambridge University Press, 2015.

François Rozet and Gilles Louppe. Score-based data assimilation. In A. Oh, T. Naumann, A. Globerson, K. Saenko, M. Hardt, and S. Levine, editors, *Advances in Neural Information Processing Systems*, volume 36, pages 40521–40541. Curran Associates, Inc., 2023a.

François Rozet and Gilles Louppe. Score-based data assimilation for a two-layer quasi-geostrophic model, 2023b. arXiv:2310.01853.

William Sacher and Peter Bartello. Sampling errors in ensemble Kalman filtering. Part I: Theory. *Monthly Weather Review*, 136:3035–3049, 2008.

Simo Särkkä and Lennart Svensson. *Bayesian filtering and smoothing*. Institute of Mathematical Statistics Textbooks. Cambridge University Press, second edition, 2023.

Johannes Schmidt-Hieber. Nonparametric regression using deep neural networks with relu activation function. *The Annals of Statistics*, 48(4):1875–1897, 2020.

Phillip Si and Peng Chen. Latent-EnSF: A latent ensemble score filter for high-dimensional data assimilation with sparse observation data, 2024. arXiv:2409.00127.

Chris Snyder, Thomas Bengtsson, Peter Bickel, and Jeff Anderson. Obstacles to high-dimensional particle filtering. *Monthly weather review*, 136:4629–4640, 2008.

Jiaming Song, Arash Vahdat, Morteza Mardani, and Jan Kautz. Pseudoinverse-guided diffusion models for inverse problems. In *International Conference on Learning Representations*, 2023a.

Jiaming Song, Qinsheng Zhang, Hongxu Yin, Morteza Mardani, Ming-Yu Liu, Jan Kautz, Yongxin Chen, and Arash Vahdat. Loss-guided diffusion models for plug-and-play controllable generation. In Andreas Krause, Emma Brunskill, Kyunghyun Cho, Barbara Engelhardt, Sivan Sabato, and Jonathan Scarlett, editors, *Proceedings of the 40th International Conference on Machine Learning*, volume 202 of *Proceedings of Machine Learning Research*, pages 32483–32498. PMLR, 23–29 Jul 2023b.

Yang Song and Stefano Ermon. Generative modeling by estimating gradients of the data distribution. In H. Wallach, H. Larochelle, A. Beygelzimer, F. d'Alché-Buc, E. Fox, and R. Garnett, editors, *Advances in Neural Information Processing Systems*, volume 32. Curran Associates, Inc., 2019.

Yang Song, Sahaj Garg, Jiaxin Shi, and Stefano Ermon. Sliced score matching: A scalable approach to density and score estimation. In Ryan P. Adams and Vibhav Gogate, editors, *Proceedings of The 35th Uncertainty in Artificial Intelligence Conference*, volume 115 of *Proceedings of Machine Learning Research*, pages 574–584. PMLR, 22–25 Jul 2020.

Yang Song, Jascha Sohl-Dickstein, Diederik P Kingma, Abhishek Kumar, Stefano Ermon, and Ben Poole. Score-based generative modeling through stochastic differential equations. In *International Conference on Learning Representations*, 2021.

Alessio Spantini, Ricardo Baptista, and Youssef Marzouk. Coupling techniques for nonlinear ensemble filtering. *SIAM Review*, 64(4):921–953, 2022.

T.J. Sullivan. *Introduction to Uncertainty Quantification*, volume 63 of *Texts in Applied Mathematics (TAM)*. Springer Cham, first edition, 2015.

Rong Tang and Yun Yang. Adaptivity of diffusion models to manifold structures. In Sanjoy Dasgupta, Stephan Mandt, and Yingzhen Li, editors, *Proceedings of The 27th International Conference on Artificial Intelligence and Statistics*, volume 238 of *Proceedings of Machine Learning*

Research, pages 1648–1656. PMLR, 02–04 May 2024.

Adam Thelen, Xiaoge Zhang, Olga Fink, Yan Lu, Sayan Ghosh, D. Byeng Youn, Michael D. Todd, Sankaran Mahadevan, Chao Hu, and Zhen Hu. A comprehensive review of digital twin – part 1: modeling and twinning enabling technologies. *Structural and Multidisciplinary Optimization*, 65(354), 2022.

Adam Thelen, Xiaoge Zhang, Olga Fink, Yan Lu, Sayan Ghosh, D. Byeng Youn, Michael D. Todd, Sankaran Mahadevan, Chao Hu, and Zhen Hu. A comprehensive review of digital twin – part 2: roles of uncertainty quantification and optimization, a battery digital twin, and perspectives. *Structural and Multidisciplinary Optimization*, 66(1), 2023.

Alexandre B. Tsybakov. *Introduction to Nonparametric Estimation*. Springer Series in Statistics (SSS). Springer New York, NY, first edition, 2009.

Santosh Vempala and Andre Wibisono. Rapid convergence of the unadjusted Langevin algorithm: Isoperimetry suffices. In H. Wallach, H. Larochelle, A. Beygelzimer, F. d'Alché-Buc, E. Fox, and R. Garnett, editors, *Advances in Neural Information Processing Systems*, volume 32. Curran Associates, Inc., 2019.

Pascal Vincent. A connection between score matching and denoising autoencoders. *Neural Computation*, 23(7):1661–1674, 2011.

Martin J. Wainwright. *High-Dimensional Statistics: A Non-Asymptotic Viewpoint*. Cambridge Series in Statistical and Probabilistic Mathematics. Cambridge University Press, 2019.

Dongze Wu and Yao Xie. Annealing flow generative model towards sampling high-dimensional and multi-modal distributions, 2024. arXiv:2409.20547.

Outline of the Supplementary Material

The supplementary material comprises several appendices containing notation summaries, additional derivations, theoretical proofs, experimental results, and implementation details:

(I) Appendix A presents a comprehensive review of related works.

(II) Appendix B provides a summary of notation used throughout the paper.

(III) Appendix C details the recursive Bayesian framework underlying our approach and presents derivations of denoising score matching.

(IV) Appendix D establishes the convergence of score-based sequential Langevin sampling. The analysis decomposes the assimilation error into three components:

(i) Langevin Monte Carlo convergence (Appendix E)

(ii) Prior error (Appendix F)

(iii) Score matching error (Appendix G)

The initial error analysis is presented in Appendix H, while Appendix I introduces auxiliary definitions and lemmas supporting the theoretical analysis.

(V) Appendix J presents additional numerical experiments, with corresponding implementation details documented in Appendix K.

Appendix A. Related work

A.1. **Diffusion models for Bayesian inverse problems.** Bayesian inverse problems are closely linked to data assimilation, as demonstrated in Section 2.4. In recent years, diffusion methods have gained prominence as an effective technique for posterior sampling in Bayesian inverse problems, such as Chung et al. (2023), Song et al. (2023a,b), Purohit et al. (2024). This section provides a comprehensive review of the existing literature on diffusion-based approaches for posterior sampling.

We first introduce the setup of Bayesian inverse problems. Suppose the forward model is defined as

$$\mathbf{U} = \mathcal{G}(\mathbf{Z}, \mathbf{W}), \quad \mathbf{Z} \sim p_{\mathbf{Z}},$$

where $\mathcal{G}$ represents a given measurement model, $p_{\mathbf{Z}}$ is a known prior distribution, and $\mathbf{W}$ is a random variable with a known distribution. As a result, the measurement likelihood $p_{\mathbf{U}|\mathbf{Z}}(\mathbf{u}|\mathbf{z})$ can be obtained from the measurement model $\mathcal{G}$ and the distribution of $\mathbf{W}$.

Bayesian inverse problems aim to estimate the posterior distribution $p_{\mathbf{Z}|\mathbf{U}}(\mathbf{z}|\mathbf{u})$ given the observation $\mathbf{u}$, the prior $p_{\mathbf{Z}}$, and the measurement likelihood $p_{\mathbf{U}|\mathbf{Z}}$. It is evident that the update step (Section 2.4) within the recursive Bayesian framework exactly corresponds to solving a Bayesian inverse problem.

Diffusion model with guidance. The mainstream technique in diffusion models for conditional or posterior sampling is guidance (Guo et al., 2024). As an illustrative example, we consider the diffusion model with the following forward process

$$\mathrm{d}\mathbf{Z}_s = -\mathbf{Z}_s \, \mathrm{d}s + \sqrt{2} \, \mathrm{d}\mathbf{B}_s, \quad \mathbf{Z}_0 \sim p_{\mathbf{Z}}, \ s \in (0, T),$$

where $(\mathbf{B}_s)_{s \geq 0}$ is a standard Brownian motion. Denote by $p_{\mathbf{Z}_s}$ the law of $\mathbf{Z}_s$ for each $s \in (0, T)$. Following Bayes' rule, the time-reversal process for sampling from the posterior distribution $p_{\mathbf{Z}|\mathbf{U}}(\cdot|\mathbf{u})$ reads (Chung et al., 2023)

$$(A.1) \qquad \mathrm{d}\bar{\mathbf{Z}}_s = \Big\{ \bar{\mathbf{Z}}_s + 2 \overbrace{\nabla_{\mathbf{z}} \log p_{\mathbf{U}|\mathbf{Z}_{T-s}}(\mathbf{u}|\bar{\mathbf{Z}}_s)}^{\text{intractable}} + 2 \overbrace{\nabla_{\mathbf{z}} \log p_{\mathbf{Z}_{T-s}}(\bar{\mathbf{Z}}_s)}^{\text{score}} \Big\} \, \mathrm{d}s + \sqrt{2} \, \mathrm{d}\mathbf{B}_s,$$
$$\bar{\mathbf{Z}}_0 \sim N(\mathbf{0}, \mathbf{I}_d), \ s \in (0, T),$$

where $p_{\mathbf{U}|\mathbf{Z}_s}(\mathbf{u}|\mathbf{z})$ is the time-dependent likelihood, and $p_{\mathbf{Z}_s}(\mathbf{z})$ is the time-dependent prior. It worth noting that the score in (A.1) can be estimated by denoising score matching (Vincent, 2011, Song et al., 2021), while the gradient of log-likelihood is typically intractable.

Linear Gaussian inverse problems. When the measurement model $\mathcal{G}$ is linear, and both the prior and the likelihood are Gaussian, that is,

$$\mathcal{G}(\mathbf{Z}, \mathbf{W}) := \mathbf{G}\mathbf{Z} + \sigma_{\mathrm{obs}}\mathbf{W}, \quad \mathbf{Z} \sim p_{\mathbf{Z}} = N(\boldsymbol{\mu}, \boldsymbol{\Sigma}), \ \mathbf{W} \sim N(\mathbf{0}, \mathbf{I}_d),$$

the gradient of time-dependent log-likelihood in (A.1) can be estimated without bias. For a detailed derivation, please refer to Guo et al. (2024, Lemma 1). However, this linear scenario corresponds to the assimilation with linear state-space model. The solution to the linear assimilation can be obtained using the ensemble Kalman filter (Särkkä and Svensson, 2023). Therefore, there is no necessity to utilize diffusion models for the linear assimilation.

Nonlinear inverse problems. Researchers' interests lie in nonlinear inverse problems, which corresponds to the nonlinear assimilation. One of the most widely-used diffusion-based approaches for nonlinear inverse problem is the diffusion posterior sampling (DPS) (Chung et al., 2023), which estimates the gradient of time-dependent log-likelihood in (A.1) by exchanging the expectation with likelihood, that is,

$$p_{\mathbf{U}|\mathbf{Z}_s}(\mathbf{u}|\mathbf{z}) = \int p_{\mathbf{U}|\mathbf{Z}_0}(\mathbf{u}|\mathbf{z}_0) p_{\mathbf{Z}_0|\mathbf{Z}_s}(\mathbf{z}_0|\mathbf{z}) \, \mathrm{d}\mathbf{z}_0$$
$$(A.2) \qquad = \mathbb{E}\big[p_{\mathbf{U}|\mathbf{Z}_0}(\mathbf{u}|\mathbf{Z}_0)|\mathbf{Z}_s = \mathbf{z} \big] \approx p_{\mathbf{U}|\mathbf{Z}_0}(\mathbf{u}|\mathbb{E}[\mathbf{Z}_0|\mathbf{Z}_s = \mathbf{z}]).$$

However, it is important to note that this approximation introduces a bias term known as Jensen's gap, as pointed out by Chung et al. (2023). Therefore, DPS can not yield a consistent estimation in nonlinear Bayesian inverse problems. In contrast, the score-based LMC proposed by this work is consistent in nonlinear scenarios, as shown in Theorem 3.2.

A.2. **Diffusion-based methods for assimilation.** In the preceding subsection, we discussed diffusion-based methods for Bayesian inverse problems. Building upon these methods, a variety of diffusion-based approaches have been developed for data assimilation, which can be broadly classified into data-driven methods and filtering methods. A comparison of these techniques, along with commonly used classical methods, is presented in Table 1.

TABLE 1. A comparison of methods for nonlinear assimilation.

Method	Consistent	Approximation or assumption
3D-Var/4D-Var	✘	(i) Linearization (ii) Gaussian prior and likelihood
SDA (Rozet and Louppe, 2023a)	✘	Jensen's gap (Chung et al., 2023)
SOAD (Li et al., 2024)	✔	Gaussian prior and likelihood
EnKF	✘	(i) Linearization (ii) Gaussian prior and likelihood
PF	✔	None
SF (Bao et al., 2024)	✘	Damping function
SSLS (ours)	✔	None

Data-driven methods for assimilation. Data-driven methods focus on estimating the posterior distribution of all latent states $\mathbf{Z} := \mathbf{X}_{[k]}$ given all available observation data $\mathbf{U} := \mathbf{Y}_{[k]}$. By substituting $\mathbf{Z}$ and $\mathbf{U}$ into the time-reversal process (A.1), this line of methods reformulate the assimialtion as a single Bayesian inverse problem (Rozet and Louppe, 2023a,b, Li et al., 2024).

The prior score in (A.1) can be approximated by utilizing random copies of $\mathbf{Z} = \mathbf{X}_{[k+1]}$ through denoising score matching, as discussed in (Rozet and Louppe, 2023a, Li et al., 2024). This characteristic makes these methods data-driven, as they rely on empirical data rather than explicit knowledge of the underlying physical models, i.e., the states transition dynamics. In these data-driven approaches, the physical mechanism is implicitly incorporated into the prior score.

Then it remains to estimate the gradient of time-dependent log-likelihood in (A.1). For example, the score-based data assimilation (SDA) (Rozet and Louppe, 2023a,b) estimates the gradient of time-dependent log-likelihood in a similar manner as DPS (A.2). In Li et al. (2024), the authors propose the state-observation augmented diffusion (SOAD) method, which involves converting a nonlinear state-space model into a linear one through variable augmentation. The gradient of time-dependent log-likelihood of augmented linear state-space model can be estimated without bias, as discussed in the previous section.

Computing the joint distribution of the states across all time steps is computationally inefficient due to the increasing dimensionality of the diffusion model as the number of time steps increases. This limitation of the data-driven methods hinders the application of these methods to high-dimensional data assimilation tasks. Additionally, data-driven methods are unable to fully leverage the underlying physical mechanisms. In contrast, the dimensionality of SSLS proposed in this study remains constant, regardless of the assimilation time. Moreover, SSLS effectively integrates physical principles with observation data.

Filtering methods for assimilation. Another category of diffusion-based assimilation methods are developed within the Bayesian filtering framework (Section 2.2), with examples

including the score-based filter (SF) (Bao et al., 2024). In the update at the $(k+1)$-th time step, SF sets $\mathbf{U} := \mathbf{Y}_{k+1}$, $\mathbf{u} := \mathbf{y}_{k+1}$, and $\mathbf{Z}_0 \sim \widehat{q}_{k+1}(\cdot|\mathbf{y}[k])$. SF estimates the prior score in(A.1) using sliced score matching (Song et al., 2020), while approximating the gradient of the time-dependent log-likelihood through a separation of variables:

$$\nabla_{\mathbf{z}} \log p_{\mathbf{U}|\mathbf{Z}_s}(\mathbf{u}|\mathbf{z}) = h(s)\nabla_{\mathbf{z}} \log p_{\mathbf{U}|\mathbf{Z}_0}(\mathbf{u}|\mathbf{z}), \quad s \in (0, T),$$

Here, the damping function h is a monotonically decreasing function in the interval $[0, T]$, with $h(0) = 1$ and $h(T) = 0$. However, this separation of variable approximation is often inconsistent, and the optimal choice of the damping function remains unresolved. In contrast, our method is consistent and does not rely on such heuristic approximations.

Appendix B. A Summary of Notations

Table 2 summarizes the notations used in Sections 2 and 3 for easy reference and cross-checking.

Table 2. The list of notations defined in Sections 2 and 3.

Symbols	Description
$\mathcal{F}_k$	The dynamics model at the k-th time step, defined as (2.1).
$\mathcal{G}_k$	The measurement model at the k-th time step, defined as (2.2).
$\mathbf{X}_k$	The state at the k-th time step.
$\mathbf{Y}_k$	The observation of $\mathbf{X}_k$.
$\widehat{\mathbf{X}}_k$	The estimated state at the k-th time step using SSLS.
$\underline{\mathbf{X}}_k$	The predicted state at the k-th time step using the dynamics model, defined as (2.8).
ρ_k	The state transition density at the k-th time step, specified by (2.1).
g_k	The measurement likelihood at the k-th time step, specified by (2.2).
π_k	The posterior at the k-th time step, defined as (2.3).
$\widehat{\pi}_k$ or $\widehat{\pi}_k^T$	The estimated posterior at the k-th time step using SSLS with terminal time T, which is the law of $\widehat{\mathbf{X}}_k$.
q_k	The prediction distribution at the k-th time step, defined as (2.4), serving as the prior in the posterior π_k.
$\widehat{q}_k$	The approximated prediction distribution at the k-th time step, defined as (2.7), which is the law of $\underline{\mathbf{X}}_k$.
$\mathbf{Z}_t$	The stochastic process specified by the Langevin diffusion (2.11).
$\widehat{\mathbf{Z}}_t$	The stochastic process specified by the score-based Langevin sampling (3.1).
$\widehat{\mathbf{b}}_k$	The drift term in the score-based Langevin Monte Carlo (3.2).
$(\beta_m)_{m=1}^M$	A sequence of inverse temperatures for annealing.
$\widehat{\mathbf{Z}}_t^m$	The stochastic process specified by the annealed Langevin Monte Carlo (2.14) with a inverse temperature β_m.
$\widehat{\mathbf{b}}_k^m$	The drift term in the score-based annealed Langevin Monte Carlo (2.15) with a inverse temperature β_m.

<div align="center">APPENDIX C. PROOFS IN SECTION 2</div>

In this section, we provide proofs in Section 2. The derivation of the recursive Bayesian framework is shown in Appendix C.1, and the proof of the denoising score matching is demonstrated in Appendix C.2.

C.1. **Recursive Bayesian framework.** This section verifies the recursion (2.6). Indeed,

$$
\begin{aligned}
&\pi_{k+1}(\mathbf{x}_{k+1}|\mathbf{y}_{[k+1]}) \\
&= \frac{p_{\mathbf{Y}_{k+1}|\mathbf{X}_{k+1},\mathbf{Y}_{[k]}}(\mathbf{y}_{k+1}|\mathbf{x}_{k+1},\mathbf{y}_{[k]})}{p_{\mathbf{Y}_{k+1}|\mathbf{Y}_{[k]}}(\mathbf{y}_{k+1}|\mathbf{y}_{[k]})} p_{\mathbf{X}_{k+1}|\mathbf{Y}_{[k]}}(\mathbf{x}_{k+1}|\mathbf{y}_{[k]}) \\
&= \frac{g_{k+1}(\mathbf{y}_{k+1}|\mathbf{x}_{k+1})}{p_{\mathbf{Y}_{k+1}|\mathbf{Y}_{[k]}}(\mathbf{y}_{k+1}|\mathbf{y}_{[k]})} \int p_{\mathbf{X}_{k+1}|\mathbf{X}_k,\mathbf{Y}_{[k]}}(\mathbf{x}_{k+1}|\mathbf{x}_k,\mathbf{y}_{[k]})\pi_k(\mathbf{x}_k|\mathbf{y}_{[k]})\,\mathrm{d}\mathbf{x}_k \\
&= \frac{g_{k+1}(\mathbf{y}_{k+1}|\mathbf{x}_{k+1})}{p_{\mathbf{Y}_{k+1}|\mathbf{Y}_{[k]}}(\mathbf{y}_{k+1}|\mathbf{y}_{[k]})} \int \rho_k(\mathbf{x}_{k+1}|\mathbf{x}_k)\pi_k(\mathbf{x}_k|\mathbf{y}_{[k]})\,\mathrm{d}\mathbf{x}_k,
\end{aligned}
$$

where the first equality follows from Bayes's rule. The second equality invokes Chapman-Kolmogorov identity and the fact that $\mathbf{Y}_{k+1}$ is independent of $\mathbf{Y}_k$ given $\mathbf{X}_{k+1}$. The last equality is owing to the fact that $\mathbf{X}_{k+1}$ is independent of $\mathbf{Y}_{[k]}$ given $\mathbf{X}_k$.

C.2. **Denoising score matching.** In this section, we provide the derivations of the denoising score matching, which has been proven by Vincent (2011), Ho et al. (2020), Song and Ermon (2019).

Let $\underline{\mathbf{X}}_{k+1}$ be a random variable drawn from the prediction distribution $\widehat{q}_{k+1}(\cdot|\mathbf{y}_{[k]})$, and let ε be a standard Gaussian noise independent of $\underline{\mathbf{X}}_{k+1}$. For each fixed noise level $\sigma > 0$, define

$$
\text{(C.1)} \qquad\qquad \underline{\mathbf{X}}_{k+1}^\sigma = \underline{\mathbf{X}}_{k+1} + \sigma\varepsilon.
$$

It is evident that $\underline{\mathbf{X}}_{k+1}^\sigma$ obeys the Gaussian smoothed prediction distribution, that is,

$$
\begin{aligned}
q_{k+1}^\sigma(\mathbf{x}^\sigma|\mathbf{y}_{[k]}) &:= \int p_{\underline{\mathbf{X}}_{k+1}^\sigma|\underline{\mathbf{X}}_{k+1}}(\mathbf{x}^\sigma|\mathbf{x})\widehat{q}_{k+1}(\mathbf{x}|\mathbf{y}_{[k]})\,\mathrm{d}\mathbf{x} \\
&= \int \underbrace{N(\mathbf{x}^\sigma;\mathbf{x},\sigma^2\mathbf{I}_d)}_{\text{Gaussian kernel}} \widehat{q}_{k+1}(\mathbf{x}|\mathbf{y}_{[k]})\,\mathrm{d}\mathbf{x}.
\end{aligned}
$$

Observe that the score of the Gaussian kernel is given as

$$
\text{(C.2)} \qquad\qquad \nabla_{\mathbf{x}^\sigma} \log p_{\underline{\mathbf{X}}_{k+1}^\sigma|\underline{\mathbf{X}}_{k+1}}(\mathbf{x}^\sigma|\mathbf{x}) = -\frac{\mathbf{x}^\sigma - \mathbf{x}}{\sigma^2}.
$$

Step (I). We first show that for each function $\mathbf{s}$,

$$
\begin{aligned}
&\mathbb{E}_{\underline{\mathbf{X}}_{k+1}^\sigma \sim p_{\underline{\mathbf{X}}_{k+1}^\sigma|\mathbf{Y}_{[k]}}(\cdot|\mathbf{y}_{[k]})}\big[\|\mathbf{s}(\underline{\mathbf{X}}_{k+1}^\sigma,\mathbf{y}_{[k]}) - \nabla_{\mathbf{x}^\sigma} \log p_{\underline{\mathbf{X}}_{k+1}^\sigma|\mathbf{Y}_{[k]}}(\underline{\mathbf{X}}_{k+1}^\sigma|\mathbf{y}_{[k]})\|_2^2\big] \\
&\text{(C.3)} \quad = \mathbb{E}_{\underline{\mathbf{X}}_{k+1} \sim \widehat{q}_{k+1}(\cdot|\mathbf{y}_{[k]})}\mathbb{E}_{\underline{\mathbf{X}}_{k+1}^\sigma \sim p_{\underline{\mathbf{X}}_{k+1}^\sigma|\underline{\mathbf{X}}_{k+1}}}\big[\|\mathbf{s}(\underline{\mathbf{X}}_{k+1}^\sigma,\mathbf{y}_{[k]}) \\
&\qquad\qquad - \nabla_{\mathbf{x}_\sigma} \log p_{\underline{\mathbf{X}}_{k+1}^\sigma|\underline{\mathbf{X}}_{k+1}}(\underline{\mathbf{X}}_{k+1}^\sigma|\underline{\mathbf{X}}_{k+1})\|_2^2\big] + c,
\end{aligned}
$$

where c is a constant independent of $\mathbf{s}$. Indeed,

$$
\mathbb{E}_{\underline{\mathbf{X}}^{\sigma}_{k+1} \sim p_{\underline{\mathbf{X}}^{\sigma}_{k+1}|\mathbf{Y}_{[k]}}(\cdot|\mathbf{y}_{[k]})}\left[\|\mathbf{s}(\underline{\mathbf{X}}^{\sigma}_{k+1}, \mathbf{y}_{[k]}) - \nabla_{\mathbf{x}_{\sigma}} \log p_{\underline{\mathbf{X}}^{\sigma}_{k+1}|\mathbf{Y}_{[k]}}(\underline{\mathbf{X}}^{\sigma}_{k+1}|\mathbf{y}_{[k]})\|_2^2\right]
$$

(C.4)
$$
= \underbrace{\mathbb{E}_{\underline{\mathbf{X}}^{\sigma}_{k+1} \sim p_{\underline{\mathbf{X}}^{\sigma}_{k+1}|\mathbf{Y}_{[k]}}(\cdot|\mathbf{y}_{[k]})}\left[\|\mathbf{s}(\underline{\mathbf{X}}^{\sigma}_{k+1}, \mathbf{y}_{[k]})\|_2^2\right]}_{(i)}
$$

$$
\underbrace{- 2\,\mathbb{E}_{\underline{\mathbf{X}}^{\sigma}_{k+1} \sim p_{\underline{\mathbf{X}}^{\sigma}_{k+1}|\mathbf{Y}_{[k]}}(\cdot|\mathbf{y}_{[k]})}\left[\mathbf{s}(\underline{\mathbf{X}}^{\sigma}_{k+1}, \mathbf{y}_{[k]}) \cdot \nabla_{\mathbf{x}_{\sigma}} \log p_{\underline{\mathbf{X}}^{\sigma}_{k+1}|\mathbf{Y}_{[k]}}(\underline{\mathbf{X}}^{\sigma}_{k+1}|\mathbf{y}_{[k]})\right]}_{(i)} + c_1,
$$

where c_1 is a constant independent of $\mathbf{s}$. For the term (i) in (C.4), we have

$$
\mathbb{E}_{\underline{\mathbf{X}}^{\sigma}_{k+1} \sim p_{\underline{\mathbf{X}}^{\sigma}_{k+1}|\mathbf{Y}_{[k]}}(\cdot|\mathbf{y}_{[k]})}\left[\|\mathbf{s}(\underline{\mathbf{X}}^{\sigma}_{k+1}, \mathbf{y}_{[k]})\|_2^2\right]
$$

$$
= \int \|\mathbf{s}(\mathbf{x}_{\sigma}, \mathbf{y}_{[k]})\|_2^2 \, p_{\underline{\mathbf{X}}^{\sigma}_{k+1}|\mathbf{Y}_{[k]}}(\mathbf{x}_{\sigma}|\mathbf{y}_{[k]}) \, \mathrm{d}\mathbf{x}_{\sigma}
$$

$$
= \int \|\mathbf{s}(\mathbf{x}_{\sigma}, \mathbf{y}_{[k]})\|_2^2 \left(\int p_{\underline{\mathbf{X}}^{\sigma}_{k+1}|\underline{\mathbf{X}}_{k+1}, \mathbf{Y}_{[k]}}(\mathbf{x}_{\sigma}|\mathbf{x}, \mathbf{y}_{[k]}) q_{k+1}(\mathbf{x}|\mathbf{y}_{[k]}) \, \mathrm{d}\mathbf{x} \right) \mathrm{d}\mathbf{x}_{\sigma}
$$

$$
= \int \|\mathbf{s}(\mathbf{x}_{\sigma}, \mathbf{y}_{[k]})\|_2^2 \left(\int p_{\underline{\mathbf{X}}^{\sigma}_{k+1}|\underline{\mathbf{X}}_{k+1}}(\mathbf{x}_{\sigma}|\mathbf{x}) q_{k+1}(\mathbf{x}|\mathbf{y}_{[k]}) \, \mathrm{d}\mathbf{x} \right) \mathrm{d}\mathbf{x}_{\sigma}
$$

$$
= \int \left(\int \|\mathbf{s}(\mathbf{x}_{\sigma}, \mathbf{y}_{[k]})\|_2^2 \, p_{\underline{\mathbf{X}}^{\sigma}_{k+1}|\underline{\mathbf{X}}_{k+1}}(\mathbf{x}_{\sigma}|\mathbf{x}) \, \mathrm{d}\mathbf{x}_{\sigma} \right) q_{k+1}(\mathbf{x}|\mathbf{y}_{[k]}) \, \mathrm{d}\mathbf{x}
$$

(C.5)
$$
= \mathbb{E}_{\underline{\mathbf{X}}_{k+1} \sim \widehat{q}_{k+1}(\cdot|\mathbf{y}_{[k]})} \mathbb{E}_{\underline{\mathbf{X}}^{\sigma}_{k+1} \sim p_{\underline{\mathbf{X}}^{\sigma}_{k+1}|\underline{\mathbf{X}}_{k+1}}}\left[\|\mathbf{s}(\underline{\mathbf{X}}^{\sigma}_{k+1}, \mathbf{y}_{[k]})\|_2^2\right],
$$

where the second equality follows from Chapman-Kolmogorov identity, the third equality is due to the fact that $\underline{\mathbf{X}}^{\sigma}_{k+1}$ is conditionally independent of $\mathbf{Y}^{[k]}$ given $\underline{\mathbf{X}}_{k+1}$. For the term (ii) in (C.4), by the same argument,

$$
\mathbb{E}_{\underline{\mathbf{X}}^{\sigma}_{k+1} \sim p_{\underline{\mathbf{X}}^{\sigma}_{k+1}|\mathbf{Y}_{[k]}}(\cdot|\mathbf{y}_{[k]})}\left[\mathbf{s}(\underline{\mathbf{X}}^{\sigma}_{k+1}, \mathbf{y}_{[k]}) \cdot \nabla_{\mathbf{x}_{\sigma}} \log p_{\underline{\mathbf{X}}^{\sigma}_{k+1}|\mathbf{Y}_{[k]}}(\underline{\mathbf{X}}^{\sigma}_{k+1}|\mathbf{y}_{[k]})\right]
$$

$$
= \int \mathbf{s}(\mathbf{x}_{\sigma}, \mathbf{y}_{[k]}) \cdot \nabla_{\mathbf{x}_{\sigma}} p_{\underline{\mathbf{X}}^{\sigma}_{k+1}|\mathbf{Y}_{[k]}}(\mathbf{x}_{\sigma}|\mathbf{y}_{[k]}) \, \mathrm{d}\mathbf{x}_{\sigma}
$$

$$
= \int \mathbf{s}(\mathbf{x}_{\sigma}, \mathbf{y}_{[k]}) \cdot \nabla_{\mathbf{x}_{\sigma}} \left(\int p_{\underline{\mathbf{X}}^{\sigma}_{k+1}|\underline{\mathbf{X}}_{k+1}}(\mathbf{x}_{\sigma}|\mathbf{x}) q_{k+1}(\mathbf{x}|\mathbf{y}_{[k]}) \, \mathrm{d}\mathbf{x} \right) \mathrm{d}\mathbf{x}_{\sigma}
$$

$$
= \int \mathbf{s}(\mathbf{x}_{\sigma}, \mathbf{y}_{[k]}) \cdot \left(\int \nabla_{\mathbf{x}_{\sigma}} p_{\underline{\mathbf{X}}^{\sigma}_{k+1}|\underline{\mathbf{X}}_{k+1}}(\mathbf{x}_{\sigma}|\mathbf{x}) q_{k+1}(\mathbf{x}|\mathbf{y}_{[k]}) \, \mathrm{d}\mathbf{x} \right) \mathrm{d}\mathbf{x}_{\sigma}
$$

$$
= \int \left(\int \mathbf{s}(\mathbf{x}_{\sigma}, \mathbf{y}_{[k]}) \cdot \nabla_{\mathbf{x}_{\sigma}} p_{\underline{\mathbf{X}}^{\sigma}_{k+1}|\underline{\mathbf{X}}_{k+1}}(\mathbf{x}_{\sigma}|\mathbf{x}) \, \mathrm{d}\mathbf{x}_{\sigma} \right) q_{k+1}(\mathbf{x}|\mathbf{y}_{[k]}) \, \mathrm{d}\mathbf{x}
$$

(C.6)
$$
= \mathbb{E}_{\underline{\mathbf{X}}_{k+1} \sim \widehat{q}_{k+1}(\cdot|\mathbf{y}_{[k]})} \mathbb{E}_{\underline{\mathbf{X}}^{\sigma}_{k+1} \sim p_{\underline{\mathbf{X}}^{\sigma}_{k+1}|\underline{\mathbf{X}}_{k+1}}}\left[\mathbf{s}(\underline{\mathbf{X}}^{\sigma}_{k+1}, \mathbf{y}_{[k]}) \cdot \nabla \log p_{\underline{\mathbf{X}}^{\sigma}_{k+1}|\underline{\mathbf{X}}_{k+1}}(\underline{\mathbf{X}}^{\sigma}_{k+1}|\underline{\mathbf{X}}_{k+1})\right].
$$

Plugging (C.5) and (C.6) into (C.4) completes the proof of (C.3).

Step (II). We next reformulate the right-hand side of (C.3) as

$$
\mathbb{E}_{\underline{\mathbf{X}}_{k+1} \sim \widehat{q}_{k+1}(\cdot|\mathbf{y}_{[k]})} \mathbb{E}_{\underline{\mathbf{X}}^{\sigma}_{k+1} \sim p_{\underline{\mathbf{X}}^{\sigma}_{k+1}|\underline{\mathbf{X}}_{k+1}}}\left[\|\mathbf{s}(\underline{\mathbf{X}}^{\sigma}_{k+1}, \mathbf{y}_{[k]}) - \nabla_{\mathbf{x}} \log p_{\underline{\mathbf{X}}^{\sigma}_{k+1}|\underline{\mathbf{X}}_{k+1}}(\underline{\mathbf{X}}^{\sigma}_{k+1}|\underline{\mathbf{X}}_{k+1})\|_2^2\right]
$$

$$
= \mathbb{E}_{\underline{\mathbf{X}}_{k+1} \sim \widehat{q}_{k+1}(\cdot|\mathbf{y}_{[k]})} \mathbb{E}_{\underline{\mathbf{X}}^{\sigma}_{k+1} \sim p_{\underline{\mathbf{X}}^{\sigma}_{k+1}|\underline{\mathbf{X}}_{k+1}}}\left[\left\|\mathbf{s}(\underline{\mathbf{X}}^{\sigma}_{k+1}, \mathbf{y}_{[k]}) + \frac{1}{\sigma^2}(\underline{\mathbf{X}}^{\sigma}_{k+1} - \underline{\mathbf{X}}_{k+1})\right\|_2^2\right]
$$

$$
= \frac{1}{\sigma^2} \mathbb{E}_{\underline{\mathbf{X}}_{k+1} \sim \widehat{q}_{k+1}(\cdot|\mathbf{y}_{[k]})} \mathbb{E}_{\boldsymbol{\varepsilon} \sim N(\mathbf{0}, \mathbf{I}_d)}\left[\|\sigma \mathbf{s}(\underline{\mathbf{X}}_{k+1} + \sigma \boldsymbol{\varepsilon}, \mathbf{y}_{[k]}) + \boldsymbol{\varepsilon}\|_2^2\right],
$$

where the first equality is due to (C.2), and the second equality used (C.1). Combining this with (C.3) yields

$$
\mathbb{E}_{\underline{\mathbf{X}}^{\sigma}_{k+1} \sim p_{\underline{\mathbf{X}}^{\sigma}_{k+1} | \mathbf{Y}_{[k]}}(\cdot | \mathbf{y}_{[k]})} \left[\| \mathbf{s}(\underline{\mathbf{X}}^{\sigma}_{k+1}, \mathbf{y}_{[k]}) - \nabla \log p_{\underline{\mathbf{X}}^{\sigma}_{k+1} | \mathbf{Y}_{[k]}}(\underline{\mathbf{X}}^{\sigma}_{k+1} | \mathbf{y}_{[k]}) \|^2_2 \right]
$$

$$
= \frac{1}{\sigma^2} \mathbb{E}_{\underline{\mathbf{X}}_{k+1} \sim \widehat{q}_{k+1}(\cdot | \mathbf{y}_{[k]})} \mathbb{E}_{\boldsymbol{\varepsilon} \sim N(\mathbf{0}, \mathbf{I}_d)} \left[\| \sigma \mathbf{s}(\underline{\mathbf{X}}_{k+1} + \sigma \boldsymbol{\varepsilon}, \mathbf{y}_{[k]}) + \boldsymbol{\varepsilon} \|^2_2 \right] + c,
$$

which achieves the population risk of the denoising score matching. Consequently,

$$
\nabla_{\mathbf{x}_{\sigma}} \log q^{\sigma}_{k+1}(\cdot | \mathbf{y}_{[k+1]}) = \arg\min_{\mathbf{s}} \mathbb{E}_{\underline{\mathbf{X}}_{k+1} \sim \widehat{q}_{k+1}(\cdot | \mathbf{y}_{[k]})} \mathbb{E}_{\boldsymbol{\varepsilon} \sim N(\mathbf{0}, \mathbf{I}_d)} \left[\| \sigma \mathbf{s}(\underline{\mathbf{X}}_{k+1} + \sigma \boldsymbol{\varepsilon}, \mathbf{y}_{[k]}) + \boldsymbol{\varepsilon} \|^2_2 \right].
$$

Finally, approximate the above population risk by its empirical counterpart yields (2.10).

APPENDIX D. PROOFS IN SECTION 3

In this section, we provide proofs of Theorems 3.2 and 3.4. We first decompose the error of the posterior distribution in Appendix D.1. The error analysis for the posterior sampling (Theorem 3.2), and the convergence of assimilation (Theorem 3.4) are proven in Appendix D.2.

D.1. **Error Decomposition.** Recall the Langevin diffusion for the $(k + 1)$-th time step of the data assimilation

$$
(D.1) \qquad d\mathbf{Z}_t = \nabla_{\mathbf{x}} \log \pi_{k+1}(\mathbf{Z}_t | \mathbf{y}_{[k+1]}) \, dt + \sqrt{2} \, d\mathbf{B}_t, \quad \mathbf{Z}_0 \sim \pi^0_{k+1}(\cdot | \mathbf{y}_{[k+1]}), \ t \geq 0.
$$

Denote by π^t_{k+1} the law of $\mathbf{Z}_t$ for each $t \geq 0$. The Langevin Monte Carlo is defined as the Euler-Maruyama discretization of the Langevin diffusion. The interpolation of the Langevin Monte Carlo is given as, for each $0 \leq \ell \leq K - 1$,

$$
(D.2) \qquad d\bar{\mathbf{Z}}_t = \nabla_{\mathbf{x}} \log \pi_{k+1}(\bar{\mathbf{Z}}_{\ell h} | \mathbf{y}_{[k+1]}) \, dt + \sqrt{2} \, d\mathbf{B}_t, \quad \ell h \leq t \leq (\ell + 1)h,
$$

where $\bar{\mathbf{Z}}_0 \sim \pi^0_{k+1}(\cdot | \mathbf{y}_{[k+1]})$. Denote by $\bar{\pi}^t_{k+1}$ the law of $\bar{\mathbf{Z}}_t$ for each $0 \leq t \leq Kh = T$. We next introduce the interpolation of the score-based Langevin Monte Carlo

$$
(D.3) \qquad d\widehat{\mathbf{Z}}_t = \widehat{\mathbf{b}}_{k+1}(\widehat{\mathbf{Z}}_{\ell h} | \mathbf{y}_{[k+1]}) \, dt + \sqrt{2} \, d\mathbf{B}_t, \quad \ell h \leq t \leq (\ell + 1)h,
$$

where $\widehat{\mathbf{Z}}_0 \sim \pi^0_{k+1}(\cdot | \mathbf{y}_{[k+1]})$, and the estimator of posterior score function is given as

$$
\widehat{\mathbf{b}}_{k+1}(\mathbf{x} | \mathbf{y}_{[k+1]}) = \nabla_{\mathbf{x}} \log g_{k+1}(\mathbf{y}_{k+1} | \mathbf{x}) + \widehat{\mathbf{s}}_{k+1}(\mathbf{x}, \mathbf{y}_{[k]}).
$$

Here the prediction score $\widehat{\mathbf{s}}_{k+1}$ is defined as (2.10). Denote by $\widehat{\pi}^t_{k+1}$ the law of $\widehat{\mathbf{Z}}_t$ for each $0 \leq t \leq Kh = T$. Recall the prediction distribution (2.4)

$$
q_{k+1}(\mathbf{x} | \mathbf{y}_{[k]}) = \int \rho_k(\mathbf{x} | \mathbf{x}_k) \pi_k(\mathbf{x}_k | \mathbf{y}_{[k]}) \, d\mathbf{x}_k,
$$

which serves as the prior in the Bayesian recursive framework. Recall the approximated prediction distribution (2.7)

$$
\widehat{q}_{k+1}(\mathbf{x} | \mathbf{y}_{[k]}) := \int \rho_k(\mathbf{x} | \mathbf{x}_k) \widehat{\pi}^T_k(\mathbf{x}_k | \mathbf{y}_{[k]}) \, d\mathbf{x}_k.
$$

The following lemma decomposes the TV distance between π_{k+1} and $\widehat{\pi}^T_{k+1}$ into three parts: the convergence of the Langevin Monte Carlo, the prior error, and the error of score matching.

Lemma D.1 (Error decomposition). *Let π_{k+1} be the stationary distribution of the Langevin diffusion* (D.1), *and let $\widehat{\pi}_{k+1}^T$ be the law of the score-based Langevin Monte Carlo* (D.3). *Then for each $k \in \mathbb{N}$,*

$$\mathrm{TV}^2 \left(\pi_{k+1}(\cdot|\mathbf{y}_{[k+1]}), \widehat{\pi}_{k+1}^T(\cdot|\mathbf{y}_{[k+1]}) \right)$$

$$\leq 2 \underbrace{\mathrm{TV}^2 \left(\pi_{k+1}(\cdot|\mathbf{y}_{[k+1]}), \bar{\pi}_{k+1}^T(\cdot|\mathbf{y}_{[k+1]}) \right)}_{\text{convergence of Langevin Monte Carlo}}$$

$$+ 4T \underbrace{\| \nabla_{\mathbf{x}} \log q_{k+1}(\cdot|\mathbf{y}_{[k]}) - \nabla_{\mathbf{x}} \log \widehat{q}_{k+1}(\cdot|\mathbf{y}_{[k]}) \|_{L^\infty(\mathbb{R}^d)}^2}_{\text{prior error}}$$

$$+ 4 \underbrace{\sum_{\ell=0}^{K-1} h \mathbb{E}_{\bar{\mathbf{Z}}_{\ell h}} \left[\| \nabla_{\mathbf{x}} \log \widehat{q}_{k+1}(\bar{\mathbf{Z}}_{\ell h}|\mathbf{y}_{[k]}) - \widehat{\mathbf{s}}_{k+1}(\bar{\mathbf{Z}}_{\ell h}, \mathbf{y}_{[k]}) \|_2^2 \right]}_{\text{score estimation error}},$$

where the expectation $\mathbb{E}_{\bar{\mathbf{Z}}_{\ell h}}[\cdot]$ is taken with respect to $\bar{\mathbf{Z}}_{\ell h} \sim \bar{\pi}_{k+1}^{\ell h}(\cdot|\mathbf{y}_{[k+1]})$.

Remark D.2. The convergence of the Langevin Monte Carlo will be analyzed in Appendix E. The prior error characterizes the error of the approximated prediction distribution $\widehat{q}_{k+1}$, which is induced by the error of the posterior distribution $\widehat{\pi}_k^T$ in the previous time step. The detailed analysis will be shown in Appendix F. Finally, we will investigate the score estimation error in Appendix G.

Proof of Lemma D.1. According to the triangular inequality of TV distance, we have

$$\mathrm{TV}^2 \left(\pi_{k+1}(\cdot|\mathbf{y}_{[k+1]}), \widehat{\pi}_{k+1}^T(\cdot|\mathbf{y}_{[k+1]}) \right)$$

$$\leq 2 \, \mathrm{TV}^2 \left(\pi_{k+1}(\cdot|\mathbf{y}_{[k+1]}), \bar{\pi}_{k+1}^T(\cdot|\mathbf{y}_{[k+1]}) \right) + 2 \, \mathrm{TV}^2 \left(\bar{\pi}_{k+1}^T(\cdot|\mathbf{y}_{[k+1]}), \widehat{\pi}_{k+1}^T(\cdot|\mathbf{y}_{[k+1]}) \right).$$

For the second term, we invoke Girsanov theorem (Chen et al., 2023) to show that

$$\mathrm{TV}^2 \left(\bar{\pi}_{k+1}^T(\cdot|\mathbf{y}_{[k+1]}), \widehat{\pi}_{k+1}^T(\cdot|\mathbf{y}_{[k+1]}) \right)$$

$$\leq 2 \, \mathrm{KL} \left(\bar{\pi}_{k+1}^T(\cdot|\mathbf{y}_{[k+1]}), \widehat{\pi}_{k+1}^T(\cdot|\mathbf{y}_{[k+1]}) \right)$$

$$\leq \sum_{\ell=0}^{K-1} h \mathbb{E}_{\bar{\mathbf{Z}}_{\ell h}} \left[\| \nabla_{\mathbf{x}} \log \pi_{k+1}(\bar{\mathbf{Z}}_{\ell h}|\mathbf{y}_{[k+1]}) - \widehat{\mathbf{b}}_{k+1}(\bar{\mathbf{Z}}_{\ell h}, \mathbf{y}_{[k+1]}) \|_2^2 \right]$$

$$= \sum_{\ell=0}^{K-1} h \mathbb{E}_{\bar{\mathbf{Z}}_{\ell h}} \left[\| \nabla_{\mathbf{x}} \log q_{k+1}(\bar{\mathbf{Z}}_{\ell h}|\mathbf{y}_{[k]}) - \widehat{\mathbf{s}}_{k+1}(\bar{\mathbf{Z}}_{\ell h}, \mathbf{y}_{[k]}) \|_2^2 \right]$$

$$\leq 2 \sum_{\ell=0}^{K-1} h \mathbb{E}_{\bar{\mathbf{Z}}_{\ell h}} \left[\| \nabla_{\mathbf{x}} \log q_{k+1}(\bar{\mathbf{Z}}_{\ell h}|\mathbf{y}_{[k]}) - \nabla_{\mathbf{x}} \log \widehat{q}_{k+1}(\bar{\mathbf{Z}}_{\ell h}|\mathbf{y}_{[k]}) \|_2^2 \right]$$

$$+ 2 \sum_{\ell=0}^{K-1} h \mathbb{E}_{\bar{\mathbf{Z}}_{\ell h}} \left[\| \nabla_{\mathbf{x}} \log \widehat{q}_{k+1}(\bar{\mathbf{Z}}_{\ell h}|\mathbf{y}_{[k]}) - \widehat{\mathbf{s}}_{k+1}(\bar{\mathbf{Z}}_{\ell h}, \mathbf{y}_{[k]}) \|_2^2 \right]$$

$$\leq 2T \| \nabla_{\mathbf{x}} \log q_{k+1}(\cdot|\mathbf{y}_{[k]}) - \nabla_{\mathbf{x}} \log \widehat{q}_{k+1}(\cdot|\mathbf{y}_{[k]}) \|_{L^\infty(\mathbb{R}^d)}^2$$

$$+ 2 \sum_{\ell=0}^{K-1} h \mathbb{E}_{\bar{\mathbf{Z}}_{\ell h}} \left[\| \nabla_{\mathbf{x}} \log \widehat{q}_{k+1}(\bar{\mathbf{Z}}_{\ell h}|\mathbf{y}_{[k]}) - \widehat{\mathbf{s}}_{k+1}(\bar{\mathbf{Z}}_{\ell h}, \mathbf{y}_{[k]}) \|_2^2 \right],$$

where the first inequality follows from Pinsker's inequality (Lemma I.5), the second inequality invokes Girsanov theorem (Chen et al., 2023), and the third inequality is due to the triangular inequality. This completes the proof. □

D.2. **Error of the posterior sampling and assimilation.**

Proof of Theorem 3.2. Substituting Lemmas E.1, F.1, and G.1 into Lemma D.1

$$(\varepsilon_{\mathrm{TV}}^{k+1})^2 \leq \frac{1}{2} \exp\Big(-\frac{T}{5C_{\mathrm{LSI}}} \Big)\eta_\chi^2 + 70dC_{\mathrm{LSI}}\lambda^2 h + 64B^4 D^4 T(\varepsilon_{\mathrm{TV}}^k)^2$$
$$+ 112C_{\mathrm{LSI}}\sqrt{\kappa B^3 D^3}\eta_\chi\Delta + 32\sqrt{\kappa B^3 D^3}T\Delta,$$

where we used Lemma I.4. This completes the proof. □

Proof of Corollary 3.3. A direct conclusion of Theorem 3.2. □

Proof of Theorem 3.4. According to Corollary 3.3, we have that for each $k \in \mathbb{N}$,

(D.4) $$(\varepsilon_{\mathrm{TV}}^{k+1})^2 \leq C_{\mathrm{LSI}}^k(CB^4 D^4)^k \log^k\Big(\frac{\eta_\chi^2}{\varepsilon^2}\Big)\big\{(\varepsilon_{\mathrm{TV}}^1)^2 + (k-1)\varepsilon^2\big\}.$$

On the other hand, if the terminal time T, the step size h, and the score matching error Δ are set, respectively, as

$$T = \Theta\Big(C_{\mathrm{LSI}} \log\Big(\frac{\eta_\chi^2}{\varepsilon^2}\Big)\Big), \quad h = \Theta\Big(\frac{\varepsilon^2}{dC_{\mathrm{LSI}}\lambda^2}\Big), \quad \Delta = \Theta\Big(\frac{\varepsilon^2}{\sqrt{\kappa B^3 D^3}(T + C_{\mathrm{LSI}}\eta_\chi)}\Big),$$

it follows from Lemma H.1 that

(D.5) $$(\varepsilon_{\mathrm{TV}}^1)^2 \lesssim C_{\mathrm{LSI}} \log\Big(\frac{\eta_\chi^2}{\varepsilon^2}\Big)\|\nabla_{\mathbf{x}} \log q_1 - \nabla_{\mathbf{x}} \log \widehat{q}_1\|_{L^\infty(\mathbb{R}^d)}^2 + \varepsilon^2.$$

Combining (D.4) and (D.5) completes the proof. □

APPENDIX E. CONVERGENCE OF LANGEVIN MONTE CARLO

In this section, we aim to analyze the convergence of the Langevin Monte Carlo

$$\mathrm{TV}^2\big(\pi_{k+1}(\cdot|\mathbf{y}_{[k+1]}), \bar{\pi}_{k+1}^T(\cdot|\mathbf{y}_{[k+1]})\big).$$

Indeed, we provide a stronger convergence result in χ^2-divergence rather than the TV distance, since bounding the error of the score matching (Appendix G) also requires the convergence results in χ^2-divergence.

Lemma E.1. *Suppose Assumptions 1 and 2 hold. Then*

$$\chi^2\big(\bar{\pi}_{k+1}^T(\cdot|\mathbf{y}_{[k+1]})\|\pi_{k+1}(\cdot|\mathbf{y}_{[k+1]})\big) \leq \exp\Big(-\frac{T}{5C_{\mathrm{LSI}}} \Big)\eta_\chi^2 + 140dC_{\mathrm{LSI}}\lambda^2 h,$$

where $T = Kh$, and the step size $h > 0$ satisfies $400dC_{\mathrm{LSI}}\lambda^2 h \leq 1$.

Remark E.2. The proof of Lemma E.1 is inspired by Lee et al. (2022, Theorem 2.1), and Chewi et al. (2024, Theorem 4). We show the proof in this section for the sake of completeness. The first term in Lemma E.1 converges to zero exponentially as the time T increases, which corresponds to the convergence of the Langevin diffusion (D.1). The second term is linear with respect to the step size h, induced by the Euler-Maruyama approximation.

Recall the Langevin Monte Carlo (D.2). For each $0 \leq \ell \leq K - 1$ and $\ell h \leq t \leq (\ell + 1)h$,

$$\bar{\mathbf{Z}}_t = \bar{\mathbf{Z}}_{\ell h} + \int_{\ell h}^t \nabla_{\mathbf{x}} \log \pi_{k+1}(\bar{\mathbf{Z}}_{\ell h}|\mathbf{y}_{[k+1]})\,\mathrm{d}s + \sqrt{2}\int_{\ell h}^t \mathrm{d}\mathbf{B}_s$$

(E.1) $$= \bar{\mathbf{Z}}_{\ell h} + (t - \ell h)\nabla_{\mathbf{x}} \log \pi_{k+1}(\bar{\mathbf{Z}}_{\ell h}|\mathbf{y}_{[k+1]}) + \sqrt{2}(\mathbf{B}_t - \mathbf{B}_{\ell h}),$$

where $\mathbf{B}_t - \mathbf{B}_{\ell h} \sim N(\mathbf{0}, (t - \ell h)\mathbf{I}_d)$ is independent of $\bar{\mathbf{Z}}_{\ell h}$.

E.1. **Differential inequality for the chi-squared divergence.** The most crucial recipe in the proof of Lemma E.1 is the following differential inequality for the χ^2-divergence, which is inspired by Chewi et al. (2024, Theorem 4) and Lee et al. (2022, Theorem 4.2).

Before proceeding, we introduce some notations and properties. Define the Radon-Nikodym derivative of $\bar{\pi}_{k+1}^t$ with respect to π_{k+1}

$$\text{(E.2)} \qquad \phi_{k+1}^t(\mathbf{x}|\mathbf{y}_{[k+1]}) := \frac{\bar{\pi}_{k+1}^t(\mathbf{x}|\mathbf{y}_{[k+1]})}{\pi_{k+1}(\mathbf{x}|\mathbf{y}_{[k+1]})}, \quad \mathbf{x} \in \mathbb{R}^d.$$

Apparently, we find

$$\text{(E.3)} \qquad \mathbb{E}_{\mathbf{Z}}[\phi_{k+1}^t(\mathbf{Z}|\mathbf{y}_{[k+1]})^2] = \mathbb{E}_{\bar{\mathbf{Z}}_t}[\phi_{k+1}^t(\bar{\mathbf{Z}}_t|\mathbf{y}_{[k+1]})].$$

Further, we define

$$\text{(E.4)} \qquad \psi_{k+1}^t(\mathbf{x}|\mathbf{y}_{[k+1]}) := \frac{\phi_{k+1}^t(\mathbf{x}|\mathbf{y}_{[k+1]})}{\mathbb{E}_{\mathbf{Z}}[\phi_{k+1}^t(\mathbf{Z}|\mathbf{y}_{[k+1]})^2]}, \quad \mathbf{x} \in \mathbb{R}^d.$$

Then it is straightforward that

$$\mathbb{E}_{\bar{\mathbf{Z}}_t}\left[\psi_{k+1}^t(\bar{\mathbf{Z}}_t|\mathbf{y}_{[k+1]})\right] = \int \psi_{k+1}^t(\mathbf{x}|\mathbf{y}_{[k+1]})\phi_{k+1}^t(\mathbf{x}|\mathbf{y}_{[k+1]})\pi_{k+1}(\mathbf{x}|\mathbf{y}_{[k+1]})\,\mathrm{d}\mathbf{x}$$

$$\text{(E.5)} \qquad = \int \frac{\phi_{k+1}^t(\mathbf{x}|\mathbf{y}_{[k+1]})^2}{\mathbb{E}_{\mathbf{Z}}[\phi_{k+1}^t(\mathbf{Z}|\mathbf{y}_{[k+1]})^2]}\pi_{k+1}(\mathbf{x}|\mathbf{y}_{[k+1]})\,\mathrm{d}\mathbf{x} = 1.$$

The following lemmas shows that the derivative of the χ^2-divergence can be bounded by two parts: Dirichlet energy and the discretization error.

Lemma E.3. *For each $\ell h \leq t \leq (\ell+1)h$, it holds that*

$$\frac{\mathrm{d}}{\mathrm{d}t}\chi^2\big(\bar{\pi}_{k+1}^t(\cdot|\mathbf{y}_{[k+1]})\|\pi_{k+1}(\cdot|\mathbf{y}_{[k+1]})\big)$$

$$\leq - \underbrace{\mathbb{E}_{\mathbf{Z}}\big[\|\nabla_{\mathbf{x}}\phi_{k+1}^t(\mathbf{Z}|\mathbf{y}_{[k+1]})\|_2^2\big]}_{\textit{Dirichlet energy}}$$

$$+ \underbrace{\mathbb{E}_{\mathbf{Z}}\big[\phi_{k+1}^t(\mathbf{Z}|\mathbf{y}_{[k+1]})^2\big]\mathbb{E}_{(\bar{\mathbf{Z}}_{\ell h},\bar{\mathbf{Z}}_t)}\big[\|\mathbf{e}_{k+1}(\bar{\mathbf{Z}}_{\ell h},\bar{\mathbf{Z}}_t|\mathbf{y}_{[k+1]})\|_2^2\psi_{k+1}^t(\bar{\mathbf{Z}}_t|\mathbf{y}_{[k+1]})\big]}_{\textit{discretization error}}$$

where the pointwise discretization error is defined as

$$\mathbf{e}_{k+1}(\mathbf{x}_{\ell h},\mathbf{x}|\mathbf{y}_{[k+1]}) := \nabla_{\mathbf{x}}\log\pi_{k+1}(\mathbf{x}_{\ell h}|\mathbf{y}_{[k+1]}) - \nabla_{\mathbf{x}}\log\pi_{k+1}(\mathbf{x}|\mathbf{y}_{[k+1]}).$$

Here the expectation $\mathbb{E}_{\mathbf{Z}}[\cdot]$ is taken with respect to $\mathbf{Z} \sim \pi_{k+1}(\cdot|\mathbf{y}_{[k+1]})$, and the expectation $\mathbb{E}_{(\bar{\mathbf{Z}}_{\ell h},\bar{\mathbf{Z}}_t)}[\cdot]$ is taken with respect to $(\bar{\mathbf{Z}}_{\ell h},\bar{\mathbf{Z}}_t) \sim \bar{\pi}_{k+1}^{\ell h,t}(\cdot|\mathbf{y}_{[k+1]})$.

Remark E.4. According to Vempala and Wibisono (2019, Lemma 6), the law of the Langevin diffusion (D.1) $\pi_{k+1}^t(\cdot|\mathbf{y}_{[k+1]})$ satisfies

$$\frac{\mathrm{d}}{\mathrm{d}t}\chi^2\big(\pi_{k+1}^t(\cdot|\mathbf{y}_{[k+1]})\|\pi_{k+1}(\cdot|\mathbf{y}_{[k+1]})\big) \leq -2\mathbb{E}_{\mathbf{Z}}\big[\|\nabla_{\mathbf{x}}\phi_{k+1}^t(\mathbf{Z}|\mathbf{y}_{[k+1]})\|_2^2\big],$$

which can also be derived from (E.8). Compared with this inequality, the differential inequality of the Langevin Monte Carlo in Lemma E.3 has an additional term known as the discretization error.

We first introduce the Fokker-Planck equation associated to the Langevin Monte Carlo (D.2), which has appeared in Chewi et al. (2024, Proposition 17).

Lemma E.5. *For each $\ell h \le t \le (\ell+1)h$, the law of Langevin Monte Carlo* (D.2) *satisfies the Fokker-Planck equation*

$$\frac{\partial}{\partial t}\bar{\pi}^t_{k+1}(\mathbf{x}|\mathbf{y}_{[k+1]}) = -\nabla_{\mathbf{x}} \cdot \left(\bar{\pi}^t_{k+1}(\mathbf{x}|\mathbf{y}_{[k+1]})\bar{\mathbf{b}}^t_{k+1}(\mathbf{x}|\mathbf{y}_{[k+1]})\right) + \Delta_{\mathbf{x}}\bar{\pi}^t_{k+1}(\mathbf{x}|\mathbf{y}_{[k+1]}),$$

where the drift term is given as

(E.6) $$\bar{\mathbf{b}}^t_{k+1}(\mathbf{x}|\mathbf{y}_{[k+1]}) = \mathbb{E}\left[\nabla_{\mathbf{x}} \log \pi_{k+1}(\bar{\mathbf{Z}}_{\ell h}|\mathbf{y}_{[k+1]})|\bar{\mathbf{Z}}_t = \mathbf{x}, \mathbf{Y}^{[k+1]} = \mathbf{y}_{[k+1]}\right].$$

Proof of Lemma E.5. Let $\bar{\pi}^{t|\ell h}_{k+1}(\cdot|\mathbf{x}_{\ell h}, \mathbf{y}_{[k+1]})$ denote the conditional distribution of $\bar{\mathbf{Z}}_t$ given $\bar{\mathbf{Z}}_{\ell h} = \mathbf{x}_{\ell h}$ and $\mathbf{Y}^{[k+1]} = \mathbf{y}_{[k+1]}$, which satisfies the Fokker-Planck equation (Pavliotis, 2014, Theorem 2.2)

$$\frac{\partial}{\partial t}\bar{\pi}^{t|\ell h}_{k+1}(\mathbf{x}|\mathbf{x}_{\ell h}, \mathbf{y}_{[k+1]})$$

(E.7) $$= \nabla_{\mathbf{x}} \cdot \left(-\bar{\pi}^{t|\ell h}_{k+1}(\mathbf{x}|\mathbf{x}_{\ell h}, \mathbf{y}_{[k+1]})\nabla_{\mathbf{x}} \log \pi_{k+1}(\mathbf{x}_{\ell h}|\mathbf{y}_{[k+1]})\right) + \Delta_{\mathbf{x}}\bar{\pi}^{t|\ell h}_{k+1}(\mathbf{x}|\mathbf{x}_{\ell h}, \mathbf{y}_{[k+1]}).$$

Multiplying both sides of the equality by $\bar{\pi}^{\ell h}_{k+1}(\mathbf{x}_{\ell h}|\mathbf{y}_{[k+1]})$ and then integrating with respect to $\mathbf{x}_{\ell h} \in \mathbb{R}^d$ deduces

$$\frac{\partial}{\partial t}\bar{\pi}^t_{k+1}(\mathbf{x}|\mathbf{y}_{[k+1]})$$

$$= \frac{\partial}{\partial t}\int \bar{\pi}^{t|\ell h}_{k+1}(\mathbf{x}|\mathbf{x}_{\ell h}, \mathbf{y}_{[k+1]})\bar{\pi}^{\ell h}_{k+1}(\mathbf{x}_{\ell h}|\mathbf{y}_{[k+1]})\,\mathrm{d}\mathbf{x}_{\ell h}$$

$$= \int \frac{\partial}{\partial t}\bar{\pi}^{t|\ell h}_{k+1}(\mathbf{x}|\mathbf{x}_{\ell h}, \mathbf{y}_{[k+1]})\bar{\pi}^{\ell h}_{k+1}(\mathbf{x}_{\ell h}|\mathbf{y}_{[k+1]})\,\mathrm{d}\mathbf{x}_{\ell h}$$

$$= -\int \nabla_{\mathbf{x}} \cdot \left(\bar{\pi}^{t|\ell h}_{k+1}(\mathbf{x}|\mathbf{x}_{\ell h}, \mathbf{y}_{[k+1]})\nabla_{\mathbf{x}} \log \pi_{k+1}(\mathbf{x}_{\ell h}|\mathbf{y}_{[k+1]})\right)\bar{\pi}^{\ell h}_{k+1}(\mathbf{x}_{\ell h}|\mathbf{y}_{[k+1]})\,\mathrm{d}\mathbf{x}_{\ell h}$$

$$+ \int \Delta_{\mathbf{x}}\bar{\pi}^{t|\ell h}_{k+1}(\mathbf{x}|\mathbf{x}_{\ell h}, \mathbf{y}_{[k+1]})\bar{\pi}^{\ell h}_{k+1}(\mathbf{x}_{\ell h}|\mathbf{y}_{[k+1]})\,\mathrm{d}\mathbf{x}_{\ell h}$$

$$= -\int \nabla_{\mathbf{x}} \cdot \left(\bar{\pi}^{t,\ell h}_{k+1}(\mathbf{x}, \mathbf{x}_{\ell h}|\mathbf{y}_{[k+1]})\nabla_{\mathbf{x}} \log \pi_{k+1}(\mathbf{x}_{\ell h}|\mathbf{y}_{[k+1]})\right)\,\mathrm{d}\mathbf{x}_{\ell h}$$

$$+ \int \Delta_{\mathbf{x}}\bar{\pi}^{t,\ell h}_{k+1}(\mathbf{x}, \mathbf{x}_{\ell h}|\mathbf{y}_{[k+1]})\,\mathrm{d}\mathbf{x}_{\ell h}$$

$$= -\nabla_{\mathbf{x}} \cdot \left(\bar{\pi}^t_{k+1}(\mathbf{x}|\mathbf{y}_{[k+1]})\int \bar{\pi}^{\ell h|t}_{k+1}(\mathbf{x}_{\ell h}|\mathbf{x}, \mathbf{y}_{[k+1]})\nabla_{\mathbf{x}} \log \pi_{k+1}(\mathbf{x}_{\ell h}|\mathbf{y}_{[k+1]})\,\mathrm{d}\mathbf{x}_{\ell h}\right)$$

$$+ \Delta_{\mathbf{x}}\bar{\pi}^t_{k+1}(\mathbf{x}|\mathbf{y}_{[k+1]})\int \bar{\pi}^{\ell h|t}_{k+1}(\mathbf{x}_{\ell h}|\mathbf{x}, \mathbf{y}_{[k+1]})\,\mathrm{d}\mathbf{x}_{\ell h}$$

$$= -\nabla_{\mathbf{x}} \cdot \left(\bar{\pi}^t_{k+1}(\mathbf{x}|\mathbf{y}_{[k+1]})\bar{\mathbf{b}}^t_{k+1}(\mathbf{x}|\mathbf{y}_{[k+1]})\right) + \Delta_{\mathbf{x}}\bar{\pi}^t_{k+1}(\mathbf{x}|\mathbf{y}_{[k+1]}),$$

where the first equality holds from Chapman-Kolmogorov identity, the third equality follows from (E.7), and the last equality invokes (E.6). This completes the proof. ☐

Now we are ready to prove Lemma E.3.

Proof of Lemma E.3. According to the definition of the χ^2-divergence, we have

$$\frac{\mathrm{d}}{\mathrm{d}t}\chi^2\big(\bar{\pi}_{k+1}^t(\cdot|\mathbf{y}_{[k+1]})\|\pi_{k+1}(\cdot|\mathbf{y}_{[k+1]})\big)$$

$$= 2\int \frac{\partial \bar{\pi}_{k+1}^t}{\partial t}(\mathbf{x}|\mathbf{y}_{[k+1]})\frac{\bar{\pi}_{k+1}^t(\mathbf{x}|\mathbf{y}_{[k+1]})}{\pi_{k+1}(\mathbf{x}|\mathbf{y}_{[k+1]})}\,\mathrm{d}\mathbf{x}$$

$$= 2\int \nabla_{\mathbf{x}}\cdot\big(-\bar{\pi}_{k+1}^t(\mathbf{x}|\mathbf{y}_{[k+1]})\bar{\mathbf{b}}_{k+1}^t(\mathbf{x}|\mathbf{y}_{[k+1]})\big)\phi_{k+1}^t(\mathbf{x}|\mathbf{y}_{[k+1]})\,\mathrm{d}\mathbf{x}$$

$$\quad + 2\int \Delta_{\mathbf{x}}\bar{\pi}_{k+1}^t(\mathbf{x}|\mathbf{y}_{[k+1]})\phi_{k+1}^t(\mathbf{x}|\mathbf{y}_{[k+1]})\,\mathrm{d}\mathbf{x}$$

$$= 2\underbrace{\mathbb{E}_{\bar{\mathbf{Z}}_t}\big[(\bar{\mathbf{b}}_{k+1}^t - \nabla_{\mathbf{x}}\log\pi_{k+1})(\bar{\mathbf{Z}}_t|\mathbf{y}_{[k+1]})\cdot\nabla_{\mathbf{x}}\phi_{k+1}^t(\bar{\mathbf{Z}}_t|\mathbf{y}_{[k+1]})\big]}_{(\star)}$$

(E.8) $$\quad - 2\mathbb{E}_{\mathbf{Z}}\big[\|\nabla_{\mathbf{x}}\phi_{k+1}^t(\mathbf{Z}|\mathbf{y}_{[k+1]})\|_2^2\big],$$

where the first inequality invokes the chain rule, the second equality holds from Fokker-Planck equation (Lemma E.5) and (E.2), and the last equation used the Green's formula and Lemma I.9. Here the expectation $\mathbb{E}_{\bar{\mathbf{Z}}_t}[\cdot]$ is taken with respect to $\bar{\mathbf{Z}}_t \sim \bar{\pi}_{k+1}^t(\cdot|\mathbf{y}_{[k+1]})$, while the expectation $\mathbb{E}_{\mathbf{Z}}[\cdot]$ is taken with respect to $\mathbf{Z} \sim \pi_{k+1}(\cdot|\mathbf{y}_{[k+1]})$. Now it remains to estimate the term $(\star)$ in (E.8). Notice that

$$\mathbb{E}_{\bar{\mathbf{Z}}_t}\big[\bar{\mathbf{b}}_{k+1}^t(\bar{\mathbf{Z}}_t|\mathbf{y}_{[k+1]})\cdot\nabla_{\mathbf{x}}\phi_{k+1}^t(\bar{\mathbf{Z}}_t|\mathbf{y}_{[k+1]})\big]$$

$$= \int \bar{\pi}_{k+1}^t(\mathbf{x}|\mathbf{y}_{[k+1]})\bar{\mathbf{b}}_{k+1}^t(\mathbf{x}|\mathbf{y}_{[k+1]})\cdot\nabla_{\mathbf{x}}\phi_{k+1}^t(\mathbf{x}|\mathbf{y}_{[k+1]})\,\mathrm{d}\mathbf{x}$$

$$= \iint \bar{\pi}_{k+1}^{\ell h,t}(\mathbf{x}_{\ell h},\mathbf{x}|\mathbf{y}_{[k+1]})\nabla_{\mathbf{x}}\log\pi_{k+1}(\mathbf{x}_{\ell h}|\mathbf{y}_{[k+1]})\cdot\nabla_{\mathbf{x}}\phi_{k+1}^t(\mathbf{x}|\mathbf{y}_{[k+1]})\,\mathrm{d}\mathbf{x}_{\ell h}\,\mathrm{d}\mathbf{x}$$

$$= \mathbb{E}_{(\bar{\mathbf{Z}}_{\ell h},\bar{\mathbf{Z}}_t)}\big[\nabla_{\mathbf{x}}\log\pi_{k+1}(\bar{\mathbf{Z}}_{\ell h}|\mathbf{y}_{[k+1]})\cdot\nabla_{\mathbf{x}}\phi_{k+1}^t(\bar{\mathbf{Z}}_t|\mathbf{y}_{[k+1]})\big],$$

where we used the definition of $\bar{\mathbf{b}}_{k+1}^t(\mathbf{x}|\mathbf{y}_{[k+1]})$ as (E.6). As a consequence,

$$(\star) = \mathbb{E}_{\bar{\mathbf{Z}}_t}\big[(\bar{\mathbf{b}}_{k+1}^t - \nabla_{\mathbf{x}}\log\pi_{k+1})(\bar{\mathbf{Z}}_t|\mathbf{y}_{[k+1]})\cdot\nabla_{\mathbf{x}}\phi_{k+1}^t(\bar{\mathbf{Z}}_t|\mathbf{y}_{[k+1]})\big]$$

$$= \mathbb{E}_{(\bar{\mathbf{Z}}_{\ell h},\bar{\mathbf{Z}}_t)}\big[\mathbf{e}_{k+1}(\bar{\mathbf{Z}}_{\ell h},\bar{\mathbf{Z}}_t|\mathbf{y}_{[k+1]})\cdot\nabla_{\mathbf{x}}\phi_{k+1}^t(\bar{\mathbf{Z}}_t|\mathbf{y}_{[k+1]})\big]$$

$$= \mathbb{E}_{(\bar{\mathbf{Z}}_{\ell h},\bar{\mathbf{Z}}_t)}\Big[\mathbf{e}_{k+1}(\bar{\mathbf{Z}}_{\ell h},\bar{\mathbf{Z}}_t|\mathbf{y}_{[k+1]})\sqrt{\phi_{k+1}^t(\bar{\mathbf{Z}}_t|\mathbf{y}_{[k+1]})}\cdot\frac{\nabla_{\mathbf{x}}\phi_{k+1}^t(\bar{\mathbf{Z}}_t|\mathbf{y}_{[k+1]})}{\sqrt{\phi_{k+1}^t(\bar{\mathbf{Z}}_t|\mathbf{y}_{[k+1]})}}\Big]$$

$$\leq \mathbb{E}_{(\bar{\mathbf{Z}}_{\ell h},\bar{\mathbf{Z}}_t)}^{\frac{1}{2}}\big[\|\mathbf{e}_{k+1}(\bar{\mathbf{Z}}_{\ell h},\bar{\mathbf{Z}}_t|\mathbf{y}_{[k+1]})\|_2^2\phi_{k+1}^t(\bar{\mathbf{Z}}_t|\mathbf{y}_{[k+1]})\big]\mathbb{E}_{\mathbf{Z}}^{\frac{1}{2}}\big[\|\nabla_{\mathbf{x}}\phi_{k+1}^t(\mathbf{Z}|\mathbf{y}_{[k+1]})\|_2^2\big]$$

$$\leq \frac{1}{2}\mathbb{E}_{(\bar{\mathbf{Z}}_{\ell h},\bar{\mathbf{Z}}_t)}\big[\|\mathbf{e}_{k+1}(\bar{\mathbf{Z}}_{\ell h},\bar{\mathbf{Z}}_t|\mathbf{y}_{[k+1]})\|_2^2\phi_{k+1}^t(\bar{\mathbf{Z}}_t|\mathbf{y}_{[k+1]})\big]$$

$$\quad + \frac{1}{2}\mathbb{E}_{\mathbf{Z}}\big[\|\nabla_{\mathbf{x}}\phi_{k+1}^t(\mathbf{Z}|\mathbf{y}_{[k+1]})\|_2^2\big]$$

$$= \frac{1}{2}\mathbb{E}_{\mathbf{Z}}\big[\phi_{k+1}^t(\mathbf{Z}|\mathbf{y}_{[k+1]})^2\big]\mathbb{E}_{(\bar{\mathbf{Z}}_{\ell h},\bar{\mathbf{Z}}_t)}\big[\|\mathbf{e}_{k+1}(\bar{\mathbf{Z}}_{\ell h},\bar{\mathbf{Z}}_t|\mathbf{y}_{[k+1]})\|_2^2\psi_{k+1}^t(\bar{\mathbf{Z}}_t|\mathbf{y}_{[k+1]})\big]$$

(E.9) $$\quad + \frac{1}{2}\mathbb{E}_{\mathbf{Z}}\big[\|\nabla_{\mathbf{x}}\phi_{k+1}^t(\mathbf{Z}|\mathbf{y}_{[k+1]})\|_2^2\big],$$

where the first inequality invokes the Cauchy-Schwarz inequality, the second inequality follows from $ab \leq (a^2 + b^2)/2$. Substituting (E.9) into (E.8) completes the proof. $\square$

E.2. **Dirichlet energy and chi-squared divergence.** We relate the Dirichlet energy to χ^2-divergence by the following lemma.

Lemma E.6. *Suppose Assumption 2 holds. Then*

$$\frac{1}{2C_{\mathrm{LSI}}}\chi^2\big(\bar{\pi}_{k+1}^t(\cdot|\mathbf{y}_{[k+1]})\|\pi_{k+1}(\cdot|\mathbf{y}_{[k+1]})\big) \leq \mathbb{E}_{\mathbf{Z}}\big[\|\nabla_{\mathbf{x}}\phi_{k+1}^t(\mathbf{Z}|\mathbf{y}_{[k+1]})\|_2^2\big].$$

Proof of Lemma E.6. A direct conclusion of Lemma I.10.   □

E.3. **Discretization error.** The main results for the discretization error is stated as follows.

Lemma E.7. *Suppose Assumptions 1 and 2 hold. Then for each $\ell h \leq t \leq (\ell+1)h$,*

$$\mathbb{E}_{\mathbf{Z}}\big[\phi_{k+1}^t(\mathbf{Z}|\mathbf{y}_{[k+1]})^2\big]\mathbb{E}_{(\bar{\mathbf{Z}}_{\ell h},\bar{\mathbf{Z}}_t)}\Big[\|\mathbf{e}_{k+1}(\bar{\mathbf{Z}}_{\ell h},\bar{\mathbf{Z}}_t|\mathbf{y}_{[k+1]})\|_2^2\psi_{k+1}^t(\bar{\mathbf{Z}}_t|\mathbf{y}_{[k+1]})\Big]$$
$$\leq 80C_{\mathrm{LSI}}\lambda^2(t-\ell h)\mathbb{E}_{\mathbf{Z}}[\|\nabla_{\mathbf{x}}\phi_{k+1}^t(\mathbf{Z}|\mathbf{y}_{[k+1]})\|_2^2] + 20d\lambda^2(t-\ell h)\mathbb{E}_{\mathbf{Z}}\big[\phi_{k+1}^t(\mathbf{Z}|\mathbf{y}_{[k+1]})^2\big],$$

where the step size $h > 0$ satisfies $4\lambda h \leq 1$.

To verify Lemma E.7, we provide some auxiliary lemmas.

Lemma E.8. *Suppose Assumption 1 holds. Then for each $\ell h \leq t \leq (\ell+1)h$,*

$$\mathbb{E}_{(\bar{\mathbf{Z}}_{\ell h},\bar{\mathbf{Z}}_t)}\Big[\|\mathbf{e}_{k+1}(\bar{\mathbf{Z}}_{\ell h},\bar{\mathbf{Z}}_t|\mathbf{y}_{[k+1]})\|_2^2\psi_{k+1}^t(\bar{\mathbf{Z}}_t|\mathbf{y}_{[k+1]})\Big]$$
$$\leq 8\lambda^2(t-\ell h)^2\mathbb{E}_{\bar{\mathbf{Z}}_t}\Big[\|\nabla_{\mathbf{x}}\log\pi_{k+1}(\bar{\mathbf{Z}}_t|\mathbf{y}_{[k+1]})\|_2^2\psi_{k+1}^t(\bar{\mathbf{Z}}_t|\mathbf{y}_{[k+1]})\Big]$$
$$+ 6\lambda^2\mathbb{E}_{(\mathbf{B}_{\ell h},\mathbf{B}_t,\bar{\mathbf{Z}}_t)}\Big[\|\mathbf{B}_t - \mathbf{B}_{\ell h}\|_2^2\psi_{k+1}^t(\bar{\mathbf{Z}}_t|\mathbf{y}_{[k+1]})\Big],$$

where the step size $h > 0$ satisfies $4\lambda h \leq 1$.

Proof of Lemma E.8. Recall the solution to the Langevin Monte Carlo (E.1), which implies

$$(E.10) \qquad \|\bar{\mathbf{Z}}_t - \bar{\mathbf{Z}}_{\ell h}\|_2^2 \leq 2(t-\ell h)^2\|\nabla_{\mathbf{x}}\log\pi_{k+1}(\bar{\mathbf{Z}}_{\ell h}|\mathbf{y}_{[k+1]})\|_2^2 + 4\|\mathbf{B}_t - \mathbf{B}_{\ell h}\|_2^2,$$

where the first inequality invokes the triangular inequality, and last inequality holds from the fact $\ell h \leq t \leq (\ell+1)h$. According to Assumption 1, we have

$$\|\nabla_{\mathbf{x}}\log\pi_{k+1}(\bar{\mathbf{Z}}_t|\mathbf{y}_{[k+1]}) - \nabla_{\mathbf{x}}\log\pi_{k+1}(\bar{\mathbf{Z}}_{\ell h}|\mathbf{y}_{[k+1]})\|_2^2$$
$$\leq \lambda^2\|\bar{\mathbf{Z}}_t - \bar{\mathbf{Z}}_{\ell h}\|_2^2$$
$$(E.11) \qquad \leq 2\lambda^2(t-\ell h)^2\|\nabla_{\mathbf{x}}\log\pi_{k+1}(\bar{\mathbf{Z}}_{\ell h}|\mathbf{y}_{[k+1]})\|_2^2 + 4\lambda^2\|\mathbf{B}_t - \mathbf{B}_{\ell h}\|_2^2,$$

where the last inequality used (E.1). As a consequence, for each step size h with $4\lambda h \leq 1$,

$$\|\nabla_{\mathbf{x}}\log\pi_{k+1}(\bar{\mathbf{Z}}_{\ell h}|\mathbf{y}_{[k+1]})\|_2^2$$
$$\leq 2\|\nabla_{\mathbf{x}}\log\pi_{k+1}(\bar{\mathbf{Z}}_t|\mathbf{y}_{[k+1]}) - \nabla_{\mathbf{x}}\log\pi_{k+1}(\bar{\mathbf{Z}}_{\ell h}|\mathbf{y}_{[k+1]})\|_2^2 + 2\|\nabla_{\mathbf{x}}\log\pi_{k+1}(\bar{\mathbf{Z}}_t|\mathbf{y}_{[k+1]})\|_2^2$$
$$\leq 4\lambda^2(t-\ell h)^2\|\nabla_{\mathbf{x}}\log\pi_{k+1}(\bar{\mathbf{Z}}_{\ell h}|\mathbf{y}_{[k+1]})\|_2^2 + 8\lambda^2\|\mathbf{B}_t - \mathbf{B}_{\ell h}\|_2^2 + 2\|\nabla_{\mathbf{x}}\log\pi_{k+1}(\bar{\mathbf{Z}}_t|\mathbf{y}_{[k+1]})\|_2^2$$
$$\leq \frac{1}{4}\|\nabla_{\mathbf{x}}\log\pi_{k+1}(\bar{\mathbf{Z}}_{\ell h}|\mathbf{y}_{[k+1]})\|_2^2 + 8\lambda^2\|\mathbf{B}_t - \mathbf{B}_{\ell h}\|_2^2 + 2\|\nabla_{\mathbf{x}}\log\pi_{k+1}(\bar{\mathbf{Z}}_t|\mathbf{y}_{[k+1]})\|_2^2,$$

where the first inequality follows from the triangular inequality. Rearranging this inequality yields

$$\|\nabla_{\mathbf{x}}\log\pi_{k+1}(\bar{\mathbf{Z}}_{\ell h}|\mathbf{y}_{[k+1]})\|_2^2$$
$$(E.12) \qquad \leq 16\lambda^2\|\mathbf{B}_t - \mathbf{B}_{\ell h}\|_2^2 + 4\|\nabla_{\mathbf{x}}\log\pi_{k+1}(\bar{\mathbf{Z}}_t|\mathbf{y}_{[k+1]})\|_2^2.$$

Then substituting (E.12) into (E.11) yields

$$\|\nabla_{\mathbf{x}} \log \pi_{k+1}(\bar{\mathbf{Z}}_t|\mathbf{y}_{[k+1]}) - \nabla_{\mathbf{x}} \log \pi_{k+1}(\bar{\mathbf{Z}}_{\ell h}|\mathbf{y}_{[k+1]})\|_2^2$$

$$\leq 8\lambda^2(t - \ell h)^2 \|\nabla_{\mathbf{x}} \log \pi_{k+1}(\bar{\mathbf{Z}}_t|\mathbf{y}_{[k+1]})\|_2^2 + \{32\lambda^4 h^2 + 4\lambda^2\}\|\mathbf{B}_t - \mathbf{B}_{\ell h}\|_2^2$$

$$(E.13) \qquad \leq 8\lambda^2(t - \ell h)^2 \|\nabla_{\mathbf{x}} \log \pi_{k+1}(\bar{\mathbf{Z}}_t|\mathbf{y}_{[k+1]})\|_2^2 + 6\lambda^2\|\mathbf{B}_t - \mathbf{B}_{\ell h}\|_2^2,$$

where we used the inequality $4\lambda h \leq 1$. Multiplying both sides of (E.13) by ψ_{k+1}^t and taking expectation complete the proof. $\qquad\square$

We bound the first term in Lemma E.7 by the following lemma, which is based on Chewi et al. (2024, Lemma 20).

Lemma E.9. *Suppose Assumption 1 holds. Then for each* $\ell h \leq t \leq (\ell + 1)h$,

$$\mathbb{E}_{\bar{\mathbf{Z}}_t}\left[\|\nabla_{\mathbf{x}} \log \pi_{k+1}(\bar{\mathbf{Z}}_t|\mathbf{y}_{[k+1]})\|_2^2 \psi_{k+1}^t(\bar{\mathbf{Z}}_t|\mathbf{y}_{[k+1]})\right]$$

$$\leq \frac{4\mathbb{E}_{\mathbf{Z}}[\|\nabla_{\mathbf{x}}\phi_{k+1}^t(\mathbf{Z}|\mathbf{y}_{[k+1]})\|_2^2]}{\mathbb{E}_{\mathbf{Z}}[\phi_{k+1}^t(\mathbf{Z}|\mathbf{y}_{[k+1]})^2]} + 2d\lambda,$$

where the expectation $\mathbb{E}_{\mathbf{Z}}[\cdot]$ *is taken with respect to* $\mathbf{Z} \sim \pi_{k+1}(\cdot|\mathbf{y}_{[k+1]})$.

Proof of Lemma E.9. According to (E.5), we define a change of measure

$$\mu_{k+1}^t(\mathbf{x}|\mathbf{y}_{[k+1]}) := \psi_{k+1}^t(\mathbf{x}|\mathbf{y}_{[k+1]})\bar{\pi}_{k+1}^t(\mathbf{x}|\mathbf{y}_{[k+1]}).$$

Then it suffices to consider the expectation under this change of measures

$$\mathbb{E}_{\widetilde{\mathbf{Z}}_t}\left[\|\nabla_{\mathbf{x}} \log \pi_{k+1}(\widetilde{\mathbf{Z}}_t|\mathbf{y}_{[k+1]})\|_2^2\right]$$

$$= \mathbb{E}_{\bar{\mathbf{Z}}_t}\left[\|\nabla_{\mathbf{x}} \log \pi_{k+1}(\bar{\mathbf{Z}}_t|\mathbf{y}_{[k+1]})\|_2^2 \psi_{k+1}^t(\bar{\mathbf{Z}}_t|\mathbf{y}_{[k+1]})\right],$$

where $\widetilde{\mathbf{Z}}_t$ is a random variable with probability density $\mu_{k+1}^t(\cdot|\mathbf{y}_{[k+1]})$. We first verify that

$$\mathbb{E}_{\widetilde{\mathbf{Z}}_t}\left[\|\nabla_{\mathbf{x}} \log \pi_{k+1}(\widetilde{\mathbf{Z}}_t|\mathbf{y}_{[k+1]})\|_2^2\right]$$

$$(E.14) \qquad \leq \underbrace{\mathbb{E}_{\widetilde{\mathbf{Z}}_t}\left[\Delta_{\mathbf{x}} \log \pi_{k+1}(\widetilde{\mathbf{Z}}_t|\mathbf{y}_{[k+1]})\right]}_{(i)} + \underbrace{\mathbb{E}_{\mathbf{Z}}\left[\nabla_{\mathbf{x}} \log \pi_{k+1}(\mathbf{Z}|\mathbf{y}_{[k+1]}) \cdot \nabla_{\mathbf{x}} \frac{\mu_{k+1}^t(\mathbf{Z}|\mathbf{y}_{[k+1]})}{\pi_{k+1}(\mathbf{Z}|\mathbf{y}_{[k+1]})}\right]}_{(ii)}.$$

Indeed, according to the Green's formula, we obtain

$$\mathbb{E}_{\widetilde{\mathbf{Z}}_t}\left[\Delta_{\mathbf{x}} \log \pi_{k+1}(\widetilde{\mathbf{Z}}_t|\mathbf{y}_{[k+1]})\right]$$

$$= \int \Delta_{\mathbf{x}} \log \pi_{k+1}(\mathbf{x}|\mathbf{y}_{[k+1]}) \frac{\mu_{k+1}^t(\mathbf{x}|\mathbf{y}_{[k+1]})}{\pi_{k+1}(\mathbf{x}|\mathbf{y}_{[k+1]})} \pi_{k+1}(\mathbf{x}|\mathbf{y}_{[k+1]})\, \mathrm{d}\mathbf{x}$$

$$= -\int \nabla_{\mathbf{x}} \log \pi_{k+1}(\mathbf{x}|\mathbf{y}_{[k+1]}) \cdot \nabla_{\mathbf{x}}\left(\frac{\mu_{k+1}^t(\mathbf{x}|\mathbf{y}_{[k+1]})}{\pi_{k+1}(\mathbf{x}|\mathbf{y}_{[k+1]})} \pi_{k+1}(\mathbf{x}|\mathbf{y}_{[k+1]})\right) \mathrm{d}\mathbf{x}$$

$$= -\mathbb{E}_{\mathbf{Z}}\left[\nabla_{\mathbf{x}} \log \pi_{k+1}(\mathbf{Z}|\mathbf{y}_{[k+1]}) \cdot \nabla_{\mathbf{x}} \frac{\mu_{k+1}^t(\mathbf{Z}|\mathbf{y}_{[k+1]})}{\pi_{k+1}(\mathbf{Z}|\mathbf{y}_{[k+1]})}\right] + \mathbb{E}_{\widetilde{\mathbf{Z}}_t}\left[\|\nabla_{\mathbf{x}} \log \pi_{k+1}(\widetilde{\mathbf{Z}}_t|\mathbf{y}_{[k+1]})\|_2^2\right].$$

For the term (i) in (E.15), it follows from Assumption 1 that

$$(E.15) \qquad \mathbb{E}_{\widetilde{\mathbf{Z}}_t}\left[\Delta_{\mathbf{x}} \log \pi_{k+1}(\widetilde{\mathbf{Z}}_t|\mathbf{y}_{[k+1]})\right] \leq d\lambda.$$

For the term (ii) in (E.15), we find

$$
\mathbb{E}_{\mathbf{Z}}\Big[\nabla_{\mathbf{x}}\log\pi_{k+1}(\mathbf{Z}|\mathbf{y}_{[k+1]})\cdot\nabla_{\mathbf{x}}\frac{\mu_{k+1}^t(\mathbf{Z}|\mathbf{y}_{[k+1]})}{\pi_{k+1}(\mathbf{Z}|\mathbf{y}_{[k+1]})}\Big]
$$

$$
= 2\mathbb{E}_{\mathbf{Z}}\Big[\nabla_{\mathbf{x}}\log\pi_{k+1}(\mathbf{Z}|\mathbf{y}_{[k+1]})\sqrt{\frac{\mu_{k+1}^t(\mathbf{Z}|\mathbf{y}_{[k+1]})}{\pi_{k+1}(\mathbf{Z}|\mathbf{y}_{[k+1]})}}\cdot\nabla_{\mathbf{x}}\sqrt{\frac{\mu_{k+1}^t(\mathbf{Z}|\mathbf{y}_{[k+1]})}{\pi_{k+1}(\mathbf{Z}|\mathbf{y}_{[k+1]})}}\Big]
$$

$$
\leq \frac{1}{2}\mathbb{E}_{\mathbf{Z}}\Big[\|\nabla_{\mathbf{x}}\log\pi_{k+1}(\mathbf{Z}|\mathbf{y}_{[k+1]})\|_2^2\frac{\mu_{k+1}^t(\mathbf{Z}|\mathbf{y}_{[k+1]})}{\pi_{k+1}(\mathbf{Z}|\mathbf{y}_{[k+1]})}\Big] + 2\mathbb{E}_{\mathbf{Z}}\Big[\|\nabla_{\mathbf{x}}\sqrt{\frac{\mu_{k+1}^t(\mathbf{Z}|\mathbf{y}_{[k+1]})}{\pi_{k+1}(\mathbf{Z}|\mathbf{y}_{[k+1]})}}\|_2^2\Big]
$$

$$
(\text{E.16}) \quad = \frac{1}{2}\mathbb{E}_{\widetilde{\mathbf{Z}}_t}\Big[\|\nabla_{\mathbf{x}}\log\pi_{k+1}(\widetilde{\mathbf{Z}}_t|\mathbf{y}_{[k+1]})\|_2^2\Big] + 2\mathbb{E}_{\mathbf{Z}}\Big[\|\nabla_{\mathbf{x}}\sqrt{\frac{\mu_{k+1}^t(\mathbf{Z}|\mathbf{y}_{[k+1]})}{\pi_{k+1}(\mathbf{Z}|\mathbf{y}_{[k+1]})}}\|_2^2\Big],
$$

where the second equality holds from the chain rule, and the inequality follows from Young's inequality. Substituting (E.15) and (E.16) into (E.14) implies

$$
(\text{E.17}) \qquad \mathbb{E}_{\widetilde{\mathbf{Z}}_t}\Big[\|\nabla_{\mathbf{x}}\log\pi_{k+1}(\widetilde{\mathbf{Z}}_t|\mathbf{y}_{[k+1]})\|_2^2\Big] \leq 4\mathbb{E}_{\mathbf{Z}}\Big[\|\nabla_{\mathbf{x}}\sqrt{\frac{\mu_{k+1}^t(\mathbf{Z}|\mathbf{y}_{[k+1]})}{\pi_{k+1}(\mathbf{Z}|\mathbf{y}_{[k+1]})}}\|_2^2\Big] + 2d\lambda.
$$

Applying Lemma I.14 to (E.17) yields

$$
\mathbb{E}_{\widetilde{\mathbf{Z}}_t}\Big[\|\nabla_{\mathbf{x}}\log\pi_{k+1}(\widetilde{\mathbf{Z}}_t|\mathbf{y}_{[k+1]})\|_2^2\Big]
$$

$$
\leq \mathbb{E}_{\widetilde{\mathbf{Z}}_t}\Big[\|\nabla_{\mathbf{x}}\log\frac{\mu_{k+1}^t(\widetilde{\mathbf{Z}}_t|\mathbf{y}_{[k+1]})}{\pi_{k+1}(\widetilde{\mathbf{Z}}_t|\mathbf{y}_{[k+1]})}\|_2^2\Big] + 2d\lambda
$$

$$
= \mathbb{E}_{\bar{\mathbf{Z}}_t}\Big[\|\nabla_{\mathbf{x}}\log\frac{\mu_{k+1}^t(\bar{\mathbf{Z}}_t|\mathbf{y}_{[k+1]})}{\pi_{k+1}(\bar{\mathbf{Z}}_t|\mathbf{y}_{[k+1]})}\|_2^2\psi_{k+1}^t(\bar{\mathbf{Z}}_t|\mathbf{y}_{[k+1]})\Big] + 2d\lambda.
$$

Finally, using Lemma I.15 completes the proof. $\qquad\square$

For the second term in Lemma E.7, we have the following result by a similar argument as Chewi et al. (2024, Lemma 19).

Lemma E.10. *Suppose Assumptions 1 and 2 hold. Then for each $\ell h \leq t \leq (\ell+1)h$,*

$$
\mathbb{E}\big[\|\mathbf{B}_t - \mathbf{B}_{\ell h}\|_2^2\psi_{k+1}^t(\bar{\mathbf{Z}}_t|\mathbf{y}_{[k+1]})\big]
$$

$$
\leq 3d(t-\ell h) + 8C_{\text{LSI}}(t-\ell h)\frac{\mathbb{E}_{\mathbf{Z}}[\|\nabla_{\mathbf{x}}\phi_{k+1}^t(\mathbf{Z}|\mathbf{y}_{[k+1]})\|_2^2]}{\mathbb{E}_{\mathbf{Z}}[\phi_{k+1}^t(\mathbf{Z}|\mathbf{y}_{[k+1]})^2]},
$$

where the expectation $\mathbb{E}_{\mathbf{Z}}[\cdot]$ is taken with respect to $\mathbf{Z} \sim \pi_{k+1}(\cdot|\mathbf{y}_{[k+1]})$.

Proof of Lemma E.10. According to Donsker-Varadhan variational principle (Lemma I.11), for each $s > 0$, we have

$$
\mathbb{E}\big[\|\mathbf{B}_t - \mathbf{B}_{\ell h}\|_2^2\psi_{k+1}^t(\bar{\mathbf{Z}}_t|\mathbf{y}_{[k+1]})\big] - \mathbb{E}[\|\mathbf{B}_t - \mathbf{B}_{\ell h}\|_2^2]
$$

$$
= \frac{1}{s}\mathbb{E}\big[s(\|\mathbf{B}_t - \mathbf{B}_{\ell h}\|_2^2 - \mathbb{E}[\|\mathbf{B}_t - \mathbf{B}_{\ell h}\|_2^2])\psi_{k+1}^t(\bar{\mathbf{Z}}_t|\mathbf{y}_{[k+1]})\big]
$$

$$
\leq \frac{1}{s}\text{KL}\big(\mu_{k+1}^t(\cdot|\mathbf{y}_{[k+1]})\|\bar{\pi}_{k+1}^t(\cdot|\mathbf{y}_{[k+1]})\big)
$$

$$
+ \frac{1}{s}\log\mathbb{E}\big[\exp\{s(\|\mathbf{B}_t - \mathbf{B}_{\ell h}\|_2^2 - \mathbb{E}[\|\mathbf{B}_t - \mathbf{B}_{\ell h}\|_2^2])\}\big].
$$

Rearranging the above inequality yields

$$\mathbb{E}\big[\|\mathbf{B}_t - \mathbf{B}_{\ell h}\|_2^2 \psi_{k+1}^t(\bar{\mathbf{Z}}_t|\mathbf{y}_{[k+1]})\big]$$

$$\leq \underbrace{\mathbb{E}[\|\mathbf{B}_t - \mathbf{B}_{\ell h}\|_2^2]}_{\text{(i)}} + \frac{1}{s}\underbrace{\mathrm{KL}\left(\mu_{k+1}^t(\cdot|\mathbf{y}_{[k+1]})\|\bar{\pi}_{k+1}^t(\cdot|\mathbf{y}_{[k+1]})\right)}_{\text{(ii)}}$$

(E.18)
$$+ \frac{1}{s}\underbrace{\log \mathbb{E}\big[\exp\{s(\|\mathbf{B}_t - \mathbf{B}_{\ell h}\|_2^2 - \mathbb{E}[\|\mathbf{B}_t - \mathbf{B}_{\ell h}\|_2^2])\}\big]}_{\text{(iii)}}.$$

For the term (i) in (E.18), it holds that

(E.19)
$$\mathbb{E}[\|\mathbf{B}_t - \mathbf{B}_{\ell h}\|_2^2] = d(t - \ell h).$$

For the term (ii) in (E.18), we find

$$\mathrm{KL}\left(\mu_{k+1}^t(\cdot|\mathbf{y}_{[k+1]})\|\bar{\pi}_{k+1}^t(\cdot|\mathbf{y}_{[k+1]})\right)$$

$$= \int \mu_{k+1}^t(\mathbf{x}|\mathbf{y}_{[k+1]}) \log \psi_{k+1}^t(\mathbf{x}|\mathbf{y}_{[k+1]})\,\mathrm{d}\mathbf{x}$$

$$= \frac{1}{2}\int \mu_{k+1}^t(\mathbf{x}|\mathbf{y}_{[k+1]}) \log \frac{\phi_{k+1}^t(\mathbf{x}|\mathbf{y}_{[k+1]})^2}{\mathbb{E}_{\bar{\mathbf{Z}}_t}[\phi_{k+1}^t(\bar{\mathbf{Z}}_t|\mathbf{y}_{[k+1]})]^2}\,\mathrm{d}\mathbf{x}$$

$$= \frac{1}{2}\int \mu_{k+1}^t(\mathbf{x}|\mathbf{y}_{[k+1]})\left\{\log \frac{\phi_{k+1}^t(\mathbf{x}|\mathbf{y}_{[k+1]})^2}{\mathbb{E}_{\bar{\mathbf{Z}}_t}[\phi_{k+1}^t(\bar{\mathbf{Z}}_t|\mathbf{y}_{[k+1]})]} - \log \mathbb{E}_{\bar{\mathbf{Z}}_t}[\phi_{k+1}^t(\bar{\mathbf{Z}}_t|\mathbf{y}_{[k+1]})]\right\}\mathrm{d}\mathbf{x}$$

$$\leq \frac{1}{2}\int \mu_{k+1}^t(\mathbf{x}|\mathbf{y}_{[k+1]}) \log \frac{\phi_{k+1}^t(\mathbf{x}|\mathbf{y}_{[k+1]})^2}{\mathbb{E}_{\bar{\mathbf{Z}}_t}[\phi_{k+1}^t(\bar{\mathbf{Z}}_t|\mathbf{y}_{[k+1]})]}\,\mathrm{d}\mathbf{x}$$

$$= \frac{1}{2}\int \mu_{k+1}^t(\mathbf{x}|\mathbf{y}_{[k+1]}) \log\left\{\psi_{k+1}^t(\mathbf{x}|\mathbf{y}_{[k+1]})\phi_{k+1}^t(\mathbf{x}|\mathbf{y}_{[k+1]})\right\}\mathrm{d}\mathbf{x}$$

$$= \frac{1}{2}\mathrm{KL}\left(\mu_{k+1}^t(\cdot|\mathbf{y}_{[k+1]})\|\pi_{k+1}(\cdot|\mathbf{y}_{[k+1]})\right)$$

$$\leq \frac{C_{\mathrm{LSI}}}{4}\mathbb{E}_{\widetilde{\mathbf{Z}}_t}\left[\big\|\nabla \log\left\{\psi_{k+1}^t(\widetilde{\mathbf{Z}}_t|\mathbf{y}_{[k+1]})\phi_{k+1}^t(\widetilde{\mathbf{Z}}_t|\mathbf{y}_{[k+1]})\right\}\big\|_2^2\right]$$

(E.20)
$$= C_{\mathrm{LSI}}\frac{\mathbb{E}_{\mathbf{Z}}[\|\nabla_{\mathbf{x}}\phi_{k+1}^t(\mathbf{Z}|\mathbf{y}_{[k+1]})\|_2^2]}{\mathbb{E}_{\mathbf{Z}}[\phi_{k+1}^t(\mathbf{Z}|\mathbf{y}_{[k+1]})^2]},$$

where the second equality holds from (E.3) and (E.4), the second inequality invokes Lemmas I.13 and I.14, and the last equality is due to Lemma I.15. Finally, we consider the term (iii) in (E.18). Applying Lemma I.12 deduces

(E.21)
$$\log \mathbb{E}\big[\exp\{s\|\mathbf{B}_t - \mathbf{B}_{\ell h}\|_2^2 - \mathbb{E}[\|\mathbf{B}_t - \mathbf{B}_{\ell h}\|_2^2]\}\big] \leq 2ds(t - \ell h),$$

provided that $4s(t - \ell h) \leq 1$. Substituting (E.19), (E.20), and (E.21) into (E.18) implies

$$\mathbb{E}\big[\|\mathbf{B}_t - \mathbf{B}_{\ell h}\|_2^2 \psi_{k+1}^t(\bar{\mathbf{Z}}_t|\mathbf{y}_{[k+1]})\big]$$

$$\leq d(t - \ell h) + \frac{C_{\mathrm{LSI}}}{s}\frac{\mathbb{E}_{\mathbf{Z}}[\|\nabla_{\mathbf{x}}\phi_{k+1}^t(\mathbf{Z}|\mathbf{y}_{[k+1]})\|_2^2]}{\mathbb{E}_{\mathbf{Z}}[\phi_{k+1}^t(\mathbf{Z}|\mathbf{y}_{[k+1]})^2]} + 2d(t - \ell h),$$

for each $s > 0$ such that $4s(t - \ell h) \leq 1$. Letting $8s(t - \ell h) = 1$ completes the proof. $\square$

With the help of the preceding three lemmas, we can now prove Lemma E.7.

Proof of Lemma E.7. Applying Lemmas E.9 and E.10 into Lemma E.8 implies

$$
\mathbb{E}_{(\bar{\mathbf{Z}}_{\ell h}, \bar{\mathbf{Z}}_t)} \Big[\|\mathbf{e}_{k+1}(\bar{\mathbf{Z}}_{\ell h}, \bar{\mathbf{Z}}_t | \mathbf{y}_{[k+1]})\|_2^2 \psi_{k+1}^t(\bar{\mathbf{Z}}_t | \mathbf{y}_{[k+1]}) \Big]
$$

$$
\leq 8\lambda^2 (t - \ell h)^2 \left\{ \frac{4\mathbb{E}_{\mathbf{Z}}[\|\nabla_{\mathbf{x}}\phi_{k+1}^t(\mathbf{Z}|\mathbf{y}_{[k+1]})\|_2^2]}{\mathbb{E}_{\mathbf{Z}}[\phi_{k+1}^t(\mathbf{Z}|\mathbf{y}_{[k+1]})^2]} + 2d\lambda \right\}
$$

$$
+ 6\lambda^2 \left\{ 3d(t - \ell h) + 8C_{\mathrm{LSI}}(t - \ell h) \frac{\mathbb{E}_{\mathbf{Z}}[\|\nabla_{\mathbf{x}}\phi_{k+1}^t(\mathbf{Z}|\mathbf{y}_{[k+1]})\|_2^2]}{\mathbb{E}_{\mathbf{Z}}[\phi_{k+1}^t(\mathbf{Z}|\mathbf{y}_{[k+1]})^2]} \right\}
$$

$$
= \left\{ 32\lambda^2(t - \ell h)^2 + 48C_{\mathrm{LSI}}\lambda^2(t - \ell h) \right\} \frac{\mathbb{E}_{\mathbf{Z}}[\|\nabla_{\mathbf{x}}\phi_{k+1}^t(\mathbf{Z}|\mathbf{y}_{[k+1]})\|_2^2]}{\mathbb{E}_{\mathbf{Z}}[\phi_{k+1}^t(\mathbf{Z}|\mathbf{y}_{[k+1]})^2]}
$$

$$
+ 16d\lambda^3(t - \ell h)^2 + 16d\lambda^2(t - \ell h)
$$

$$
\leq 80C_{\mathrm{LSI}}\lambda^2(t - \ell h) \frac{\mathbb{E}_{\mathbf{Z}}[\|\nabla_{\mathbf{x}}\phi_{k+1}^t(\mathbf{Z}|\mathbf{y}_{[k+1]})\|_2^2]}{\mathbb{E}_{\mathbf{Z}}[\phi_{k+1}^t(\mathbf{Z}|\mathbf{y}_{[k+1]})^2]} + 20d\lambda^2(t - \ell h),
$$

where the last inequality holds from $4\lambda h \leq 1$. This completes the proof. □

E.4. **Proof of the convergence of Langevin Monte Carlo.** Combining Lemmas E.3, E.6, and E.7 achieves the following recursion of χ^2-divergence.

Lemma E.11. *Suppose Assumptions 1 and 2 hold. Then for each $0 \leq \ell \leq K - 1$,*

$$
\chi^2\big(\bar{\pi}_{k+1}^{(\ell+1)h}(\cdot|\mathbf{y}_{[k+1]})\|\pi_{k+1}(\cdot|\mathbf{y}_{[k+1]})\big)
$$

$$
\leq \exp\Big(-\frac{h}{5C_{\mathrm{LSI}}} \Big) \chi^2\big(\bar{\pi}_{k+1}^{\ell h}(\cdot|\mathbf{y}_{[k+1]})\|\pi_{k+1}(\cdot|\mathbf{y}_{[k+1]})\big) + 20d\lambda^2 h^2,
$$

where the step size $h > 0$ satisfies $400dC_{\mathrm{LSI}}\lambda^2 h \leq 1$.

Proof of Lemma E.11. Plugging Lemma E.7 into Lemma E.3 implies

$$
\frac{\mathrm{d}}{\mathrm{d}t}\chi^2\big(\bar{\pi}_{k+1}^t(\cdot|\mathbf{y}_{[k+1]})\|\pi_{k+1}(\cdot|\mathbf{y}_{[k+1]})\big)
$$

$$
\leq -\mathbb{E}_{\mathbf{Z}}\Big[\big\|\nabla_{\mathbf{x}}\phi_{k+1}^t(\mathbf{Z}|\mathbf{y}_{[k+1]})\big\|_2^2\Big] + 80C_{\mathrm{LSI}}\lambda^2 h\mathbb{E}_{\mathbf{Z}}[\|\nabla_{\mathbf{x}}\phi_{k+1}^t(\mathbf{Z}|\mathbf{y}_{[k+1]})\|_2^2]
$$

$$
+ 20d\lambda^2(t - \ell h)\mathbb{E}_{\mathbf{Z}}[\phi_{k+1}^t(\mathbf{Z}|\mathbf{y}_{[k+1]})^2]
$$

$$
\text{(E.22)} \qquad \leq -\frac{4}{5}\underbrace{\mathbb{E}_{\mathbf{Z}}\Big[\big\|\nabla_{\mathbf{x}}\phi_{k+1}^t(\mathbf{Z}|\mathbf{y}_{[k+1]})\big\|_2^2\Big]}_{\text{(i)}} + 20d\lambda^2(t - \ell h)\underbrace{\mathbb{E}_{\mathbf{Z}}[\phi_{k+1}^t(\mathbf{Z}|\mathbf{y}_{[k+1]})^2]}_{\text{(ii)}},
$$

where the second inequality invokes $400C_{\mathrm{LSI}}\lambda^2 h \leq 1$. For the term (i) in (E.22), it follows from Lemma E.6 that

$$
\text{(E.23)} \qquad \frac{1}{2C_{\mathrm{LSI}}}\chi^2\big(\bar{\pi}_{k+1}^t(\cdot|\mathbf{y}_{[k+1]})\|\pi_{k+1}(\cdot|\mathbf{y}_{[k+1]})\big) \leq \mathbb{E}_{\mathbf{Z}}\Big[\big\|\nabla_{\mathbf{x}}\phi_{k+1}^t(\mathbf{Z}|\mathbf{y}_{[k+1]})\big\|_2^2\Big].
$$

For the term (ii) in (E.22), using the definition of χ^2-divergence and (E.2),

$$
\text{(E.24)} \qquad \mathbb{E}_{\mathbf{Z}}[\phi_{k+1}^t(\mathbf{Z}|\mathbf{y}_{[k+1]})^2] \leq \chi^2\big(\bar{\pi}_{k+1}^t(\cdot|\mathbf{y}_{[k+1]})\|\pi_{k+1}(\cdot|\mathbf{y}_{[k+1]})\big) + 1.
$$

Substituting (E.23) and (E.24) into (E.22) yields that for h satisfying $100dC_{\mathrm{LSI}}\lambda^2 h \leq 1$,

$$
\frac{\mathrm{d}}{\mathrm{d}t}\chi^2\big(\bar{\pi}_{k+1}^t(\cdot|\mathbf{y}_{[k+1]})\|\pi_{k+1}(\cdot|\mathbf{y}_{[k+1]})\big)
$$

$$
\text{(E.25)} \qquad \leq -\frac{1}{5C_{\mathrm{LSI}}}\chi^2\big(\bar{\pi}_{k+1}^t(\cdot|\mathbf{y}_{[k+1]})\|\pi_{k+1}(\cdot|\mathbf{y}_{[k+1]})\big) + 20d\lambda^2 h.
$$

Multiplying both sides of (E.25) by $\exp(\frac{t}{5C_{\text{LSI}}})$ deduces

(E.26) $$\frac{\mathrm{d}}{\mathrm{d}t}\Big(\exp\Big(\frac{t}{5C_{\text{LSI}}}\Big)\chi^2\big(\bar{\pi}^t_{k+1}(\cdot|\mathbf{y}_{[k+1]})\|\pi_{k+1}(\cdot|\mathbf{y}_{[k+1]}))\Big)\le 20d\lambda^2 h\exp\Big(\frac{t}{5C_{\text{LSI}}}\Big).$$

Before proceeding, we verify a useful inequality

(E.27) $$\exp\Big(\frac{h}{5C_{\text{LSI}}}\Big)-1\le\frac{h}{5C_{\text{LSI}}}.$$

In fact, since that $400C_{\text{LSI}}\lambda^2 h\le 1$ and $C_{\text{LSI}}\lambda\ge 1$ (Lemma I.8), it holds that

$$0<\frac{h}{5C_{\text{LSI}}}\le\frac{h}{5C_{\text{LSI}}}\frac{1}{400C_{\text{LSI}}\lambda^2 h}<1,$$

which implies (E.27) directly. Then integrating both sides of (E.26) from ℓh to $(\ell+1)h$ yields

$$\chi^2\big(\bar{\pi}^{(\ell+1)h}_{k+1}(\cdot|\mathbf{y}_{[k+1]})\|\pi_{k+1}(\cdot|\mathbf{y}_{[k+1]})\big)$$
$$\le\exp\Big(-\frac{h}{5C_{\text{LSI}}}\Big)\chi^2\big(\bar{\pi}^{\ell h}_{k+1}(\cdot|\mathbf{y}_{[k+1]})\|\pi_{k+1}(\cdot|\mathbf{y}_{[k+1]})\big)$$
$$+100dC_{\text{LSI}}\lambda^2 h\exp\Big(-\frac{h}{5C_{\text{LSI}}}\Big)\Big\{\exp\Big(\frac{h}{5C_{\text{LSI}}}\Big)-1\Big\}$$
$$\le\exp\Big(-\frac{h}{5C_{\text{LSI}}}\Big)\chi^2\big(\bar{\pi}^{\ell h}_{k+1}(\cdot|\mathbf{y}_{[k+1]})\|\pi_{k+1}(\cdot|\mathbf{y}_{[k+1]})\big)+20d\lambda^2 h^2,$$

where the last inequality invokes (E.27). This completes the proof. □

Proof of Lemma E.1. It is straightforward from Lemma E.11 that

$$\chi^2\big(\bar{\pi}^{\ell h}_{k+1}(\cdot|\mathbf{y}_{[k+1]})\|\pi_{k+1}(\cdot|\mathbf{y}_{[k+1]})\big)$$
$$\le\exp\Big(-\frac{\ell h}{5C_{\text{LSI}}}\Big)\chi^2\big(\pi^0_{k+1}(\cdot|\mathbf{y}_{[k+1]})\|\pi_{k+1}(\cdot|\mathbf{y}_{[k+1]})\big)+\frac{20d\lambda^2 h^2}{1-\exp(-\frac{h}{5C_{\text{LSI}}})}$$
$$\le\exp\Big(-\frac{\ell h}{5C_{\text{LSI}}}\Big)\chi^2\big(\pi^0_{k+1}(\cdot|\mathbf{y}_{[k+1]})\|\pi_{k+1}(\cdot|\mathbf{y}_{[k+1]})\big)+140dC_{\text{LSI}}\lambda^2 h,$$

where the last inequality used $1-\exp(-\frac{h}{5C_{\text{LSI}}})\ge\frac{3h}{20C_{\text{LSI}}}$ for $0<\frac{h}{5C_{\text{LSI}}}\le\frac{1}{4}$. Indeed, combining the condition $400dC_{\text{LSI}}\lambda^2 h\le 1$ and Lemma I.8 implies $4h\lambda\le 1$, which deduces that $\frac{h}{5C_{\text{LSI}}}\le\frac{1}{20C_{\text{LSI}}\lambda}\le\frac{1}{4}$. This completes the proof. □

APPENDIX F. PRIOR ERROR

In this section, we bound the prior error

$$\|\nabla_{\mathbf{x}}\log q_{k+1}(\cdot|\mathbf{y}_{[k]})-\nabla_{\mathbf{x}}\log\widehat{q}_{k+1}(\cdot|\mathbf{y}_{[k]})\|_{L^\infty(\mathbb{R}^d)},$$

where $\widehat{q}_{k+1}$ is defined as (2.7)

$$\widehat{q}_{k+1}(\mathbf{x}|\mathbf{y}_{[k]}):=\int\rho_k(\mathbf{x}|\mathbf{x}_k)\widehat{\pi}^T_k(\mathbf{x}_k|\mathbf{y}_{[k]})\,\mathrm{d}\mathbf{x}_k.$$

The main result is stated as follows.

Lemma F.1. *Suppose Assumption 3 holds. Then for each $\mathbf{x}\in\mathbb{R}^d$,*

$$\|\nabla_{\mathbf{x}}\log q_{k+1}(\mathbf{x}|\mathbf{y}_{[k]})-\nabla_{\mathbf{x}}\log\widehat{q}_{k+1}(\mathbf{x}|\mathbf{y}_{[k]})\|_\infty\le 4B^2D^2\varepsilon^k_{\text{TV}}.$$

Before proceeding, we introduce two auxiliary lemmas.

Lemma F.2. *Suppose Assumption 3 holds. Then for each $\mathbf{x}\in\mathbb{R}^d$,*

$$|q_{k+1}(\mathbf{x}|\mathbf{y}_{[k]})-\widehat{q}_{k+1}(\mathbf{x}|\mathbf{y}_{[k]})|\le 2B\varepsilon^k_{\text{TV}}.$$

Proof of Lemma F.2. It is straightforward that for each $\mathbf{x} \in \mathbb{R}^d$,

$$|q_{k+1}(\mathbf{x}|\mathbf{y}_{[k]}) - \widehat{q}_{k+1}(\mathbf{x}|\mathbf{y}_{[k]})| \leq \int \rho_k(\mathbf{x}|\mathbf{x}_k)|\pi_k(\mathbf{x}_k|\mathbf{y}_{[k]}) - \widehat{\pi}_k^T(\mathbf{x}_k|\mathbf{y}_{[k]})| \, d\mathbf{x}_k$$

$$\leq 2B \, \mathrm{TV}(\pi_k(\cdot|\mathbf{y}_{[k]}), \widehat{\pi}_k^T(\cdot|\mathbf{y}_{[k]})),$$

where the first inequality follows from the Jensen's inequality, and the second inequality invokes Assumption 3 (i) and the Hölder's inequality. This completes the proof. $\qquad\square$

Lemma F.3. *Suppose Assumption 3 holds. Then for each $\mathbf{x} \in \mathbb{R}^d$,*

$$\|\nabla_{\mathbf{x}} q_{k+1}(\mathbf{x}|\mathbf{y}_{[k]}) - \nabla_{\mathbf{x}} \widehat{q}_{k+1}(\mathbf{x}|\mathbf{y}_{[k]})\|_{\infty} \leq 2B\varepsilon_{\mathrm{TV}}^k.$$

Proof of Lemma F.3. It is straightforward that for each $\mathbf{x} \in \mathbb{R}^d$,

$$\left| \frac{\partial q_{k+1}}{\partial x_i}(\mathbf{x}|\mathbf{y}_{[k]}) - \frac{\partial \widehat{q}_{k+1}}{\partial x_i}(\mathbf{x}|\mathbf{y}_{[k]}) \right|$$

$$\leq \int \left| \frac{\partial \rho_k}{\partial x_i}(\mathbf{x}|\mathbf{x}_k) \right| |\pi_k(\mathbf{x}_k|\mathbf{y}_{[k]}) - \widehat{\pi}_k^T(\mathbf{x}_k|\mathbf{y}_{[k]})| \, d\mathbf{x}_k$$

$$\leq 2B \, \mathrm{TV}(\pi_k(\cdot|\mathbf{y}_{[k]}), \widehat{\pi}_k^T(\cdot|\mathbf{y}_{[k]})),$$

where the first inequality follows from the Jensen's inequality, and the second inequality invokes Assumption 3 (ii) and the Hölder's inequality. This completes the proof. $\qquad\square$

With the help of Lemmas F.2 and F.3, we now prove the Lemma F.1.

Proof of Lemma F.1. According to Assumption 3, we find

(F.1) $$\left| \left(\frac{1}{q_{k+1}} \frac{\partial q_{k+1}}{\partial x_i} \right)(\mathbf{x}|\mathbf{y}_{[k]}) \right| \leq BD, \quad \mathbf{x} \in \mathbb{R}^d.$$

Notice that $\widehat{q}_{k+1}(\cdot|\mathbf{y}_{[k+1]})$ is close to $q_{k+1}(\cdot|\mathbf{y}_{[k+1]})$ given that $\widehat{\pi}_k^T(\cdot|\mathbf{y}_{[k]})$ is close to $\pi_k(\cdot|\mathbf{y}_{[k]})$. Without loss of generality, we assume $\nabla_{\mathbf{x}} \log \widehat{q}_{k+1}(\cdot|\mathbf{y}_{[k+1]})$ also satisfies the above inequality. Then it is straightforward that

$$\left| \left(\frac{1}{q_{k+1}} \frac{\partial q_{k+1}}{\partial x_i} \right)(\mathbf{x}|\mathbf{y}_{[k]}) - \left(\frac{1}{\widehat{q}_{k+1}} \frac{\partial \widehat{q}_{k+1}}{\partial x_i} \right)(\mathbf{x}|\mathbf{y}_{[k]}) \right|$$

$$\leq \left| \frac{1}{q_{k+1}(\mathbf{x}|\mathbf{y}_{[k]})} \frac{\partial q_{k+1}}{\partial x_i}(\mathbf{x}|\mathbf{y}_{[k]}) - \frac{1}{q_{k+1}(\mathbf{x}|\mathbf{y}_{[k]})} \frac{\partial \widehat{q}_{k+1}}{\partial x_i}(\mathbf{x}|\mathbf{y}_{[k]}) \right|$$

$$+ \left| \frac{1}{q_{k+1}(\mathbf{x}|\mathbf{y}_{[k]})} \frac{\partial \widehat{q}_{k+1}}{\partial x_i}(\mathbf{x}|\mathbf{y}_{[k]}) - \frac{1}{\widehat{q}_{k+1}(\mathbf{x}|\mathbf{y}_{[k]})} \frac{\partial \widehat{q}_{k+1}}{\partial x_i}(\mathbf{x}|\mathbf{y}_{[k]}) \right|$$

$$\leq \frac{1}{q_{k+1}(\mathbf{x}|\mathbf{y}_{[k]})} \left| \frac{\partial q_{k+1}}{\partial x_i}(\mathbf{x}|\mathbf{y}_{[k]}) - \frac{\partial \widehat{q}_{k+1}}{\partial x_i}(\mathbf{x}|\mathbf{y}_{[k]}) \right|$$

$$+ \frac{1}{q_{k+1}(\mathbf{x}|\mathbf{y}_{[k]})} \left| \left(\frac{1}{\widehat{q}_{k+1}} \frac{\partial \widehat{q}_{k+1}}{\partial x_i} \right)(\mathbf{x}|\mathbf{y}_{[k]}) \right| |\widehat{q}_{k+1}(\mathbf{x}|\mathbf{y}_{[k]}) - q_{k+1}(\mathbf{x}|\mathbf{y}_{[k]})|$$

$$\leq D \left| \frac{\partial q_{k+1}}{\partial x_i}(\mathbf{x}|\mathbf{y}_{[k]}) - \frac{\partial \widehat{q}_{k+1}}{\partial x_i}(\mathbf{x}|\mathbf{y}_{[k]}) \right| + D^2 B |\widehat{q}_{k+1}(\mathbf{x}|\mathbf{y}_{[k]}) - q_{k+1}(\mathbf{x}|\mathbf{y}_{[k]})|$$

$$\leq 4D^2 B^2 \, \mathrm{TV}(\pi_k(\cdot|\mathbf{y}_{[k]}), \widehat{\pi}_k^T(\cdot|\mathbf{y}_{[k]})),$$

where the first inequality follows from the triangular inequality, the third inequality is due to Assumption 3, and the last inequality invokes Lemmas F.2 and F.3. This completes the proof. $\qquad\square$

This section focuses on the error of the score matching, which is inspired by the proof of Tang and Yang (2024, Lemma B.4).

Lemma G.1. *Suppose Assumptions 1, 3, 2, and 4 hold. Then*

$$\sum_{\ell=0}^{K-1} h\mathbb{E}_{\bar{\mathbf{Z}}_{\ell h}}\big[\|\nabla_{\mathbf{x}} \log \widehat{q}_{k+1}(\bar{\mathbf{Z}}_{\ell h}|\mathbf{y}_{[k]}) - \widehat{\mathbf{s}}_{k+1}(\bar{\mathbf{Z}}_{\ell h}, \mathbf{y}_{[k]})\|_2^2\big]$$

$$\leq 28 C_{\mathrm{LSI}}\sqrt{\kappa B^3 D^3}\eta_\chi \Delta + 8\sqrt{\kappa B^3 D^3}T\Delta,$$

where the step size $h > 0$ satisfies $400 d C_{\mathrm{LSI}}\lambda^2 h \leq 1$.

Lemma G.2. *Suppose Assumptions 3 and 4 hold. Then for each $0 \leq \ell \leq K - 1$,*

$$\mathbb{E}_{\bar{\mathbf{Z}}_{\ell h}}\big[\|\nabla_{\mathbf{x}} \log \widehat{q}_{k+1}(\bar{\mathbf{Z}}_{\ell h}|\mathbf{y}_{[k]}) - \widehat{\mathbf{s}}_{k+1}(\bar{\mathbf{Z}}_{\ell h}, \mathbf{y}_{[k]})\|_2^2\big]$$

$$\leq 2\sqrt{\kappa B^3 D^3}\Delta\big(\chi^2\big(\bar{\pi}_{k+1}^{\ell h}(\cdot|\mathbf{y}_{[k+1]})\|\pi_{k+1}(\cdot|\mathbf{y}_{[k+1]})\big) + 1\big)^{\frac{1}{2}}.$$

Proof of Lemma G.2. For the simplicity of the notation, we define

$$\varpi_{k+1}^2(\mathbf{x}, \mathbf{y}_{[k]}) := \|\nabla_{\mathbf{x}} \log \widehat{q}_{k+1}(\mathbf{x}|\mathbf{y}_{[k]}) - \widehat{\mathbf{s}}_{k+1}(\mathbf{x}, \mathbf{y}_{[k]})\|_2^2.$$

According to Assumption 3, the boundedness of the prediction score is derived by (F.1). Without loss of generality, we assume $\nabla_{\mathbf{x}} \log \widehat{q}_{k+1}(\cdot|\mathbf{y}_{[k]})$ and $\widehat{\mathbf{s}}_{k+1}(\cdot, \mathbf{y}_{[k]})$ also satisfies this inequality. As a consequence, $\varpi_{k+1}^2(\mathbf{x}, \mathbf{y}_{[k]}) \leq 4B^2 D^2$ for each $\mathbf{x} \in \mathbb{R}^d$. It is straightforward that

$$\mathbb{E}_{\bar{\mathbf{Z}}_{\ell h}}^2\big[\varpi_{k+1}^2(\bar{\mathbf{Z}}_{\ell h}, \mathbf{y}_{[k]})\big]$$

$$= \bigg(\int \varpi_k^2(\mathbf{x}, \mathbf{y}_{[k+1]}) \frac{\bar{\pi}_{k+1}^{\ell h}(\mathbf{x}|\mathbf{y}_{[k+1]})}{\pi_{k+1}(\mathbf{x}|\mathbf{y}_{[k+1]})}\pi_{k+1}(\mathbf{x}|\mathbf{y}_{[k+1]})\,\mathrm{d}\mathbf{x}\bigg)^2$$

$$\text{(G.1)} \qquad \leq \underbrace{\int \varpi_{k+1}^4(\mathbf{x}, \mathbf{y}_{[k]})\pi_{k+1}(\mathbf{x}|\mathbf{y}_{[k+1]})\,\mathrm{d}\mathbf{x}}_{\text{(i)}} \underbrace{\int \bigg(\frac{\bar{\pi}_{k+1}^{\ell h}(\mathbf{x}|\mathbf{y}_{[k+1]})}{\pi_{k+1}(\mathbf{x}|\mathbf{y}_{[k+1]})}\bigg)^2 \pi_{k+1}(\mathbf{x}|\mathbf{y}_{[k+1]})\,\mathrm{d}\mathbf{x}}_{\text{(ii)}},$$

where the inequality invokes the Cauchy-Schwarz inequality. For the term (i) in (G.1),

$$\int \varpi_{k+1}^4(\mathbf{x}, \mathbf{y}_{[k]})\pi_{k+1}(\mathbf{x}|\mathbf{y}_{[k+1]})\,\mathrm{d}\mathbf{x}$$

$$= \int \varpi_{k+1}^4(\mathbf{x}, \mathbf{y}_{[k]}) \frac{\pi_{k+1}(\mathbf{x}|\mathbf{y}_{[k+1]})}{q_{k+1}(\mathbf{x}|\mathbf{y}_{[k]})} \frac{q_{k+1}(\mathbf{x}|\mathbf{y}_{[k]})}{\widehat{q}_{k+1}(\mathbf{x}|\mathbf{y}_{[k]})}\widehat{q}_{k+1}(\mathbf{x}|\mathbf{y}_{[k]})\,\mathrm{d}\mathbf{x}$$

$$\leq \kappa B D \int \varpi_{k+1}^4(\mathbf{x}, \mathbf{y}_{[k]})\widehat{q}_{k+1}(\mathbf{x}|\mathbf{y}_{[k]})\,\mathrm{d}\mathbf{x}$$

$$\text{(G.2)} \qquad \leq 4\kappa B^3 D^3 \int \varpi_{k+1}^2(\mathbf{x}, \mathbf{y}_{[k]})\widehat{q}_{k+1}(\mathbf{x}|\mathbf{y}_{[k]})\,\mathrm{d}\mathbf{x} \leq 4\kappa B^3 D^3 \Delta^2,$$

where the first inequality holds from Assumption 3 and the inequalities

$$\bigg|\frac{q_{k+1}(\mathbf{x}|\mathbf{y}_{[k]})}{\widehat{q}_{k+1}(\mathbf{x}|\mathbf{y}_{[k]})}\bigg| \leq BD, \qquad \frac{\pi_{k+1}(\mathbf{x}|\mathbf{y}_{[k+1]})}{q_{k+1}(\mathbf{x}|\mathbf{y}_{[k]})} = \frac{g_{k+1}(\mathbf{y}_{k+1}|\mathbf{x})}{\int g_{k+1}(\mathbf{y}_{k+1}|\mathbf{x})q_{k+1}(\mathbf{x}|\mathbf{y}_{[k]})\,\mathrm{d}\mathbf{x}} \leq \kappa,$$

the second inequality is due to the boundedness of $\varpi_{k+1}^2(\mathbf{x}, \mathbf{y}_{[k+1]})$, and the last inequality is owing to Assumption 4. For the term (ii) in (G.1),

$$
\begin{aligned}
&\int \Big(\frac{\bar{\pi}_{k+1}^{\ell h}(\mathbf{x}|\mathbf{y}_{[k+1]})}{\pi_{k+1}(\mathbf{x}|\mathbf{y}_{[k+1]})} \Big)^2 \pi_{k+1}(\mathbf{x}|\mathbf{y}_{[k+1]}) \, \mathrm{d}\mathbf{x} \\
&\quad = \chi^2 \big(\bar{\pi}_{k+1}^{\ell h}(\cdot|\mathbf{y}_{[k+1]}) \| \pi_{k+1}(\cdot|\mathbf{y}_{[k+1]}) \big) + 1.
\end{aligned}
$$

(G.3)

Substituting (G.2) and (G.3) into (G.1) completes the proof. $\qquad\square$

Proof of Lemma G.1. By a same argument as the proof of Lemma E.1, we have

$$
\text{(G.4)} \qquad \sum_{\ell=0}^{K-1} \exp\Big(-\frac{\ell h}{10 C_{\mathrm{LSI}}}\Big) \le \frac{20 C_{\mathrm{LSI}}}{3h},
$$

provided that the step size $h > 0$ satisfies $400 d C_{\mathrm{LSI}} \lambda^2 h \le 1$. Summing both sides of Lemma G.2 with respect to $0 \le \ell \le K-1$ yields

$$
\begin{aligned}
& \sum_{\ell=0}^{K-1} h \mathbb{E}_{\bar{\mathbf{Z}}_{\ell h}} \Big[\| \nabla_{\mathbf{x}} \log \widehat{q}_{k+1}(\bar{\mathbf{Z}}_{\ell h}|\mathbf{y}_{[k]}) - \widehat{\mathbf{s}}_{k+1}(\bar{\mathbf{Z}}_{\ell h}, \mathbf{y}_{[k]}) \|_2^2 \Big] \\
& \le 2\sqrt{\kappa B^3 D^3} h \Delta \sum_{\ell=0}^{K-1} \Big(\exp\Big(-\frac{\ell h}{5 C_{\mathrm{LSI}}}\Big) \chi^2 \big(\pi_{k+1}^0(\cdot|\mathbf{y}_{[k+1]}) \| \pi_{k+1}(\cdot|\mathbf{y}_{[k+1]}) \big) + 2 \Big)^{\frac{1}{2}} \\
& \le 4\sqrt{\kappa B^3 D^3} h \Delta \Big\{ \sum_{\ell=0}^{K-1} \exp\Big(-\frac{\ell h}{10 C_{\mathrm{LSI}}}\Big) \chi^2 \big(\pi_{k+1}^0(\cdot|\mathbf{y}_{[k+1]}) \| \pi_{k+1}(\cdot|\mathbf{y}_{[k+1]}) \big)^{\frac{1}{2}} + 2K \Big\} \\
& \le 28 C_{\mathrm{LSI}} \sqrt{\kappa B^3 D^3} \Delta \chi^2 \big(\pi_{k+1}^0(\cdot|\mathbf{y}_{[k+1]}) \| \pi_{k+1}(\cdot|\mathbf{y}_{[k+1]}) \big)^{\frac{1}{2}} + 8\sqrt{\kappa B^3 D^3} T \Delta,
\end{aligned}
$$

where the first inequality invokes Lemmas G.2 and E.1, and the inequality $400 d C_{\mathrm{LSI}} \lambda^2 h \le 1$. The second inequality is due to $\sqrt{a+b} \le 2\sqrt{a} + 2\sqrt{b}$ for $a, b \ge 0$, and the last inequality follows from (G.4) and $T = Kh$. This completes the proof. $\qquad\square$

APPENDIX H. CONVERGENCE ANALYSIS FOR THE INITIAL STEP

In this section, we consider the assimilation in the first time step. The Langevin diffusion is given as

$$
\text{(H.1)} \qquad \mathrm{d}\mathbf{Z}_t = \nabla_{\mathbf{x}} \log \pi_1(\mathbf{Z}_t|\mathbf{y}_1) \, \mathrm{d}t + \sqrt{2}\, \mathrm{d}\mathbf{B}_t, \quad \mathbf{Z}_0 \sim \pi_1^0(\cdot|\mathbf{y}_1),\ t \ge 0.
$$

Denote by π_1^t the law of $\mathbf{Z}_t$ for each $t \ge 0$. The Langevin Monte Carlo is defined as the Euler-Maruyama discretization of the Langevin diffusion. The interpolation of the Langevin Monte Carlo is given as, for each $0 \le \ell \le K-1$,

$$
\text{(H.2)} \qquad \mathrm{d}\bar{\mathbf{Z}}_t = \nabla_{\mathbf{x}} \log \pi_1(\bar{\mathbf{Z}}_{\ell h}|\mathbf{y}_{[k+1]}) \, \mathrm{d}t + \sqrt{2}\, \mathrm{d}\mathbf{B}_t, \quad \ell h \le t \le (\ell+1)h,
$$

where $\bar{\mathbf{Z}}_0 \sim \pi_1^0(\cdot|\mathbf{y}_1)$. Denote by $\bar{\pi}_1^t$ the law of $\bar{\mathbf{Z}}_t$ for each $0 \le t \le Kh = T$. We next introduce the interpolation of the score-based Langevin Monte Carlo

$$
\text{(H.3)} \qquad \mathrm{d}\widehat{\mathbf{Z}}_t = \widehat{\mathbf{b}}_1(\widehat{\mathbf{Z}}_{\ell h}|\mathbf{y}_{[k+1]}) \, \mathrm{d}t + \sqrt{2}\, \mathrm{d}\mathbf{B}_t, \quad \ell h \le t \le (\ell+1)h,
$$

where $\widehat{\mathbf{Z}}_0 \sim \pi_1^0(\cdot|\mathbf{y}_1)$, and the estimator of posterior score function is given as

$$
\widehat{\mathbf{b}}_1(\mathbf{x}|\mathbf{y}_1) = \nabla_{\mathbf{x}} \log g_1(\mathbf{y}_1|\mathbf{x}) + \widehat{\mathbf{s}}_1(\mathbf{x}).
$$

Here $\widehat{\mathbf{s}}_1$ is an estimator of $\nabla_{\mathbf{x}} \log \widehat{q}_1$. Denote by $\widehat{\pi}_{k+1}^t$ the law of $\widehat{\mathbf{Z}}_t$ for each $0 \le t \le Kh = T$.

The main result in this section is stated as the following lemma.

Lemma H.1. *Suppose Assumptions 1, 2, 3, and 4 hold. Then for each ternimal time $T = Kh$,*

$$(\varepsilon_{\mathrm{TV}}^1)^2 \lesssim \exp\Big(-\frac{T}{5C_{\mathrm{LSI}}}\Big)\eta_\chi^2 + dC_{\mathrm{LSI}}\lambda^2 h + \sqrt{\kappa B^3 D^3}(T + C_{\mathrm{LSI}}\eta_\chi)\Delta$$
$$+ T\|\nabla_{\mathbf{x}}\log q_1 - \nabla_{\mathbf{x}}\log\widehat{q}_1\|_{L^\infty(\mathbb{R}^d)}^2,$$

where the step size h and the initial distribution $\pi_k^0(\cdot|\mathbf{y}_{[k]})$ satisfies

$$h \le \mathcal{O}\Big(\frac{1}{dC_{\mathrm{LSI}}\lambda^2}\Big), \quad \chi^2\big(\pi_1^0(\cdot|\mathbf{y}_1)\|\pi_1(\cdot|\mathbf{y}_1)\big) \le \eta_\chi^2.$$

By an argument similar to Lemma D.1, we decompose the error of the initial time step of the assimilation as the following lemma.

Lemma H.2. *Let π_1 be the stationary distribution of the Langevin diffusion (H.1), and let $\widehat{\pi}_1^T$ be the law of the score-based Langevin Monte Carlo (H.3). Then*

$$\mathrm{TV}^2\big(\pi_1(\cdot|\mathbf{y}_1), \widehat{\pi}_1^T(\cdot|\mathbf{y}_1)\big)$$
$$\le 2\underbrace{\mathrm{TV}^2\big(\pi_1(\cdot|\mathbf{y}_1), \bar{\pi}_1^T(\cdot|\mathbf{y}_1)\big)}_{\text{convergence of Langevin Monte Carlo}} + 4T\underbrace{\|\nabla_{\mathbf{x}}\log q_1 - \nabla_{\mathbf{x}}\log\widehat{q}_1\|_{L^\infty(\mathbb{R}^d)}^2}_{\text{prior error}}$$
$$+ 4\underbrace{\sum_{\ell=0}^{K-1} h\mathbb{E}_{\bar{\mathbf{Z}}_{\ell h}}\Big[\|\nabla_{\mathbf{x}}\log\widehat{q}_1(\bar{\mathbf{Z}}_{\ell h}) - \widehat{\mathbf{s}}_1(\bar{\mathbf{Z}}_{\ell h})\|_2^2\Big]}_{\text{score estimation error}},$$

where the expectation $\mathbb{E}_{\bar{\mathbf{Z}}_{\ell h}}[\cdot]$ is taken with respect to $\bar{\mathbf{Z}}_{\ell h} \sim \bar{\pi}_{k+1}^{\ell h}(\cdot|\mathbf{y}_{[k+1]})$.

The convergence of the Langevin Monte Carlo can be obtained by Lemma E.1, while the score estimation error can be estimated by an argument similar to Lemma G.1 as follows.

Lemma H.3. *Suppose Assumptions 1, 2, 3, and 4 hold. Then*

$$\sum_{\ell=0}^{K-1} h\mathbb{E}_{\bar{\mathbf{Z}}_{\ell h}}\Big[\|\nabla_{\mathbf{x}}\log\widehat{q}_1(\bar{\mathbf{Z}}_{\ell h}) - \widehat{\mathbf{s}}_1(\bar{\mathbf{Z}}_{\ell h})\|_2^2\Big]$$
$$\le 28C_{\mathrm{LSI}}\sqrt{\kappa B^3 D^3}\eta_\chi\Delta + 8\sqrt{\kappa B^3 D^3}T\Delta,$$

where the step size $h > 0$ satisfies $400dC_{\mathrm{LSI}}\lambda^2 h \le 1$.

Proof of Lemma H.1. For the simplicity of the notation, we define

$$\varpi_1^2(\mathbf{x}) := \|\nabla_{\mathbf{x}}\log\widehat{q}_1(\mathbf{x}) - \widehat{\mathbf{s}}_1(\mathbf{x})\|_2^2.$$

According to Assumption 3, $\|\nabla_{\mathbf{x}}\log q_1(\mathbf{x})\|_\infty \le BD$. Without loss of generality, we assume $\nabla_{\mathbf{x}}\log\widehat{q}_1(\mathbf{x})$ and $\widehat{\mathbf{s}}_1(\mathbf{x})$ also satisfies this inequality. As a consequence, $\varpi_1^2(\mathbf{x}) \le 4B^2 D^2$ for each $\mathbf{x} \in \mathbb{R}^d$. It is straightforward that

$$\mathbb{E}_{\bar{\mathbf{Z}}_{\ell h}}^2\big[\varpi_1^2(\bar{\mathbf{Z}}_{\ell h})\big] = \Big(\int \varpi_1^2(\mathbf{x})\frac{\bar{\pi}_1^{\ell h}(\mathbf{x}|\mathbf{y}_1)}{\pi_1(\mathbf{x}|\mathbf{y}_1)}\pi_1(\mathbf{x}|\mathbf{y}_1)\,\mathrm{d}\mathbf{x}\Big)^2$$
$$\le \int \varpi_1^4(\mathbf{x})\pi_1(\mathbf{x}|\mathbf{y}_1)\,\mathrm{d}\mathbf{x}\int \Big(\frac{\bar{\pi}_1^{\ell h}(\mathbf{x}|\mathbf{y}_1)}{\pi_1(\mathbf{x}|\mathbf{y}_1)}\Big)^2\pi_1(\mathbf{x}|\mathbf{y}_1)\,\mathrm{d}\mathbf{x},$$

(H.4)
$$= \underbrace{\int \varpi_1^4(\mathbf{x})\pi_1(\mathbf{x}|\mathbf{y}_1)\,\mathrm{d}\mathbf{x}}_{(\star)}\big(\chi^2\big(\bar{\pi}_1^{\ell h}(\cdot|\mathbf{y}_1)\|\pi_1(\cdot|\mathbf{y}_1)\big) + 1\big),$$

where the inequality invokes the Cauchy-Schwarz inequality. For the term $(\star)$ in (H.4),

$$
\int \varpi_1^4(\mathbf{x})\pi_1(\mathbf{x}|\mathbf{y}_1)\,\mathrm{d}\mathbf{x}
$$

$$
= \int \varpi_1^4(\mathbf{x})\frac{\pi_1(\mathbf{x}|\mathbf{y}_1)}{q_1(\mathbf{x})}\frac{q_1(\mathbf{x})}{\widehat{q}_1(\mathbf{x})}\widehat{q}_1(\mathbf{x})\,\mathrm{d}\mathbf{x} \le \kappa BD \int \varpi_1^4(\mathbf{x})\widehat{q}_1(\mathbf{x})\,\mathrm{d}\mathbf{x}
$$

(H.5)
$$
\le 4\kappa B^3 D^3 \int \varpi_1^2(\mathbf{x})\widehat{q}_1(\mathbf{x})\,\mathrm{d}\mathbf{x} \le 4\kappa B^3 D^3 \Delta^2,
$$

where the first inequality holds from Assumption 3 and the inequalities

$$
\left|\frac{q_1(\mathbf{x})}{\widehat{q}_1(\mathbf{x})}\right| \le BD, \quad \frac{\pi_1(\mathbf{x}|\mathbf{y}_1)}{q_1(\mathbf{x})} = \frac{g_1(\mathbf{y}_1|\mathbf{x})}{\int g_1(\mathbf{y}_1|\mathbf{x})q_1(\mathbf{x})\,\mathrm{d}\mathbf{x}} \le \kappa,
$$

the second inequality is due to the boundedness of $\varpi_1^2(\mathbf{x})$, and the last inequality is owing to Assumption 4. Substituting (H.5) into (H.4) implies

$$
\mathbb{E}_{\bar{\mathbf{Z}}_{\ell h}}\left[\|\nabla_{\mathbf{x}} \log \widehat{q}_1(\bar{\mathbf{Z}}_{\ell h}) - \widehat{\mathbf{s}}_1(\bar{\mathbf{Z}}_{\ell h})\|_2^2\right] \le 2\sqrt{\kappa B^3 D^3}\Delta\left(\chi^2\left(\bar{\pi}_1^{\ell h}(\cdot|\mathbf{y}_1)\|\pi_1(\cdot|\mathbf{y}_1)\right) + 1\right)^{\frac{1}{2}}.
$$

Finally, by the same argument as the proof of Lemma G.1, we completes the proof. $\qquad\square$

APPENDIX I. AUXILIARY DEFINITIONS AND LEMMAS

We first introduce total variation (TV) distance, χ^2-divergence, and the Kullback-Leibler (KL) divergence.

Definition I.1 (Total variation distance)**.** The total variation (TV) distance between two distributions μ and π is defined as

$$
\mathrm{TV}(\mu,\pi) = \frac{1}{2}\int |\mu(\mathbf{x}) - \pi(\mathbf{x})|\,\mathrm{d}\mathbf{x}.
$$

Definition I.2 (Chi-squared divergence)**.** The χ^2-divergence between two distributions μ and π is defined as

$$
\chi^2(\mu\|\pi) = \int \left(\frac{\mu(\mathbf{x})}{\pi(\mathbf{x})}\right)^2\pi(\mathbf{x})\,\mathrm{d}\mathbf{x} - 1 = \int \left(\frac{\mu(\mathbf{x})}{\pi(\mathbf{x})} - 1\right)^2\pi(\mathbf{x})\,\mathrm{d}\mathbf{x}.
$$

Definition I.3 (Kullback-Leibler divergence)**.** The KL-divergence between two distributions μ and π is defined as

$$
\mathrm{KL}(\mu\|\pi) = \int \mu(\mathbf{x})\log\frac{\mu(\mathbf{x})}{\pi(\mathbf{x})}\,\mathrm{d}\mathbf{x}.
$$

We then show the relationships between them.

Lemma I.4. *For two distributions μ and π,*

$$
\mathrm{TV}^2(\mu,\pi) \le \frac{1}{4}\chi^2(\mu\|\pi).
$$

Proof of Lemma I.4. It is straightforward that

$$
\mathrm{TV}^2(\mu,\pi) = \frac{1}{4}\left(\int |\mu(\mathbf{x}) - \pi(\mathbf{x})|\,\mathrm{d}\mathbf{x}\right)^2
$$

$$
\le \frac{1}{4}\left(\int \frac{(\mu(\mathbf{x}) - \pi(\mathbf{x}))^2}{\pi(\mathbf{x})}\,\mathrm{d}\mathbf{x}\right)\left(\int \pi(\mathbf{x})\,\mathrm{d}\mathbf{x}\right)
$$

$$
= \frac{1}{4}\int \left(\frac{\mu(\mathbf{x})}{\pi(\mathbf{x})} - 1\right)^2\pi(\mathbf{x})\,\mathrm{d}\mathbf{x} = \frac{1}{4}\chi^2(\mu\|\pi),
$$

where the inequality follows from the Cauchy-Schwarz inequality. The proof is complete. $\qquad\square$

The proof of Lemmas I.5 and I.6 can be found in Tsybakov (2009, Lemmas 2.5 and 2.7).

Lemma I.5 (Pinsker's inequality). *For two distributions μ and π,*

$$\mathrm{TV}^2(\mu, \pi) \leq \frac{1}{2} \mathrm{KL}(\mu \| \pi).$$

Lemma I.6. *For two distributions μ and π,*

$$\mathrm{KL}(\mu \| \pi) \leq \log(1 + \chi^2(\mu \| \pi)) \leq \chi^2(\mu \| \pi).$$

Proof of Lemma I.6. It is straightforward that

$$
\begin{aligned}
\mathrm{KL}(\mu \| \pi) &= \int \mu(\mathbf{x}) \log \frac{\mu(\mathbf{x})}{\pi(\mathbf{x})} \, \mathrm{d}\mathbf{x} = \mathbb{E}_{\mathbf{X} \sim \mu}\Big[\log \frac{\mu(\mathbf{X})}{\pi(\mathbf{X})}\Big] \\
&\leq \log \mathbb{E}_{\mathbf{X} \sim \mu}\Big[\frac{\mu(\mathbf{X})}{\pi(\mathbf{X})}\Big] = \log \int \Big(\frac{\mu(\mathbf{x})}{\pi(\mathbf{x})}\Big)^2 \pi(\mathbf{x}) \, \mathrm{d}\mathbf{x} \\
&= \log(1 + \chi^2(\mu \| \pi)) \leq \chi^2(\mu \| \pi),
\end{aligned}
$$

where the inequality follows from the Jensen's inequality. The proof is complete. $\qquad\square$

Definition I.7 (Poincaré inequality). A distributoin π satisfies a Poincaré inequality with constant C_{PI}, that is, for each function $f \in C_0^\infty(\mathbb{R}^d)$,

$$\mathrm{Var}(f) \leq C_{\mathrm{PI}} \mathbb{E}\big[\|\nabla f\|_2^2\big],$$

where the expectation and variance are taken with respect to the distribution π.

Notice that the log-Sobolev inequality implies a Poincaré inequality with the same constant. Thus Lee et al. (2022, Lemma E.5) gives the following lemma.

Lemma I.8. *Let π be a distribution such that $\log \pi$ is C^1 and λ-smooth. Further, π satisfies the log-Sobolev inequality with constant C_{LSI}. Then $\lambda C_{\mathrm{LSI}} \geq 1$.*

Lemma I.9. *For two distributions μ and π, it holds that*

$$\int \Delta\mu(\mathbf{x}) \frac{\mu(\mathbf{x})}{\pi(\mathbf{x})} \, \mathrm{d}\mathbf{x} + \int \mu(\mathbf{x}) \nabla \log \pi(\mathbf{x}) \cdot \nabla \frac{\mu(\mathbf{x})}{\pi(\mathbf{x})} \, \mathrm{d}\mathbf{x} = \mathbb{E}_\pi\Big[\big\|\nabla\frac{\mu}{\pi}\big\|_2^2\Big].$$

Proof of Lemma I.9. It is straightforward that

$$
\begin{aligned}
&-\int \Delta\mu(\mathbf{x}) \frac{\mu(\mathbf{x})}{\pi(\mathbf{x})} \, \mathrm{d}\mathbf{x} - \int \mu(\mathbf{x}) \nabla \log \pi(\mathbf{x}) \cdot \nabla \frac{\mu(\mathbf{x})}{\pi(\mathbf{x})} \, \mathrm{d}\mathbf{x} \\
&= \int \nabla\mu(\mathbf{x}) \cdot \nabla\frac{\mu(\mathbf{x})}{\pi(\mathbf{x})} \, \mathrm{d}\mathbf{x} - \int \frac{\mu(\mathbf{x})}{\pi(\mathbf{x})} \nabla\pi(\mathbf{x}) \cdot \nabla\frac{\mu(\mathbf{x})}{\pi(\mathbf{x})} \, \mathrm{d}\mathbf{x} \\
&= \int \pi(\mathbf{x})\Big(\frac{\nabla\mu(\mathbf{x})}{\pi(\mathbf{x})} - \frac{\mu(\mathbf{x})\nabla\pi(\mathbf{x})}{\pi(\mathbf{x})^2}\Big) \cdot \nabla\frac{\mu(\mathbf{x})}{\pi(\mathbf{x})} \, \mathrm{d}\mathbf{x} \\
&= \int \big\|\nabla\frac{\mu(\mathbf{x})}{\pi(\mathbf{x})}\big\|_2^2 \pi(\mathbf{x}) \, \mathrm{d}\mathbf{x} = \mathbb{E}_\pi\Big[\big\|\nabla\frac{\mu}{\pi}\big\|_2^2\Big],
\end{aligned}
$$

where the first equality holds from Green's formula. This completes the proof. $\qquad\square$

Lemma I.10. *Let π be a distribution satisfies the log-Sobolev inequality with constant C_{LSI}. Then for each distribution μ, it holds that*

$$\frac{1}{2C_{\mathrm{LSI}}} \chi^2(\mu \| \pi) \leq \mathbb{E}_\pi\Big[\big\|\nabla\frac{\mu}{\pi}\big\|_2^2\Big].$$

NONLINEAR ASSIMILATION VIA SCORE-BASED SEQUENTIAL LANGEVIN SAMPLING 51

Proof of Lemma I.10. Recall the log-Sobolev inequality

$$\text{Ent}_\pi(f^2) \leq 2C_{\text{LSI}}\mathbb{E}_\pi\big[\|\nabla f\|_2^2\big]. \tag{I.1}$$

Substituting $f(\mathbf{x}) = (\mu(\mathbf{x})/\pi(\mathbf{x}))^{q/2}$ into the left-hand side of (I.4) deduces

$$
\begin{aligned}
\text{Ent}_\pi\left(\frac{\mu^q}{\pi^q}\right) &= q\int \frac{\mu(\mathbf{x})^q}{\pi(\mathbf{x})^q}\log\frac{\mu(\mathbf{x})}{\pi(\mathbf{x})}\pi(\mathbf{x})\,\mathrm{d}\mathbf{x} - \int\frac{\mu(\mathbf{x})^q}{\pi(\mathbf{x})^q}\pi(\mathbf{x})\,\mathrm{d}\mathbf{x}\log\int\frac{\mu(\mathbf{x})^q}{\pi(\mathbf{x})^q}\pi(\mathbf{x})\,\mathrm{d}\mathbf{x}\\
&= q\partial_q\int\frac{\mu(\mathbf{x})^q}{\pi(\mathbf{x})^q}\pi(\mathbf{x})\,\mathrm{d}\mathbf{x} - \int\frac{\mu(\mathbf{x})^q}{\pi(\mathbf{x})^q}\pi(\mathbf{x})\,\mathrm{d}\mathbf{x}\log\int\frac{\mu(\mathbf{x})^q}{\pi(\mathbf{x})^q}\pi(\mathbf{x})\,\mathrm{d}\mathbf{x},
\end{aligned}
$$

where the last equality used the chain rule. As a consequence,

$$
\begin{aligned}
&\left(\int\frac{\mu(\mathbf{x})^q}{\pi(\mathbf{x})^q}\pi(\mathbf{x})\,\mathrm{d}\mathbf{x}\right)^{-1}\text{Ent}_\pi\left(\frac{\mu^q}{\pi^q}\right)\\
&= q\partial_q\log\int\frac{\mu(\mathbf{x})^q}{\pi(\mathbf{x})^q}\pi(\mathbf{x})\,\mathrm{d}\mathbf{x} - \log\int\frac{\mu(\mathbf{x})^q}{\pi(\mathbf{x})^q}\pi(\mathbf{x})\,\mathrm{d}\mathbf{x}\\
&= q\partial_q\left\{(q-1)\left(\frac{1}{q-1}\log\int\frac{\mu(\mathbf{x})^q}{\pi(\mathbf{x})^q}\pi(\mathbf{x})\,\mathrm{d}\mathbf{x}\right)\right\} - \log\int\frac{\mu(\mathbf{x})^q}{\pi(\mathbf{x})^q}\pi(\mathbf{x})\,\mathrm{d}\mathbf{x}\\
&= \frac{q}{q-1}\log\int\frac{\mu(\mathbf{x})^q}{\pi(\mathbf{x})^q}\pi(\mathbf{x})\,\mathrm{d}\mathbf{x} - \log\int\frac{\mu(\mathbf{x})^q}{\pi(\mathbf{x})^q}\pi(\mathbf{x})\,\mathrm{d}\mathbf{x}\\
&\quad + q(q-1)\partial_q\left(\frac{1}{q-1}\log\int\frac{\mu(\mathbf{x})^q}{\pi(\mathbf{x})^q}\pi(\mathbf{x})\,\mathrm{d}\mathbf{x}\right)\\
&\geq \frac{1}{q-1}\log\int\frac{\mu(\mathbf{x})^q}{\pi(\mathbf{x})^q}\pi(\mathbf{x})\,\mathrm{d}\mathbf{x},
\end{aligned}
$$

where the inequality invokes the fact that the Rényi divergence is monotonic in the order q (Vempala and Wibisono, 2019, Lemma 11). Hence by setting $q = 2$,

$$
\begin{aligned}
\text{Ent}_\pi\left(\frac{\mu^2}{\pi^2}\right) &\geq \left(\int\frac{\mu(\mathbf{x})^2}{\pi(\mathbf{x})^2}\pi(\mathbf{x})\,\mathrm{d}\mathbf{x}\right)\log\int\frac{\mu(\mathbf{x})^2}{\pi(\mathbf{x})^2}\pi(\mathbf{x})\,\mathrm{d}\mathbf{x}\\
&\geq \left(\chi^2(\mu\|\pi)+1\right)\log\left(\chi^2(\mu\|\pi)+1\right) \geq \chi^2(\mu\|\pi),
\end{aligned} \tag{I.2}
$$

where the last inequality holds from $(x+1)\log(x+1) \geq x$ for each $x \geq 0$. Combining (I.1) and (I.2) completes the proof. $\square$

We next introduce Donsker-Varadhan variational principle (Rassoul-Agha and Seppäläinen, 2015, Theorem 5.4).

Lemma I.11. *Let μ and π be two distributions. Then for each function $\phi : \mathbb{R}^d \to \mathbb{R}$,*

$$\mathbb{E}_\mu[\phi] \leq \text{KL}(\mu\|\pi) + \log\mathbb{E}_\pi[\exp(\phi)].$$

The following lemma provides the Chernoff bound for χ^2-distribution, which can be found in Wainwright (2019, Example 2.8) and Duchi (2024, Example 4.1.13).

Lemma I.12. *Let Let $\mathbf{X} = (X_1,\ldots,X_d)$ be a vector of independent Gaussian random variables with zero mean and σ^2-variance. Then*

$$\log\mathbb{E}\big[\exp\{s(\|\mathbf{X}\|_2^2 - \mathbb{E}[\|\mathbf{X}\|_2^2])\}\big] \leq 2ds\sigma^2.$$

Proof of Lemma I.12. Before proceeding, we consider the Chernoff bound for the Z^2 with $Z \sim N(0,1)$. For $4\lambda < 1$, we have

$$\mathbb{E}[\exp(\lambda(Z^2 - \mathbb{E}[Z^2]))] = \frac{1}{\sqrt{2\pi}} \int \exp(\lambda(z^2 - 1)) \exp\left(-\frac{z^2}{2}\right) \mathrm{d}z$$

(I.3)
$$= \frac{\exp(-\lambda)}{\sqrt{1 - 2\lambda}} \leq \exp(2\lambda^2),$$

where the inequality holds from $-\log(1 - 2\lambda) \leq 2\lambda + 4\lambda^2$ for $4\lambda \leq 1$.

We next turn to verify the Chernoff bound for the χ^2 random variable with d degrees of freedom, denoted by $Y \sim \chi_n^2$. Note that $Y \overset{\mathrm{d}}{=} \sum_{i=1}^d Z_i^2$ where $Z_1, \ldots, Z_d \sim^{\text{i.i.d.}} N(0,1)$. Then for $4\lambda < 1$,

$$\log \mathbb{E}\big[\exp\{\lambda(Y - \mathbb{E}[Y])\}\big]$$

$$= \log \mathbb{E}\Big[\exp\Big\{\sum_{i=1}^d \lambda(Z_i^2 - \mathbb{E}[Z_i^2])\Big\}\Big] = \sum_{i=1}^d \log \mathbb{E}[\lambda(Z_i^2 - \mathbb{E}[Z_i^2])] \leq 2d\lambda^2,$$

where the inequality follows from (I.3). Setting $\lambda = s\sigma^2$ completes the proof. $\qquad\square$

The next lemma shows that the KL divergence can be bounded by the Fisher information.

Lemma I.13. *Suppose the distribution π satisfies the log-Sobolev inequality with constant C_{LSI}. Then for each distribution μ,*

$$\mathrm{KL}(\mu \| \pi) \leq 2C_{\mathrm{LSI}} \mathbb{E}_\pi\Big[\|\nabla \sqrt{\tfrac{\mu}{\pi}}\|_2^2\Big].$$

Proof of Lemma I.13. Recall the log-Sobolev inequality

(I.4)
$$\mathrm{Ent}_\pi(f^2) \leq 2C_{\mathrm{LSI}} \mathbb{E}_\pi\big[\|\nabla f\|_2^2\big].$$

Substituting $f^2(\mathbf{x}) = \mu(\mathbf{x})/\pi(\mathbf{x})$ into the left-hand side of (I.4) deduces

$$\mathrm{Ent}_\pi\left(\frac{\mu}{\pi}\right) = \int \frac{\mu(\mathbf{x})}{\pi(\mathbf{x})} \log \frac{\mu(\mathbf{x})}{\pi(\mathbf{x})} \pi(\mathbf{x})\, \mathrm{d}\mathbf{x} - \int \frac{\mu(\mathbf{x})}{\pi(\mathbf{x})} \pi(\mathbf{x})\, \mathrm{d}\mathbf{x} \log \int \frac{\mu(\mathbf{x})}{\pi(\mathbf{x})} \pi(\mathbf{x})\, \mathrm{d}\mathbf{x}$$

$$= \int \mu(\mathbf{x}) \log \frac{\mu(\mathbf{x})}{\pi(\mathbf{x})}\, \mathrm{d}\mathbf{x} = \mathrm{KL}(\mu \| \pi).$$

As a consequence,

$$\mathrm{KL}(\mu \| \pi) = \mathrm{Ent}_\pi\left(\frac{\mu}{\pi}\right) \leq 2C_{\mathrm{LSI}} \mathbb{E}_\pi\Big[\|\nabla \sqrt{\tfrac{\mu}{\pi}}\|_2^2\Big].$$

This completes the proof. $\qquad\square$

Lemma I.14. *For two distributions μ and π, it holds that*

$$\mathbb{E}_\mu\Big[\|\nabla \log \tfrac{\mu}{\pi}\|_2^2\Big] = 4\mathbb{E}_\pi\Big[\|\nabla \sqrt{\tfrac{\mu}{\pi}}\|_2^2\Big].$$

Proof of Lemma I.14. It is straightforward that

$$\mathbb{E}_\mu\Big[\|\nabla \log \tfrac{\mu}{\pi}\|_2^2\Big] = \int \|\nabla \log \frac{\mu(\mathbf{x})}{\pi(\mathbf{x})}\|_2^2 \mu(\mathbf{x})\, \mathrm{d}\mathbf{x} = \int \frac{\pi(\mathbf{x})}{\mu(\mathbf{x})} \|\nabla \frac{\mu(\mathbf{x})}{\pi(\mathbf{x})}\|_2^2 \pi(\mathbf{x})\, \mathrm{d}\mathbf{x}$$

$$= 4\int \|\frac{1}{2}\sqrt{\frac{\pi(\mathbf{x})}{\mu(\mathbf{x})}} \nabla \frac{\mu(\mathbf{x})}{\pi(\mathbf{x})}\|_2^2 \pi(\mathbf{x})\, \mathrm{d}\mathbf{x} = 4\int \|\nabla \sqrt{\frac{\mu(\mathbf{x})}{\pi(\mathbf{x})}}\|_2^2 \pi(\mathbf{x})\, \mathrm{d}\mathbf{x}$$

$$= 4\mathbb{E}_\pi\Big[\|\nabla \sqrt{\tfrac{\mu}{\pi}}\|_2^2\Big],$$

which completes the proof. □

Lemma I.15. *Let μ and π be two distributions. Define ϕ as $\mathrm{d}\mu = \phi\,\mathrm{d}\pi$, and define $\psi\mathbb{E}_\pi[\phi^2] = \phi$. Then the following equality holds*

$$\mathbb{E}_\mu\big[\psi\|\nabla\log(\psi\phi)\|_2^2\big] = \frac{4\mathbb{E}_\pi[\|\nabla_\mathbf{x}\phi\|_2^2]}{\mathbb{E}_\pi[\phi^2]}.$$

Proof of Lemma I.15. It is straightforward that

$$\|\nabla\log(\psi\phi)\|_2^2 = \|\nabla\log\frac{\phi^2}{\mathbb{E}_\pi[\phi^2]}\|_2^2 = 4\|\nabla\log\phi\|_2^2 = \frac{4\|\nabla_\mathbf{x}\phi\|_2^2}{\phi^2}.$$

As a consequence,

$$\mathbb{E}_\mu\big[\psi\|\nabla\log(\psi\phi)\|_2^2\big] = \frac{4}{\mathbb{E}_\pi[\phi^2]}\int\frac{\|\nabla_\mathbf{x}\phi(\mathbf{x})\|_2^2}{\phi(\mathbf{x})}\mu(\mathbf{x})\,\mathrm{d}\mathbf{x} = \frac{4\mathbb{E}_\pi[\|\nabla_\mathbf{x}\phi\|_2^2]}{\mathbb{E}_\pi[\phi^2]},$$

which completes the proof. □

APPENDIX J. ADDITIONAL NUMERICAL EXPERIMENTS

(1) Section J.1 showcases the application of SSLS to a linear Gaussian state-space model, highlighting its capability to accurately estimate the posterior distribution even in the presence of initial prior distribution shifts.

(2) Section J.2 focuses on applying SSLS to the Lorenz-96 model and comparing it with APF. The primary objective here is to assess the robustness of SSLS against initial prior distribution shifts, while also evaluating the impact of ensemble size on its performance across various metrics.

J.1. **Linear Gaussian state-space model.** To begin with, we look into a one-dimensional linear Gaussian state-space model, for which the ground truth posterior can be computed by the Kalman filter (Särkkä and Svensson, 2023). The state-space model is defined as

$$\begin{aligned} X_{k+1} &= X_k + V_k, & V_k &\sim N(0,5), \\ Y_k &= X_k + W_k, & W_k &\sim N(0,0.2), \end{aligned} \tag{J.1}$$

where $k \in \mathbb{N}$, and the initial prior distribution is set as $X_1 \sim N(0,1)$. The SSLS ensemble size is 500.

Assimilation with exact initial prior. We begin by considering the case where the SSLS is carried out with the exact initial prior. The experimental results are shown in the top row of Figure 10, indicating that the distribution of the SSLS ensemble closely aligns with the ground truth posterior throughout all time steps, given that the SSLS is conducted without the initial prior distribution shift. This empirical finding validates the theoretical conclusions outlined in Theorem 3.4.

Assimilation with inexact initial prior. In practical scenarios, the initial prior distribution is typically intractable. Therefore, it is essential to assess the robustness of the SSLS against the initial prior distribution shift. In this experiment, the SSLS is initialized by an inexact prior of $N(-10,1)$, and the outcomes are presented in the bottom row of Figure 10. The results demonstrate that, even in the presence of an initial prior distribution shift, the SSLS ensemble closely matches the ground truth posterior distribution after a small number of time steps, despite prominent estimation errors in initial few time steps.
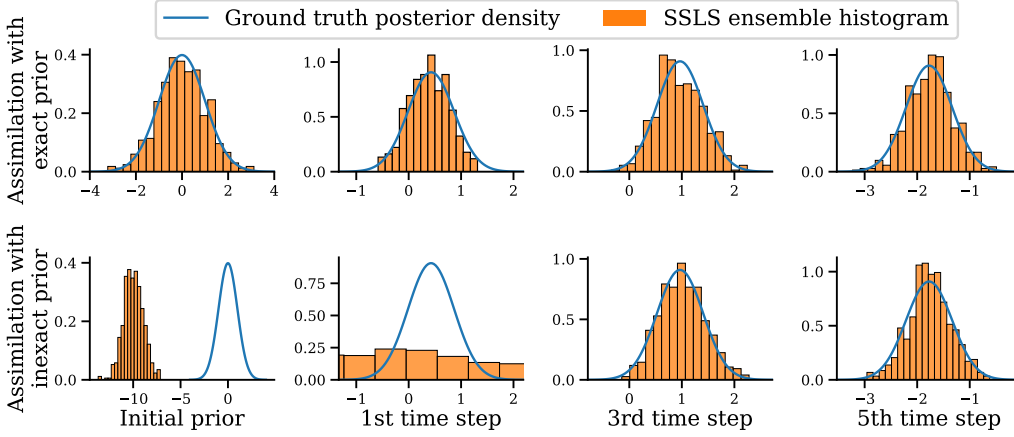
FIGURE 10. Posterior distributions estimated by SSLS in a linear Gaussian state-space model (J.1). (a) The top row shows the histogram of the SSLS ensemble with an exact initial prior distribution. (b) The bottom row demonstrates the histogram of the SSLS ensemble with an inexact initial prior distribution.

Recall that Theorem 3.4 provides an error bound that increases with the number of time step. Nonetheless, this error bound may be too loose to accurately depict empirical findings, as it solely characterizes a worst-case scenario. Therefore, establishing a tighter error bound that precisely reflects experimental observations remains an open question. This gap between theoretical understandings and experimental observations will be explored in greater depth in future work.

J.2. **Lorenz-96.** Lorenz-96 is a widely-used benchmark in the field of numerical weather forecasting (Majda and Harlim, 2012, Reich and Cotter, 2015, Evensen et al., 2022, Spantini et al., 2022), which is defined by a set of nonlinear ODEs representing the spatial discretization of a time-dependent PDE

$$(J.2) \qquad \frac{\mathrm{d}}{\mathrm{d}t} Z_{t,i} = (Z_{t,i+1} - Z_{t,i-2})Z_{t,i-1} - Z_{t,i} + F, \quad 1 \le i \le d.$$

In this experiment, we consider the twenty-dimensional Lorenz-96 system. We set a constant forcing parameter $F = 8$, resulting in a fully chaotic dynamic (Majda and Harlim, 2012), where slightly different initial conditions lead to extremely different trajectories.

The dynamics model is defined by discretizing (J.2) using the fourth-order explicit Runge-Kutta method with time step δt. The states at discrete times are denoted by $(\mathbf{X}_k)_{k \in \mathbb{N}}$ with $\mathbf{X}_k = (Z_{k\delta t,1}, \ldots, Z_{k\delta t,d})^\top$. At each time step $k \in \mathbb{N}$, we employ a linear measurement model with Gaussian additive noise

$$(J.3) \qquad\qquad \mathbf{Y}_k = \mathbf{X}_k + \sigma_{\mathrm{obs}}\mathbf{W}_k,$$

where $\mathbf{W}_k \sim N(\mathbf{0}, \mathbf{I}_d)$ denotes the measurement noise.

Baseline. To mitigate the degeneracy of the APF, a small amount of Gaussian noise $N(0, 10^{-1}\mathbf{I}_d)$ is incorporated into the state at each iteration of the Runge-Kutta method (Spantini et al., 2022). To ensure a fair comparison, the ensemble size for both APF and SSLS is set to 500. To showcase the robustness of SSLS against the initial prior distribution, we

intentionally set the initial distribution of both SSLS and APF away from the ground truth initial prior. See Appendix K for more details on training parameters.

Metrics for assimilation. To quantitatively measure the performance of SSLS and study the impact of ensemble size on the assimilation performance, we focus on four metrics as Spantini et al. (2022), including

   (i) RMSE: the root mean squared error,
  (ii) spread: the root mean trace of the ensemble covariance matrix,
 (iii) coverage probability: the coverage probability of the intervals given by the empirical 2.5% and 97.5% quantiles of each marginal of the ensemble, and
 (iv) CRPS: the continuous ranked probability score (Gneiting et al., 2007, Bröcker, 2012).

The RMSE quantifies the discrepancy between estimated states and reference states, while the spread indicates the concentration of the ensemble particles. The coverage probability assesses the likelihood that a marginal confidence interval includes the reference states. The CRPS is a statistical metric used to assess the accuracy of the estimated posterior by comparing it to the observed data. It measures the discrepancy between the cumulative distribution function of the estimated posterior and the cumulative distribution function of the observations. A lower CRPS value indicates a better alignment between the estimated posterior and observed distributions, indicating a more accurate estimate.
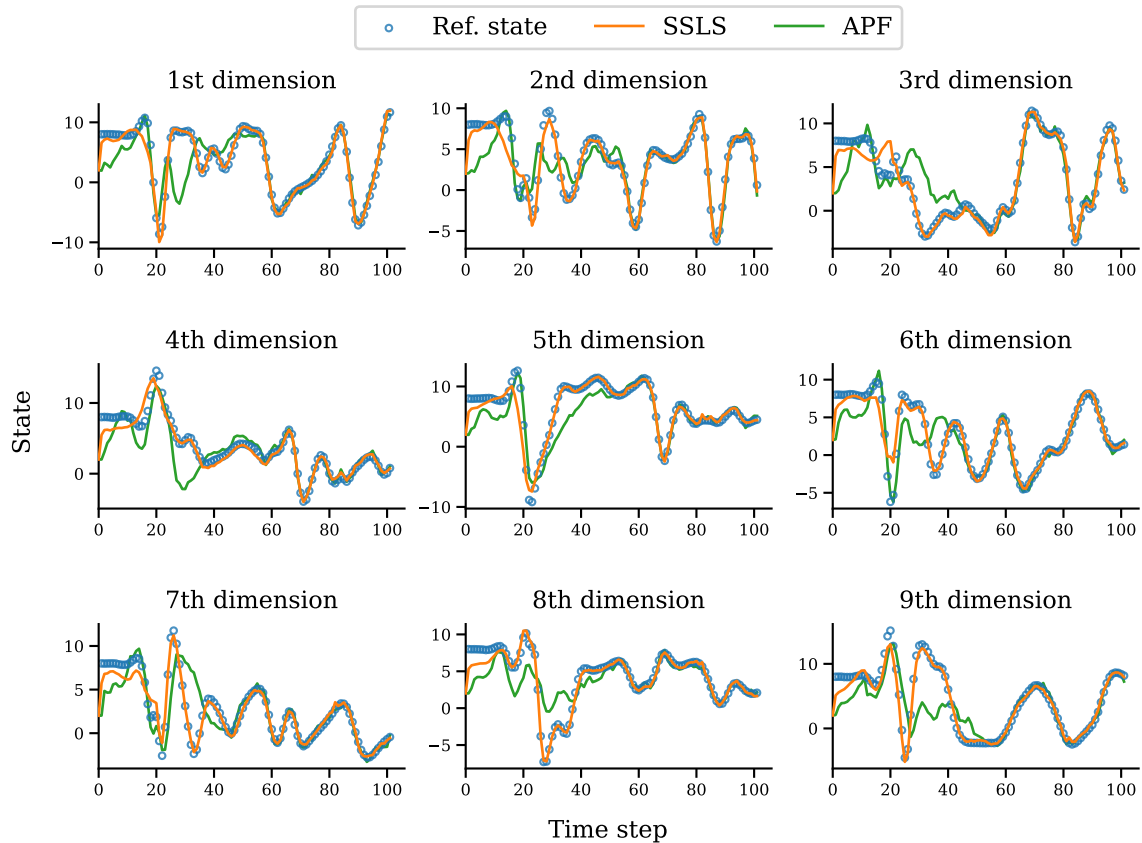

FIGURE 11. Evolution of the reference states, the SSLS ensemble mean, and the APF ensemble mean for Lorenz-96 (J.2).
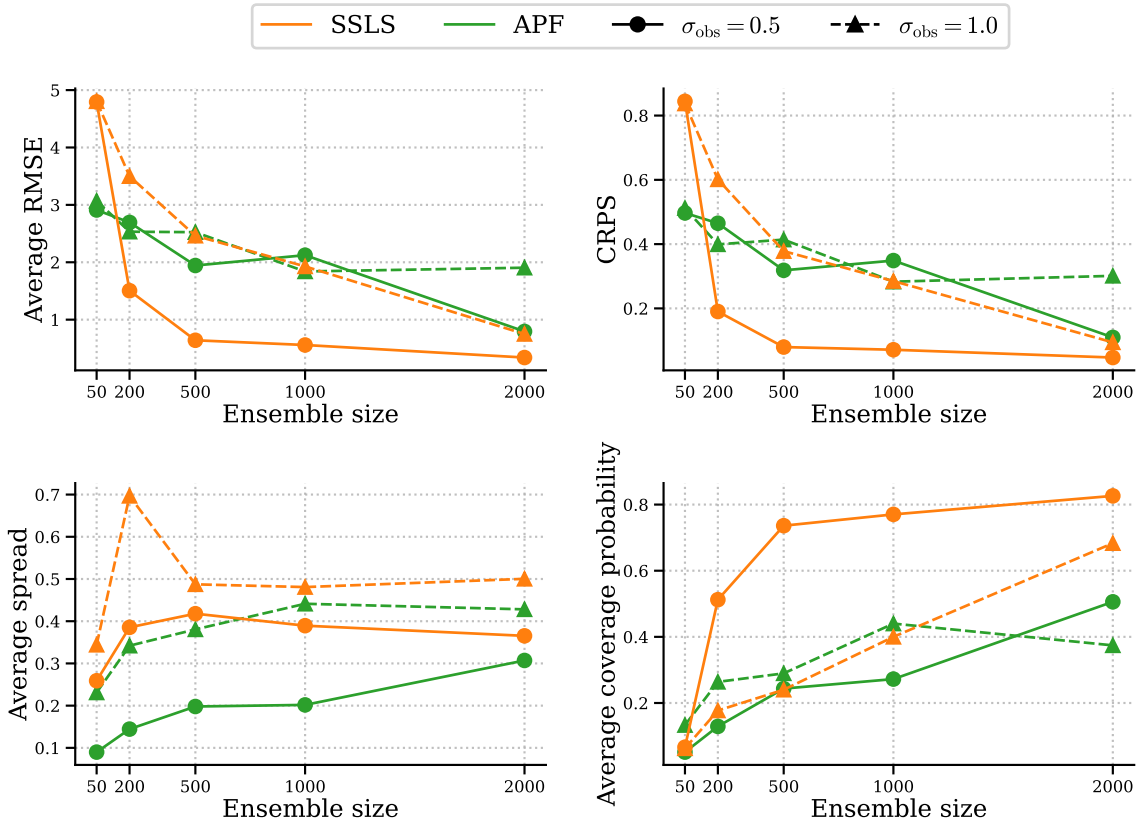
FIGURE 12. Performance metrics of SSLS and APF for Lorenz-96 (J.2). For each ensemble size, metrics are averaged over elements of the estimated states and time steps.

Experimental results. Figure 11 demonstrates the evolution of the first nine elements of the states estimated by SSLS and APF, respectively. Despite an initial prior distribution shift, SSLS effectively corrects this error within a few subsequent assimilation steps, whereas APF requires a significantly longer assimilation time to compensate for the initial prior distribution shift. These empirical observations are consistent with those of the previous experiment. Figure 12 presents four metrics for both SSLS and APF with different ensemble size.

(i) **RMSE**: The average RMSE of both SSLS and APF decreases as the ensemble size increases, which is consistent with our theoretical findings. Specifically, the discussions below Assumption 4 indicates that the score matching error in SSLS approaches zero as the ensemble size increases towards infinity. Consequently, the assimilation error decreases as the ensemble size increases, as evidenced by the results in Theorem 3.4. Additionally, Figure 12 illustrates that SSLS performs better than APF for ensemble sizes exceeding 200.

(ii) **CRPS**: As depicted in the upper right portion of Figure 12, the average CRPS of SSLS decreases significantly as the ensemble size increases. This trend suggests an enhanced alignment between the estimated posterior distribution and the observation data. Furthermore, for ensemble sizes exceeding 500, SSLS demonstrates lower CRPS values compared to the APF, underscoring the superior effectiveness of SSLS in posterior estimation.

(iii) **Spread and coverage probability**: The bottom row of Figure 12 demonstrates that the coverage probability of SSLS noticeably grows with the increase in ensemble size, while the spread remains relatively stable. Moreover, Figure 12 indicates that at a low noise level of $\sigma_{\text{obs}} = 0.5$, SSLS exhibits a much higher coverage probability compared to APF, despite having a larger average spread. This disparity can be attributed to particle degeneracy in APF.

For further discussion on this experiment, please refer to Appendix K.

APPENDIX K. EXPERIMENTAL DETAILS

K.1. **Double-well problem.** For the first problem, we adopt a residual neural network with 2 hidden layers to learn for the prior score. The width of each hidden layer is set as 128, and the activation functions is chosen as the sigmoid function. During the learning procedure, we apply the denoising score match method Vincent (2011) with a noise level 0.1 to improve the training efficiency. After that, the gradient of log posterior can be explicitly evaluated.

In the implementation of APF and EnKF, the ensemble size is set as $n = 1000$, same to the sample size used in SSLS. Among all the three methods, the initial state distribution is defined as the normal distribution $N(-1, 0.15^2)$.

K.2. **Lorenz 96 model.** For the Lorenz 96 problem, we adopt a 1D UNet to learn for the prior score. The channels are 32, 64 and 128, and the activation functions is chosen as the ReLU function. During the learning procedure, we apply the denoising score match method Vincent (2011) with a noise level 0.1 to improve the training efficiency. After that, the gradient of log posterior can be explicitly evaluated.

In the implementation of APF, if unspecified, the ensemble size is set as $n = 500$, same to the sample size used in SSLS. The initial state distribution is defined as the normal distribution $N(\mathbf{0}, \mathbf{I}_{20})$.

The superiority of SSLS in Figure 11 can also be understood using Figure 13. Starting from a bad initial guess, the width of assimilation band of the APF ensemble (the maximum difference between any two samples in the ensemble) becomes narrowing rapidly, due to the imbalanced distribution of the likelihood value. This phenomenon greatly reduces the efficiency of APF. On the contrary, SSLS adopts a continues network function to approximate the prior distribution, the better generalization ability increases the coverage probability for
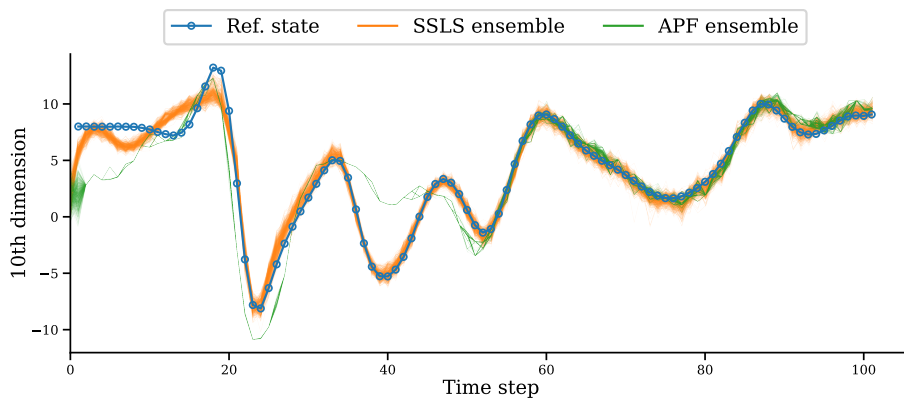

FIGURE 13. Evolution of x_{10} of the true states, the SSLS ensemble and the APF ensemble on REFERENCE LORENZ.
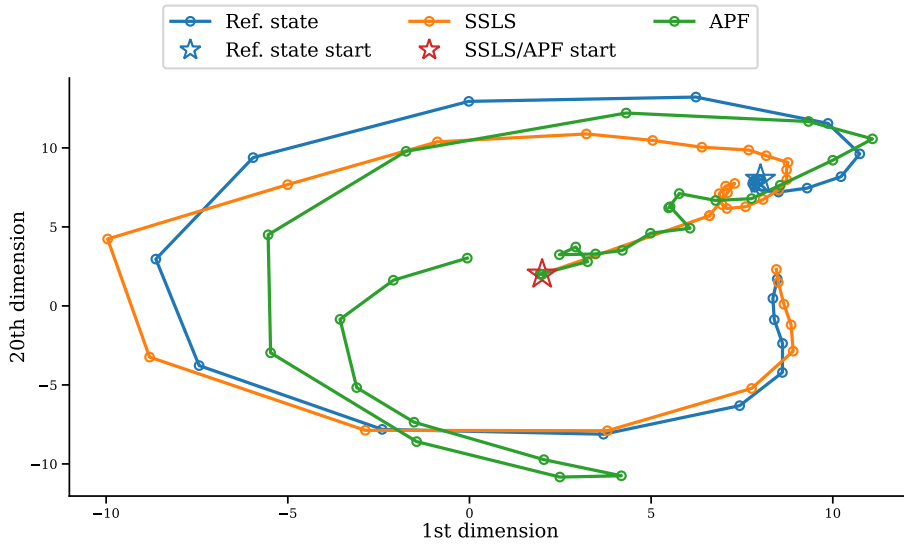
FIGURE 14. Trajectory of the true states, the SSLS estimation and the APF estimation for a Lorenz 96 system. The trajectory is visualized in the x_1-x_{20} space.
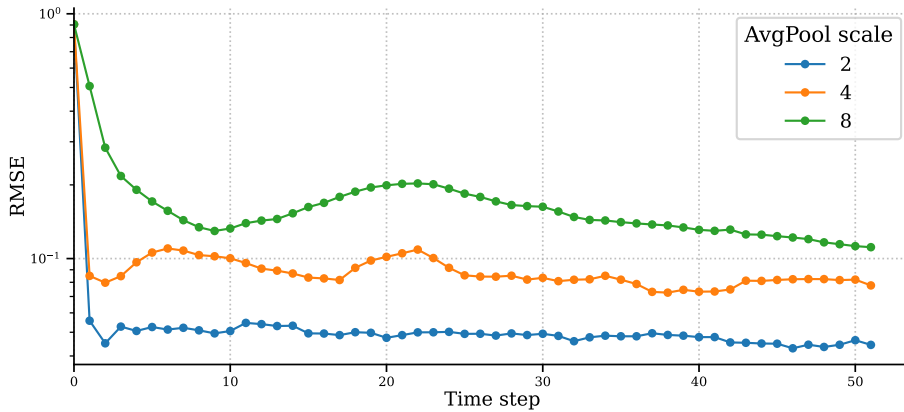

FIGURE 15. RMSE of SSLS assimilated states at different average pooling scale. Time 0 corresponds to RMSE from the expectation of the prior distribution, when the assimilation has not taken place. The three lines share the same starting RMSE as they share the same guess on the prior distribution.

the true state. In Figure 14, we compare the predicted trajectories of SSLS and APF with true state in the x_1-x_{20} space, which again verifies this advantage.

K.3. **Kolmogorov flow.** For the Kolmogorov flow problem, we adopt a 2D UNet to learn for the prior score. During the learning procedure, we apply the denoising score match method Vincent (2011) with a noise level 0.2 to improve the training efficiency. After that, the gradient of log posterior can be explicitly evaluated. The sample size used in SSLS is set as $n = 500$.

To further study the evolution of error, we also compare the RMSE of SSLS under different average pooling scale in Figure 15, which demonstrates at the early stage of assimilation (eliminating the effect of initial lag error), the RMSE would decreases rapidly to a small value,

and then maintain stable. Furthermore, a larger pooling scale would make the problem more difficult , resulting a slower decrease of RMSE, converging to a higher value.

K.4. **Numerical stability improvements.** Throughout our numerical experiments, we mainly adopt two numerical improvements on the original algorithm for stability.

(i) The first improvement is that, before matching the score function of the prior distribution at each step, we normalize the samples to zero mean and identity covariance. Then we match the score function on the normalized distribution, from which we obtain the original score function after affine transformation.

(ii) Another improvement is that, we manually clip the score function of estimated posterior score by its L^2-norm to ensure the stability of the score-based Langevin sampling.